UNIVERSITY OF SOUTHAMPTON
Faculty of Physical and Applied Sciences
Optoelectronics Research Centre

Development of Bismuth Doped Silica Fibres for High Power Sources & Long Wavelength Generation from Ytterbium Doped Fibre Lasers

Mridu P. Kalita

Thesis for the degree of Doctor of Philosophy

December 2010

UNIVERSITY OF SOUTHAMPTON

Abstract

Faculty of Physical and Applied Sciences
Optoelectronics Research Centre

Doctor of Philosophy

by Mridu P. Kalita

A detailed study of fabrication and characterisation of bismuth (Bi) doped silica optical fibre has been investigated. Three different fibre fabrication techniques were applied to study the possible influence on Bi-luminescence: modified chemical vapour deposition (MCVD) and the solution doping technique, MCVD chemical-in-crucible deposition technique and the powder-in-tube (PIT) technique. Spectroscopic absorption and Bi luminescence and fluorescence decay properties under different pumping wavelengths and with different host glass compositions are presented and provide important information for device applications. The influence of unsaturable loss on laser performance is investigated. The feasibility of direct laser diode pumping of Bi-doped fibre lasers at the wavelengths of 915 and 975 nm was examined by measuring excited state absorption in Bi-doped silicate fibres for the wavelength range of 900 -1300 nm. Enhancement in spectroscopic properties of Bi-doped fibre, by H_2-loading, has been examined.

Bi-doped fibre laser operating in the wavelength region of 1160-1179 nm has been demonstrated. The fibre laser performance at 1179 nm was investigated incorporating different cooling arrangements. The operation of Bi-doped fibre amplifier at 1179 nm, in both low and high input signal regime, was also examined.

An all-fibre, narrow-linewidth, high power Yb-doped silica fibre laser at 1179 nm has been demonstrated. Furthermore, theoretical work confirms that the proposed laser architecture can be easily scaled to higher power.

Contents

List of Figures

List of Tables

Declaration of Authorship

I, Mridu P. Kalita, declare that the thesis entitled, 'Development of Bismuth Doped Silica Fibres for High Power Sources and Long Wavelength Generation from Ytterbium Doped Fibre Lasers' and the work presented in this thesis are my own. I confirm that:

- This work was done wholly or mainly while in candidature for a research degree at this University.
- Where any part of this thesis has previously been submitted for a degree or any other qualification at this University or any other institution, this has been clearly stated.
- Where I have consulted the published work of others, this is always clearly attributed.
- Where I have quoted from the work of others, the source is always given. With the exception of such quotations, this thesis is entirely my own work.
- I have acknowledged all main sources of help.
- Where the thesis is based on work done by myself jointly with others, I have made clear exactly what was done by others and what I have contributed myself.
- Parts of this work have been published as the journal papers and conference contributions listed in Appendix A.

Signed: _____

Date: _____

Acknowledgements

I am grateful to all the people who have helped and inspired me during my PhD. First of all I would like to thank my supervisor Dr. Jayanta Sahu, for his patience, support, and guidance throughout my PhD, whilst allowing me the room to work in my own way. I would also like to thank all the members of the Specialty Silica Fibre Fabrication Group, especially Dr. Seongwoo Yoo for dedicating enormous amount of time and effort showing me the ropes when I started and assisting during the most difficult moments of my PhD. Sincere thanks to Dr. Alex Boyland, Andrew Webb and Rob Standish for their help and support on many occasions.

I wish to express my gratitude to Dr. Morten Ibsen for his help and support on numerous occasions including fabricating the fibre Bragg gratings. I would also like to thank Prof. Johan Nilsson for his advice and many helpful discussions during the course of PhD. Special thanks to Dr. Christophe Codemard and Dr. Shaif-ul Alam for sharing their expertise in fibre lasers.

I am thankful to all the administration staff and in particular to Mrs. Eve Smith, for her outstanding support, from the start to the very end. Finally, thanks to all my friends at the ORC and outside who have supported and encouraged me through the years.

I am grateful to my parents and family members, for their love, support and encouragement, without which I could never have reached this point. And special thanks to Dadu for keeping me sane through it all.

Last but by no means the least, thank you Nikita, for always being there right beside me.

To Ma, Deuta and Pehi

"It has often been said that 'nature is simple' - illusion!"

L. Brillouin

Abbreviations

AOM	**A**cousto **O**ptic **M**odulator
ASE	**A**mplified **S**pontaneous **E**mission
CW	**C**ontinuous **W**ave
DCF	**D**ouble **C**lad **F**ibre
DM	**D**ichroic **M**irror
EDAX	**E**nergy **D**ispersive **X**-ray **S**pectroscopy
ESA	**E**xcited **S**tate **A**bsorption
FBG	**F**ibre **B**ragg **G**rating
FOG	**F**ibre **O**ptic **G**yroscope
FWHM	**F**ull **W**idth **H**alf **M**aximum
GSA	**G**round **S**tate **A**bsorption
HR	**H**igh **R**eflection
HT	**H**igh **T**ransmission
MOPA	**M**aster **O**scillator **P**ower **A**mplifier
NA	**N**umerical **A**perture
NIR	**N**ear **I**nfra **R**ed
OCT	**O**ptical **C**oherence **T**omography
OC	**O**utput **C**oupler
ORC	**O**ptoelectronic **R**esearch **C**entre
OSA	**O**ptical **S**pectrum **A**nalyser
OTDR	**O**ptical **T**ime **D**omain **R**eflectometer

OVD	**O**utside **V**apour **D**eposition
PIT	**P**owder **i**n **T**ube
RE	**R**are **E**arth
RIP	**R**efractive **I**ndex **P**rofile
SIMS	**S**econdary **I**on **M**ass **S**pectrometry
SBS	**S**timulated **B**rillouin **S**cattering
SRS	**S**timulated **R**aman **S**cattering
UV	**U**ltra **V**iolet
VAD	**V**apour **A**xial **D**eposition
WDM	**W**avelength **D**ivision **M**ultiplexing

Chapter 1

Introduction

The thesis describes the development of Bi-doped silica fibre for high power sources at the 1178 nm wavelength band. The luminescence properties of Bi-doped fibre and its dependance on various factors were investigated, with an aim to improve its device performances. The thesis also reports the long wavelength generation from Yb-doped fibre lasers at the 1178 nm band.

1.1 Motivation

Over the past decades silica fibre has revolutionised optical communications by allowing low propagation loss, high gain and large bandwidth transmission of data over long distances [1, 2]. To date the 1 and 1.5 μm wavelength bands, that correspond to the emissions from Yb and Er-doped fibres, have been widely explored in silica to generate high powers. Lately, Yb-doped cladding pumped fibre lasers at 1 μm have demonstrated several kilo-watt of output power, in continuous wave (CW) operation [3]. However, the working wavelength bands of the rare earth (RE) doped lasers are from 0.9-2.1 μm with significant spectral gaps between them. Especially, fibre laser in the 1 - 1.3 μm wavelength band are attractive to

fill the gap in the low-loss transmission window of silica fibre where no efficient active fibre exists. Moreover, the availability of suitable lasers in this wavelength region will allow for the creation of efficient visible lasers, in particular yellow light sources, by frequency doubling, which is promising for opthalmology [4] and dermatological applications [5]. There is, especially for narrow linewidth laser, considerable interest in the 589 nm light to excite a layer of sodium atoms in the mesosphere, which serves as a guide star source for adaptive optics applications in astronomy [6]. The fibre laser and amplifier at this spectral region is also important for many other applications, for example low-coherence, high-brightness sources for interferometric sensing applications such as Optical Coherence Tomography (OCT) [7] and the fibre optic gyroscope (FOG) [8]. The availability of a compact, versatile, efficient, and high-brightness, broad-bandwidth light source in the 1 - 1.3 μm region would be an important advantage for future high power optical communication technologies.

The first fibre laser was demonstrated in the 1960's in a Nd-doped glass fibre, pumped by a flash lamp [9, 10]. With the development of modified chemical vapour deposition (MCVD) and the solution doping process for low loss RE doped fibre fabrication [1, 11], and at the same time, with the availability of semiconductor pump lasers, fibre lasers have replaced many conventional bulk counterparts in many industrial applications. Because fibre lasers are compact and robust compared to other types of high-power, high-brightness light sources, and provide attractive features, such as the potential for single mode and single frequency operations, they are always a favourable candidate for high power sources. Whereas fibre Raman converters can work in the spectral region not covered by the RE ions, they have drawbacks such as limited spectral control and require high power consumption and this makes the system complicated. Also, the long fibre lengths required for Raman conversion leads to a broadening of the emission spectrum

which is disadvantageous for frequency doubling and many other applications. Many researchers investigated praseodymium doped zirconium barium lanthanum aluminium sodium fluoride (ZBLAN) fibre amplifiers to utilize the second window for optical amplification. However, ZBLAN glass suffers from narrow bandwidth (25 nm) [12, 13] and is weak, both in chemical durability and mechanical strength, and cannot be fusion-spliced to silica-based fibre. Transition metal ions such as Cr^{4+} and Ni^{2+} have much broader bandwidths (∼300 nm) [14, 15], but the efficiency in a glass host is generally low. It is therefore appropriate and necessary to search for an alternative fibre material, which is efficient and economical for a 1300 nm amplifier.

Recently, Fujimoto and Nakatsuka reported broadband near infrared luminescence in Bi-doped silica glass [16]. The luminescence spans in the range of 1100 - 1500 nm, depending on co-dopants, and can be excited by a wide range of excitation wavelengths, with broad overlapping absorption peaks at 500, 700 and 800 nm. Since then, there have been numerous studies reported on the infrared luminescence of Bi-doped glasses. In the next chapter, the current understanding of luminescence in Bi-doped glasses and fibres will be reviewed.

The aim of the thesis is to develop an efficient and high power Bi-doped fibre source in the 1178 nm wavelength region. This involves fabrication and characterization of a number of fibres of different host glass compositions under different fabrication conditions. Three different fibre fabrication techniques were applied to study the possible influence on Bi-luminescence: MCVD and the solution doping technique, MCVD chemical-in-crucible deposition technique and the powder-in-tube (PIT) technique. Bi-doped fibres were fabricated with different host glass compositions and Bi concentrations suitable for different device demonstrations and for spectroscopic study.

1.2 Summary of contents

The content of the thesis is arranged as follows. The current chapter presents the motivations and objectives of the thesis. Chapter 2 describes brief review of the well known MCVD and the solution doping technique, which is widely used commercially for fabrication of RE doped silica preforms, followed by optical fibre drawing. An overview of the current progress on Bi-doped glasses and fibres and the possible origin of Bi luminescence is discussed in Section 2.3. Section 2.4 details the recent results on the long wavelength generation from Yb-doped fibre lasers. In Chapter 3, Bi and Yb-doped fibres fabricated by the MCVD technique and also by the novel MCVD chemical-in-crucible deposition technique are discussed. Later the PIT technique for the fabrication of Bi-doped fibre is discussed, in which a silica tube is filled up with a mixture of SiO_2, Bi_2O_3 and Al_2O_3 powders, before drawing into fibre. In Chapter 4, a detailed description of the basic spectroscopic properties of Bi-doped fibre are given. The impact of unsaturable absorption and pump excited state absorption (ESA) on laser performances are also discussed. In Chapter 5, the performance of Bi-doped fibre laser and amplifier at 1179 nm, are investigated. The work on Yb-doped fibre laser at 1179 nm is presented in Chapter 6. Finally, Chapter 7 summarises the main results and achievements of this thesis and describes possible areas for further development.

References

[1] S. Poole, D. Payne, and M. Fermann, "Fabrication of low-loss optical fibres containing rare-earth ions," *Electronics Letters* **21**(17), pp. 737–738, 1985.

[2] S. Sudo, *Optical fibre amplifiers: materials, devices and applications*, Artech House, 1997.

[3] Y. Jeong, J. K. Sahu, D. N. Payne, and J. Nilsson, "Ytterbium-doped large-core fiber laser with 1.36 kW continuous-wave output power," *Optics Express* **12**(25), pp. 6088–6092, 2004.

[4] C. F. Blodi, S. R. Russell, J. S. Pulido, and J. C. Folk, "Direct and feeder vessel photocoagulation of retinal angiomas with dye yellow laser," *Ophthalmology* **97**(6), pp. 791–795, 1990.

[5] N. S. Sadick and R. Weiss, "The utilization of a new yellow light laser (578 nm) for the treatment of class I red telangiectasia of the lower extremities," *Dermatologic Surgery* **28**(1), pp. 21–25, 2002.

[6] C. E. Max, S. S. Olivier, H. W. Friedman, K. An, K. Avicola, B. V. Beeman, H. D. Bissinger, J. M. Brase, G. V. Erbert, D. T. Gavel, K. Kanz, M. C. Liu, B. Macintosh, K. P. Neeb, J. Patience, and K. E. Waltjen, "Image improvement from a sodium-layer laser guide star adaptive optics system," *Science* **277**(5332), pp. 1649–1652, 1997.

[7] J. Schmitt, "Optical coherence tomography (OCT): a review," *IEEE Journal of Selected Topics in Quantum Electronics* **5**(4), pp. 1205 –1215, 1999.

[8] A. Lawrence, *Optical Fiber Communications, Volume 1: Fiber Fabrication*, Springer, 1998.

[9] E. Snitzer, "Proposed fiber cavities for optical masers," *Journal of Applied Physics* **32**(1), pp. 36–39, 1961.

[10] E. Snitzer, "Optical maser action of Nd^{+3} in a barium crown glass," *Physical Review Letter* **7**(12), pp. 444–446, 1961.

[11] J. E. Townsend, S. B. Poole, and D. N. Payne, "Solution-doping technique for fabrication of rare-earth-doped optical fibers," *Electronics Letters* **23**(7), pp. 329–331, 1987.

[12] Y. Miyajima, T. Sugawa, and Y. Fukasaku, "38.2 dB amplification at 1.31 μm and possibility of 0.98 μm pumping in Pr^{3+} doped fluoride fibre," *Electronics Letters* **27**(19), pp. 1706–1707, 1991.

[13] T. J. Whitley, "A review of recent system demonstrations incorporating 1.3 μm praseodymium-doped fluoride fiber amplifiers," *Journal of Lightwave Technology* **13**(5), pp. 744–760, 1995.

[14] S. Tanabe and X. Feng, "Temperature variation of near-infrared emission from Cr^{4+} in aluminate glass for broadband telecommunication," *Applied Physics Letters* **77**(6), pp. 818–820, 2000.

[15] T. Suzuki and Y. Ohishi, "Broadband 1400 nm emission from Ni^{2+} in zinc-alumino-silicate glass," *Applied Physics Letters* **84**(19), pp. 3804–3806, 2004.

[16] Y. Fujimoto and M. Nakatsuka, "Infrared luminescence from bismuth-doped silica glass," *Japanese Journal of Applied Physics* **40**(3B), pp. L279–L281, 2001.

Chapter 2

Background

2.1 Introduction

The purpose of this chapter is to introduce the basic concepts and information essential in understanding the content of the thesis. The standard modified chemical vapour deposition (MCVD) and the solution doping technique for preform fabrication are detailed followed by the fibre drawing techniques in section 2.2. Section 2.3 presents the recent results on the luminescence properties of Bi-doped glasses and fibre lasers. Section 2.4 gives a brief overview of the long wavelength operation of Yb-doped fibre sources.

2.2 Fabrication of the Bi-doped optical fibres

2.2.1 Fabrication of the preform

Low loss optical fibre fabrication typically involves two main stages: preform fabrication and then drawing the preform into a fibre. Special vapour deposition techniques have been developed for the fibre preform fabrication, and there are

three well known conventional techniques used for making silica optical preforms: Outside Vapour Deposition (OVD) [1], Vapour Axial Deposition (VAD) [2] and MCVD [3]. The key procedure in all of the three techniques is based on a vapour phase reaction, which is the oxidation of chloride or halide vapours. The MCVD process, the most versatile among all these techniques, is used widely because of its ability to produce low loss and high quality active fibres.

2.2.1.1 Modified chemical vapour deposition and the solution doping technique

The MCVD process involves high temperature oxidation of halides of the required elements in a gas phase to form oxide particles which is later deposited on to the inner surface of a silica substrate tube. The preform is fabricated starting with the deposition of an inner cladding and finishing with a core by forming glassy layers of pure or doped silica. Finally, the tube is collapsed to form a solid rod. Halide precursors such as $SiCl_4$, $GeCl_4$ and $POCl_3$ are vapourised and delivered into the substrate tube by a carrier gas, usually oxygen (O_2), using bubbler systems containing a liquid form of the precursor. The halides undergo high temperature oxidation in the presence of O_2 and the resultant soot particles are deposited on the tube wall, and subsequently consolidated into a glassy layer. The principle of mass transfer mechanism responsible for this process is known as thermophoresis [4], which states that particles suspended in a gas with a temperature gradient will move in the direction of the decreasing temperature. The balanced oxidation reactions involved are shown in equation 2.1.

$$
\begin{aligned}
SiCl_4(g) + O_2(g) &\leftrightarrow SiO_2(s) + 2Cl_2(g) \\
GeCl_4(g) + O_2(g) &\leftrightarrow GeO_2(s) + 2Cl_2(g) \\
4POCl_3(g) + 3O_2(g) &\leftrightarrow 2P_2O_5(s) + 6Cl_2(g)
\end{aligned} \tag{2.1}
$$

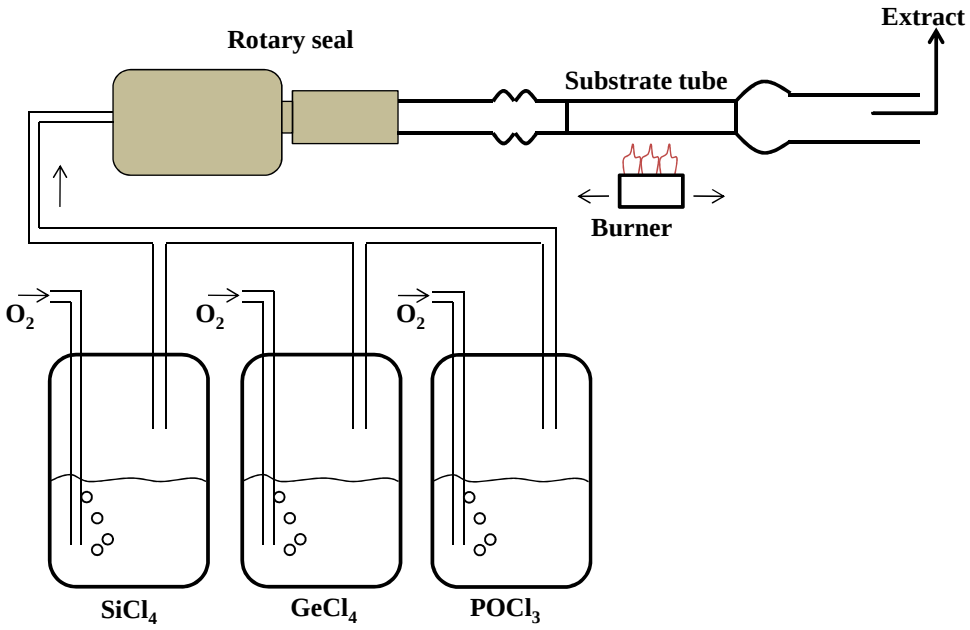

FIGURE 2.1: Schematic of the modified chemical vapour deposition process for preform fabrication.

The MCVD set up consists of a chemical delivery system and a glass working lathe, as shown in Fig. 2.1. In the chemical delivery system, the chemicals are stored in bubblers made of glass, which are housed in constant-temperature baths to maintain the liquid chemicals at the desired temperature. The bubblers consist of an inlet for O_2, which has a plate at the base where the O_2 gas is passed through the halide as small bubbles and an outlet for the O_2 mixed with halide vapour. The rate at which O_2 is passed through the bubbler can be controlled by using mass flow controller; which determines the quantity of halide transferred to the

glass working lathe. The gases are mixed together in a single pipeline before being transferred over to the lathe.

The second part of the set up is the glass working lathe, which has rotating clamps, to hold the high quality silica glass tube to be worked upon. The burner, moved by a motor-driven carriage, can traverse along the length of the glass tube. The temperature of the burner can be controlled by the flow of hydrogen and oxygen using mass flow controller. A pyrometer and an output diameter monitor, moving simultaneously with the burner, measures the temperature and diameter of the hot zone of the tube. It also has a rotary seal at one end to allow the passage of gas into the tubes, and an extract at the other end to remove the hazardous gases and particles produced during the process.

For the preform fabrication, three tubes: a start-up tube, a deposition tube and a soot tube of larger dimension are connected together. The deposition tube is where the chemicals are deposited as a glass and forms the future preform. The start-up tube allows the chemicals to reach the deposition tube without wasting any materials and the soot tube collects the reacted materials which have not been deposited and at the same time keeps the gas flow unblocked. Before connection, all the tubes are cleaned with de-ionised water and then acetone to remove any contamination. The standard deposition tube used at the Optoelectronics Research Centre (ORC) has an inner diameter of 16 mm, an outside diameter of 20 mm, with a typical length of 500 mm (F300 from Heraeus). The first step in the MCVD process is cleaning of the inner surface of the deposition tube by etching approximately 100 μm of silica, using a flow of sulphur-hexa-fluoride (SF_6) which also helps to smoothen the inner wall of the tube. The next stage is the deposition of 5 to 7 cladding layers at a temperature of around 2150^{o}C, which acts as a buffer layer between the tube and the core. It also helps to reduce the irregularities of

the inner wall of the tube and the scattering loss due to that. The burner traverses down the tube in the direction of the gas flow, creating a hot zone, where the chemicals react. The resultant glass soot particles formed are moved in the direction of the lower temperature zone and are deposited on the tube. As the hot zone passes over the deposited glass soot, it is consolidated into a glass film at the inner wall of the tube. An essential process for the incorporation of rare-earth or transition metal ions is the solution doping [5] as the low vapour pressures of these compounds make it difficult to use the standard MCVD method. After cladding deposition, the burner temperature is reduced to 1500 - 1600^{o}C so that whilst the soot is formed and deposited, the temperature of the tube is not high enough to consolidate these particles. This results in a layer of porous silica, whose structure is determined by the temperature. In case of low deposition temperature, the soot can easily be removed from the tube during the doping or sintering process, while high temperature can make the penetration of rare-earth or dopant ions impossible. After removing the tube from the lathe, a dilute solution of the required dopants in methanol is prepared and is pumped slowly into the tube. The solution can be any combination of rare earth, bismuth or aluminium chloride, as required. In order to control the concentration of the dopants in the silica host, the concentration of the solution was properly adjusted. The tube is soaked for an hour to ensure complete diffusion, and then drained slowly. The soot is first dried vertically in the air and then joined on the lathe and rotate for hours, while flowing N_2/O_2 through. Next stage is the consolidation, or sintering, of the soot into a transparent glass layer. The temperature required for sintering is controlled carefully in order to prevent the evaporation of the chlorides before the oxidation reaction occurs. $GeCl_4$ and $POCl_3$ were also incorporated during consolidation process when required.

In order to obtain the desired refractive index profile, the relative proportions of

halide constituents such as germanium, phosphorous etc. need to be adjusted for each pass. In the final glass layer, the amount of each dopant depends on the reactant composition, gas flow rates and on the details of the formation, deposition and consolidation of the gas particles [6]. The deposition temperature is generally high enough so that the oxidation reactions (equations 2.1) are not limited by reaction kinetics but by reaction equilibrium [7]. For example $SiCl_4$ reacts almost 100% to form SiO_2 above a specific temperature, while, $GeCl_4$ has a temperature above which the $GeCl_4$ conversion is reduced; which means that 100% conversion of $GeCl_4$ is not achieved during the MCVD process. At the same time, the equilibrium in equation 2.1 shifts towards $GeCl_4$ at high chlorine concentrations, which results from the complete oxidation of $SiCl_4$, and as a result the oxidation efficiency of $GeCl_4$ is further reduced [8]. It is also worth noting that, not all the particles formed in the oxidation reactions deposit on the tube wall. Particles below a certain critical size stay in the gas stream, reducing the deposition efficiency. The deposition efficiency has been shown to depend on the ratio of the temperature of the gas and the tube wall and the reaction temperature [7]. The gas temperature is affected by burner speed, ambient temperature and tube wall thickness. The deposition efficiency is particularly low for GeO_2, 40-70% [3, 6–8].

After consolidating the soot, the tube is collapsed at a temperature above 2000^{o}C. The tube collapses down to a solid rod due to the surface tension and the reduced viscosity of the glass. The outer surface is fire polished at the end of preform fabrication process and later drawn into the fibre via fibre drawing process.

A commercial preform refractive index profiler (Photon Kinetics PK2600) was used to measure the refractive index of all the preform used in this study. Here, the preform is clamped to a chuck vertically and immersed in a tank containing liquid with higher index to silica. The preform can be rotated to obtain scans at different rotational angles and at the same time, several longitudinal positions

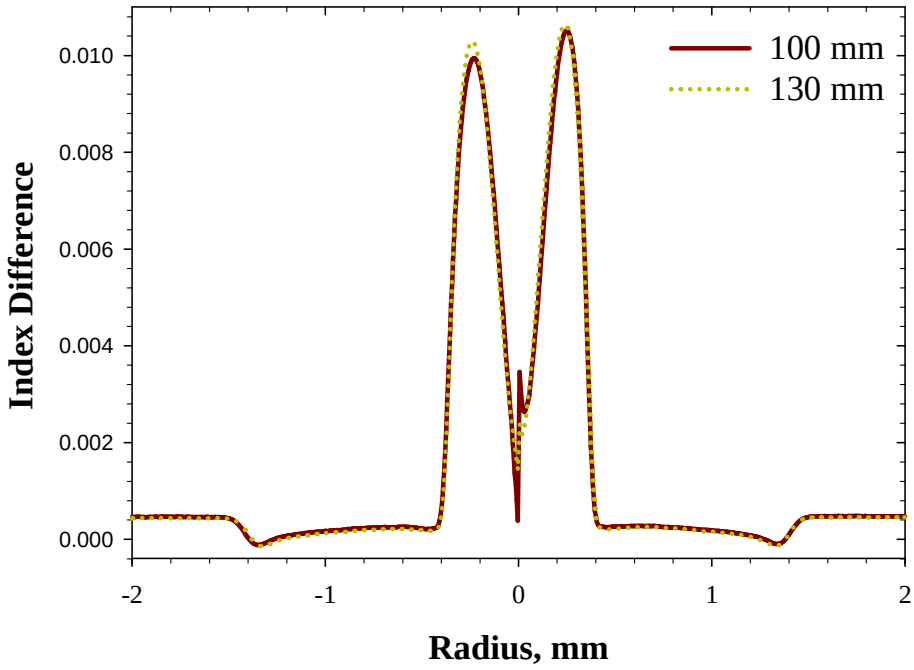

FIGURE 2.2: Refractive index profile of the Bi-doped MCVD preform.

can be measured in a single measurement routine. Figure 2.2 shows the refractive index profile of the germano-alumino-silicate preform L30103, measured by the PK2600 refractive index profiler. The germanium doped core has a central dip. At temperatures above about 1900^{o}C, GeO_2 can be converted to GeO, according to the reaction [6]:

$$GeO_2(s) \leftrightarrow GeO(g) + \frac{1}{2}O_2(g) \tag{2.2}$$

Due to the high temperatures, during collapsing process, the above reaction can occur and may cause Ge-depletion from the surface of the innermost layer because of greater volatility of GeO, causing central dip in the refractive index profile. The central dip can be compensated by adding a small amount of $GeCl_4$ during the collapse process.

2.2.2 Preform processing

In some cases, in order to improve the properties of the resultant fibre, it is necessary to process the preform. For instance, in order to improve the pump absorption for cladding pumping, the broken circular symmetry of the preform is required. In order to achieve this, preform can be milled to break the circular symmetry. All the double clad fibres (DCF) used in this work was 'D'-shaped, to increase the pump absorption.

2.2.3 Optical fibre drawing

The final part of the fibre fabrication process is to draw the preform into fibre on a drawing tower. The preform is vertically fed in to a furnace, and is heated above the glass softening temperature. The soft glass is then drawn into a fibre due to gravity and a pulling force provided by a capstan. The schematic of typical drawing tower is shown in Fig. 2.3. The preform is mounted in a chuck with x-y positioning stage in order to align the preform in the centre of the furnace in such a way that a small length of glass, is situated bellow the centre of the hot zone. The furnace is purged with argon to provide an inert atmosphere and to protect the furnace element from oxidising and hence reducing the particle contamination and increasing element lifetime. The furnace top and bottom irises are carefully adjusted, together with the inert gas flow to provide laminar flow of a sufficient quantity to maximize fibre strength and minimize diameter variations characteristic of turbulent gas flows. The preform is heated slowly until the glass softens at around 2000^{o}C, and the glass is then pulled onto a capstan, which draws the fibre at a constant rate. During the drawing process, the preform is fed into the furnace at an appropriate speed. According to the conservation of mass, the

preform feed speed and fibre draw speed are related by the equation,

$$\frac{v_p}{v_f} = \frac{D_f^2}{D_p^2} \tag{2.3}$$

where v_p is the preform feed speed and and v_f is the fibre draw speed, while D_p and D_f are preform and fibre diameters respectively.

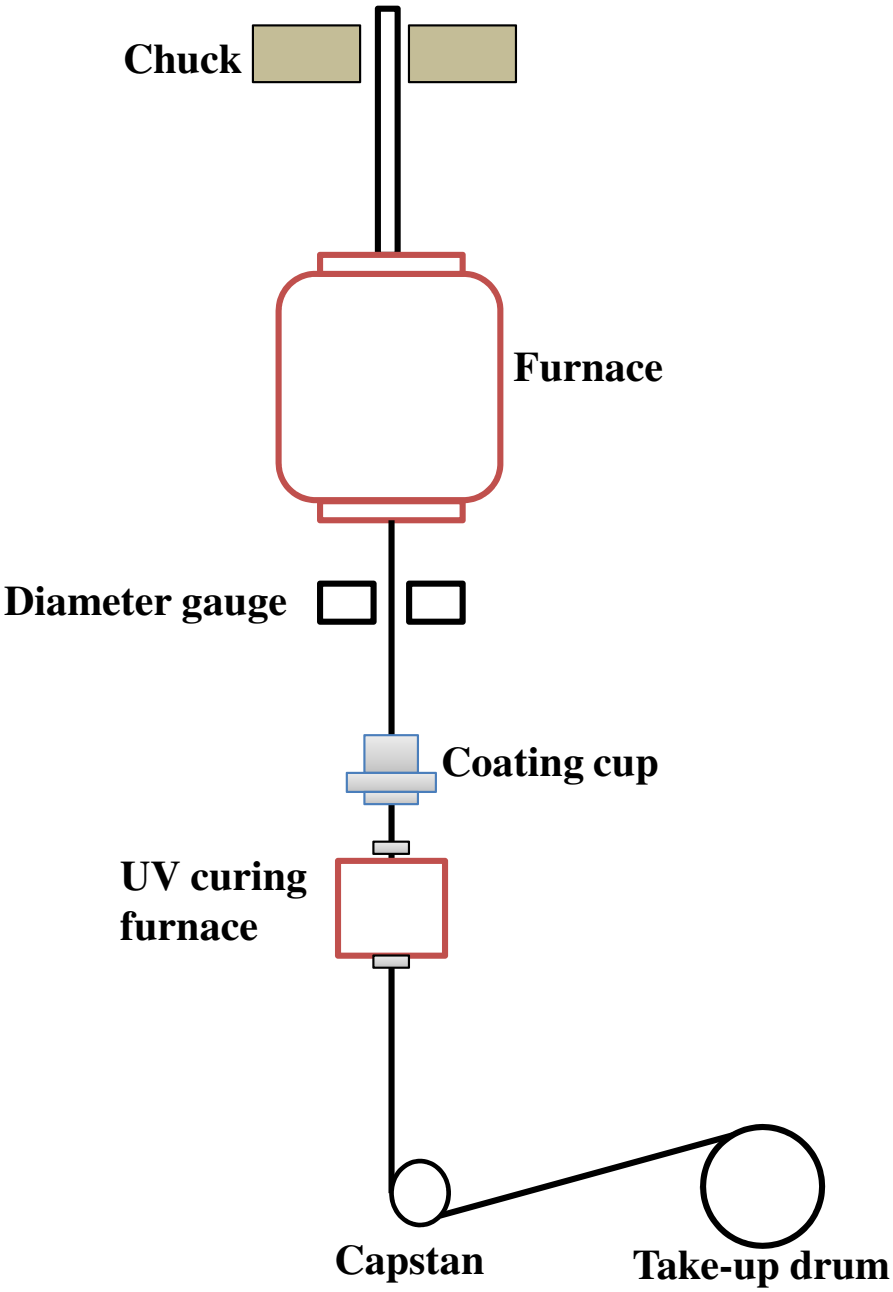

FIGURE 2.3: Schematic diagram of the fibre drawing tower.

A laser diameter gauge, situated bellow the furnace, is used to monitor the fibre diameter which delivers feedback to control the capstan speed as necessary to maintain the desired fibre diameter. Then, the fibre enters a coating cup in the polymer coating assembly, which contains a viscous acrylate fluid. The coating protects the fibre from environment and also provides optical interface for the guided light. Low index polymer is used to fabricate double clad fibres. The coating material is subsequently cured in a UV furnace where the coating is solidified. The typical coating diameter of the fibres used here are $\sim$250 μm with fibre diameter of 125 μm. Generally two types of coating methods are used namely gravity fed coating and pressurised coating. The fibre then passes round the capstan, which provides the force to draw the fibre and is then wrapped onto a take-up drum. In addition to drawing fibres, the fibre tower can be used to draw canes as well.

2.3 Luminescence properties of Bi-doped glasses and fibres

2.3.1 Bi-doped glasses

Visible luminescence from Bi-doped crystals and glasses are well known and have been investigated previously [9–18]. In fact, laser action in Bi atoms and molecules in a gas phase as an active medium, was demonstrated in the visible and infrared region [19–21]. Recently, Fujimata and Nakatsuka reported infrared luminescence from Bi-doped alumino-silicate glass fabricated by the melting-quenching technique [22] and also demonstrated optical amplification at 1300 nm when excited at 800 nm [23]. Peng et. al [24] demonstrated broad infrared luminescence from Bi-doped germanate glass prepared by conventional melting-quenching technique. Absorption peaks at 500, 700, 800 and 1000 nm were observed while emission at

1300 nm with a full width half maximum (FWHM) of 320 nm when excited at 808 nm, was also observed. It was suggested that Al was necessary for Bi luminescence. Bi-doped barium-aluminium-borate glasses were also fabricated by the same group and absorption peaks at 300, 500, 700 and 800 nm were observed while emission shifts from 1252 to 1300 nm depending on BaO concentration [25]. Subsequently, Bi-doped alumino-phosphate glasses have also been developed and investigated [26]. It was observed that in alumino-phosphate hosts, the photoluminescence peak is red shifted about 50 nm in comparison to silica host. Peng et. al also studied the Li_2O-Al_2O_3-ZnO-SiO_2 glass co-doped with Bi_2O_3 and suggested that the luminescent properties of Bi-doped glass depends on the glass compositions [27]. In another report, Bi and Ta co-doped germanium oxide glasses were studied, where the Bi luminescence at 1300 nm was attributed to Bi clusters [28]. Peng et al. also investigated infrared luminescence from Bi-doped zinc aluminosilicate glasses and glass-ceramics and reported decreased luminescence with increasing heat treatment for crystallisation [29]. Apart from this, the optical properties of a variety of Bi-doped glasses including silicate [30–34], germanate [34–37], borate [38, 39] and phosphate [38] have been investigated.

Table 2.1 shows compositions of some selected Bi-doped glasses along with their luminescence properties. The glasses were prepared by conventional melting-quenching technique. The typical Bi absorption peaks at 500, 700 and 800 nm were observed in almost all glasses and most luminescence measurements were carried out with excitation at these bands. In some report, co-doping with Al considerably enhances the efficiency of infrared emission. It was thought that Al acts to disperse the Bi ions, also observed in Al co-doped rare earth ions in a glass, and prevent clustering [29].

After analysing the spectroscopic properties of the Bi-doped glasses in table 2.1, it can be concluded that the luminescence position and bandwidth depends mainly

Composition (mol%)	λ_p (nm)	λ_e (nm)	FWHM (nm)	τ (μs)	Reference
97.5 SiO_2:2.2 Al_2O_3:0.3 Bi_2O_3	500	750	140	3.62	[22]
		1140	220	630	
	700	1122	160	∼700	
	800	1250	300	—	
75 SiO_2:10 Li_2O:14 Al_2O_3:1 Bi_2O_3	808	1265	318	456	[40]
75 SiO_2:10 Li_2O:14 Ta_2O_5:1 Bi_2O_3	808	1300	268	420	
75 SiO_2:10 Na_2O:10 Al_2O_3:1 Bi_2O_3	808	1310	360	489	
65 SiO_2:30 SrO:5 Al_2O_3:2 Bi_2O_3	808	1300	200	400	[30]
65 SiO_2:30 BaO:5 Al_2O_3:2 Bi_2O_3	808	1305	—	—	
65 SiO_2:30 CaO:5 Al_2O_3:2 Bi_2O_3	808	1325	—	—	
94.5 GeO_2:5 Al_2O_3:0.5 Bi_2O_3	532	1247	295	—	[35]
	632	1263	281	—	
	808	1300	320	—	
96 GeO_2:3 Ta_2O_5:0.5 Bi_2O_3	808	1310	402	243	[28]
75 GeO_2:20 MgO:5 Al_2O_3:1 Bi_2O_3	808	1290	330	—	[36]
	980	1150	315	264	
75 GeO_2:20 CaO:5 Al_2O_3:1 Bi_2O_3	808	1290	300	—	
	980	1150	440	157	
75 GeO_2:20 SrO:5 Al_2O_3:1 Bi_2O_3	808	1290	225	—	
	980	1150	510	1725	
87.4 GeO_2:6 PbO:6 Al_2O_3:0.6 Bi_2O_3	808	1230	291	378	[37]
75 B_2O_3:20 BaO:5 Al_2O_3:2 Bi_2O_3	532	1148	244	—	[25]
	808	1272	230	370	
82 P_2O_5:17 Al_2O_3:1 Bi_2O_3	405	1210	235	—	[26]
	514	1173	207	—	
	808	1300	300	500	
	980	1194	—	—	
59 P_2O_5:12 B_2O_3:5 La_2O_3	530	690	100	4	[38]
:17 Li_2O:6 Al_2O_3:1 Bi_2O_3		1150	—	—	
	800	1270	290	220	
	980	1125	—	290	

TABLE 2.1: Optical properties of Bi-doped glasses

on the excitation wavelength and also on the glass composition. Absorption peaks at 500, 700, and 800 nm was observed while a weaker and less defined peaks at 1000 nm was also observed in germanate glasses. The near-infrared emission can be excited by pumping into any of these absorption bands. The lifetime of the near infrared emission was as long as 1725 μs [36] and also the luminescence was very broad (up to 500 nm) [36]. In most cases the infrared luminescence was observed if the glass contains Al or Ta.

2.3.2 Bi-doped fibre lasers and amplifiers

In 2005, Dvoyrin et al. first reported the fabrication and spectroscopic characterisation of Bi-doped fibres by the modified chemical vapour deposition (MCVD) and solution doping technique [41, 42]. Absorption bands around 500, 700, 800 and 1000 nm, while luminescence at 750 and 1050-1200 nm band, with 676 nm excitation were observed in the Bi-doped fibres. With 1000 nm excitation, only one luminescence band at 1200 nm was observed, which shifts to longer wavelength with increasing germanium content in the core. The fluorescence lifetime was reported to be around 1 ms. Subsequently, realisation of Bi-doped fibre laser in the range of 1.15 - 1.21 μm was reported, when pumped at 1.06 μm, but the slope efficiency achieved was not more than 10% at 1146 nm [43]. An increase in the efficiency up to 21%, in the high pump power region, was also reported; however an 80 m long fibre was required for the laser experiments due to its low pump absorption of 0.3 dB/m [44]. The maximum output power was 15 W at 1160 nm, when pumped at 1070 nm in a 100%-50% laser cavity. The presence of unsaturable loss at the pump wavelength was suggested as the reason for the lower efficiency in the Bi-doped fibre laser. The output power was limited by Raman Stokes generation at a pump power higher than 60 W. The Bi-doped fibre laser was also used to generate yellow light, but the efficiency was as low as 2.5%. Another experiment

on a Bi-doped fibre laser, which utilized a similarly low Bi concentration fibre, also used an 80 m long Bi-doped fibre [45]. It was observed that the the luminescence spectra of Bi-doped preforms and fibres were essentially different, where the preform luminescence is comparable to the already mentioned Bi-doped glass samples (Table 2.1). It was suggested that, oxygen reducing atmosphere during preform drawing can modify the valency state of Bi, leading to different luminescence properties in fibre and preform [45]. An average power of 125 mW at 589 nm with frequency doubling was also achieved using the same fibre [46]. Up to date, the maximum laser efficiency achieved is 32%, when water cooled (20^{o}C), using 55 m long fibre [47].

At the same time, pulsed Bi-doped fibre laser was demonstrated, among them Q-switched Yb-Bi fibre laser [48] and mode-locked Bi-doped fibre laser [49, 50]. Eventually, laser generation at the longer wavelength was also achieved in Bi-doped fibres. In ref. [51], lasing in the wavelength band of 1442-1460 nm, in an alumino-silicate fibre at -30^{o}C, with 1343-1356 nm excitation was reported but the efficiency was estimated to be less than 0.1%. Using alumina free phospho-germano-silicate fibre, laser emission in the wavelength band of 1300-1470 nm, with a slope efficiency of 1-3% was achieved, by pumping at 1205-1230 nm [52, 53]. Using a laser cavity of 100%-90%, Bi laser action in the wavelength band of 1470-1500 nm, was also realised using similar fibre [54]. The maximum slope efficiency achieved was 4.2%, at 1500 nm. In the same report, laser generation from a germano-silicate fibre was also reported, with an efficiency up-to 3%, at 1500 nm. It is worth noting here that fluorescence at 1425 nm was also observed in an alumina free Bi-doped silica fibre fabricated with granulated oxides, but the fibre was badly guiding due to slight difference in refractive index between the core and the cladding [55]. Broad luminescence at 1450 nm was also achieved with 808 nm pumping, in a germano-silicate Bi-doped fibre [56]

After analysing the Bi-doped fibre lasers reported so far, the maximum laser efficiency achieved is 32%, using 55 m long fibre. For reasons such as background loss and nonlinearities, shorter fibres are generally preferred, but it appears that low Bi concentration has prevented progress towards shorter fibres. Indeed, 0.005% of Bi by wt. was set as an upper limit for Bi laser action [46]. There are possibly two challenges in increasing the Bi concentration. First, the desired infrared luminescence is only achievable when the Bi ions sit in proper sites [22]. Hence, increasing the Bi concentration beyond what the number of appropriate sites permit may cause unsaturable absorption or, at best, have no effect. Secondly, as the lasing wavelength is located in the tail of the pump absorption band, high Bi concentration gives rise to additional signal loss like an unsaturable loss. Depending on the excited-state lifetime, this can lead to high thresholds in long devices of high Bi concentration. Despite these challenges, it is imperative to develop efficient, high Bi concentration, fibre for short fibre laser operation and avoid any unwanted nonlinear effects for cladding pumped Bi-doped fibre laser.

Compared to Bi-doped fibre lasers, there has not been many report on Bi-doped fibre amplifiers. Optical pump on-off gain in Bi-doped glass was first reported in 2003 [23]. After that amplification was observed in various bulk glasses [57–59] and also in Bi-doped fibres [60, 61]. In 2007, a 10.6 dB small signal optical gain at 1300 nm, with 810 nm excitation, in a Bi-doped fibre, fabricated by the rod in tube method, has been reported [61]. Also, in other Bi fibres fabricated by the chemical vapor deposition processes, 10 dB on-off gain at 1120 nm [62] and 5-13 dB gain in the 1100-1300 nm range [52] have been observed. On-off gain in the wavelength band of 1240-1485 nm, was also reported in a phospho-germano-silicate fibre with pumping at 1205, 1230 and 808 nm [53]. Positive net gain at 1430-1495 nm wavelengths by pumping the fibre at 1343 nm was also observed [51]. To date, investigations of the gain characteristics of Bi-doped fibre amplifiers have

focused on the small input signal regime, but in the full dynamic range, particularly for high seed power, has not been studied. However, Bi-doped fibre amplifiers behaviour in the high signal power regime is important for applications as power amplifiers.

2.3.3 Origin of Bi luminescence

The actual nature of the Bi luminescent centre is still controversial and has been attributed to the electronic transition of Bi^{5+} [22, 42], $\{[AlO_{4/2}]^{-}, Bi^{+}\}$ [41], Bi^{+} [25, 26, 42, 56, 63], Bi^{2+} [64], Bi_2^{-}, Bi_2^{2-}, Bi_2/Bi_2^{-} [65, 66], BiO_4 [67] or even Bi clusters [28].

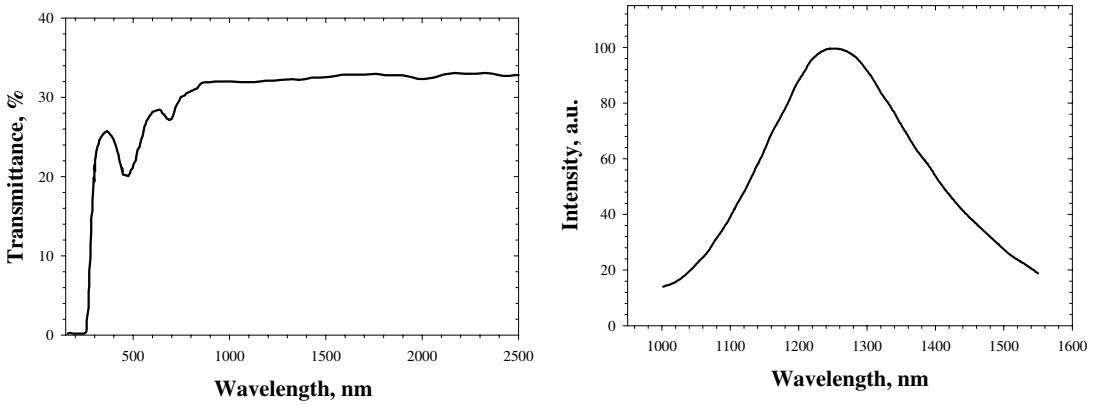

(a) (b)

FIGURE 2.4: (a) Transmission spectrum and (b) luminescence spectrum at 800 nm excitation of Bi-doped silica glass [22].

Fujimoto and Nakatsuka suggested Bi^{5+} as the Bi luminescent centre, with absorption and emission occurring between the ground state $^1S_0$ and the excited states $^3D_{3,2,1}$ and $^1D_2$. Absorption peaks at 500, 700 and 800 nm were observed with corresponding emission peaks at 750, 1120 and 1250 nm. Fig. 2.4 shows the transmittance and emission spectrum at 800 nm excitation of such Bi-doped silica glass [22]. However, based on the optical basicity theory proposed by Duffy [68],

the observed variation of emission quenching with host acidity suggested to other researchers that the Bi luminescent centre is a low valence state such as Bi^{+} or a Bi cluster [25]. But at the same time, a model based on a single Bi^{+} centre failed to explain the unusual variation of the near infrared emission spectrum of Bi with pump wavelengths. It has been observed in many studies that the Bi emission is red-shifted when pumping at 800 nm, compared to when pumping at 500, 700 or 1000 nm [22, 26, 35]. This suggests the existence of two distinct sites in the glass for the Bi luminescent centre with different energy separations between the ground state and the first excited state. This two-site model was also used by Hughes et al. to explain the different emission spectrum and lifetime properties as a function of PbO content in a Bi-doped lead-germanate glass, when excited at 800 nm [69]. Further evidence for the two-site model was obtained by studying the effect of thermal processing in Bi-doped fibre and preform [45, 63]. It was observed that the 1300 nm emission from Bi was present in the preform, but was either absent or diminished in the corresponding fibre. It was suggested that the luminescent centre responsible for the long wavelength generation is thermally unstable compared to the one responsible for 1150 nm emission.

Another model that has been proposed is the dual-valency model, in which the Bi luminescence is ascribed to the low valency state such as Bi^{+} and Bi^{2+} ions [70]. Recently, models based on more complex optical centers have received attention, such as Bi_2^{-}, Bi_2^{2-}, Bi_2/Bi_2^{-} dimers [65, 66] and BiO molecular orbital [67]. In the molecular orbital model, it was found that the wavelength and lifetime of the infrared emission depend mostly on the wave-functions of the oxygen tetrahedron, and only weakly on the metal ion. This model was further supported by the optically detected magnetic resonance measurements, which reveal two distinct and low values of the g factor associated with the near infrared emission in the region of 1100-1300 nm [71]. The energy level scheme that results from the molecular

orbital calculations consists of singlet and triplet states. Strong absorption occurs on the allowed transitions from the ground state to higher singlet states, and this is followed by non-radiative cross-over to the triplet states. The triplet states are metastable due to the spin selection rule, and emit light in the visible and near infrared with a long radiative lifetime.

In another report, the search for Bi luminescent centre was extended to point defects and localized states in glasses [72]. Colour centres related to the point defects in glasses (oxygen vacancies, non-bridging oxygen hole centres, oxygen deficient centres, unterminated bonds) might be formed under heat treatment at high temperature [73].

The issue of the origin of broadband near infrared luminescence in Bi-doped glass is far from settled, and further fundamental researches are necessary to fully understand the mechanism behind Bi luminescence.

2.4 Yb-doped fibre laser at longer wavelengths

Yb-doped silica fibre is an extremely successful gain medium that operates efficiently in the wavelength region of 1030-1100 nm, with excellent beam quality and multi kilowatt of output power level [74–76]. These outstanding properties can be attributed to several attractive features of Yb^{3+} ions, such as broad absorption band for pumping, small quantum defect between pump and emission wavelengths and sufficiently long metastable lifetime. As a result, it finds many applications such as material processing, marking, medicine, spectroscopy etc. to name a few.

Substantial attention has been paid in the field of development of Yb-doped fibre laser to increase the output power. On the other hand, there was not much

report on the spectral properties of Yb-doped fibre, in particular to extend the spectral range towards longer wavelengths. In ref. [77] an Yb-doped silica fibre laser had been tuned from 1020 to 1140 nm with possibility of extending the lasing wavelengths to increase the number of applications that can be achieved with such a fibre laser. Different approaches have been proposed to operate Yb-doped fibre lasers in the long wavelength (1120-1180 nm) range [47, 78–84]. Using conventional Yb-doped alumino-silicate fibre, an output of 121 mW at 1150 nm was achieved with a slope efficiency of 21%, by pumping at 977 nm [78]. By employing a high-Q resonator design in conjunction with a double clad Yb-doped fibre, up to 6.5 W output at 1178 nm was also obtained [79]. Another approach includes core pumping of a Yb-doped fibre at 1070 nm with simultaneous heating of the fibre above 70^{o}C to improve the absorption cross-section [80]. The maximum slope efficiency, with respect to pump power was 45% at 1160 nm, with a maximum output power of 3.3 W. However, the low emission cross-section at these wavelengths and the gain competition from shorter wavelengths lead to the generation of amplified spontaneous emission (ASE) and parasitic lasing at high pump power, limiting the utilisable gain and power scaling, making the operation a challenging work. Other alternatives have been proposed to overcome those issues, such as cladding pumped Yb-doped all-solid photonic bandgap fibres for suppression of ASE at 1030 nm [82]. Also, by using the spectral filtering properties of photonic bandgap fibres, with a Raman fibre laser seeded master oscillator power amplifier (MOPA) configuration, 32 W output at 1156 nm and 30 W output at 1178 nm has been realised [83]. Power scaling in those fibre was limited by onset of parasitic lasing at the short wavelength region and with modification in fabrication process an output power of 167 W has been reported recently [85]. However, complex system structure and therefore difficult fabrication conditions with the additional possibility of photodarkening, when pumped at 915-976 nm; make such a laser impractical for industrial use. In another work, Goto et al. in ref. [84] reported a narrow

linewidth Yb-doped hybrid micro-structured fibre, which offers better cladding pumping efficiency than a standard photonic bandgap fibre; but the output power was limited due to high loss present in the fibre.

References

[1] P. Schultz, "Fabrication of optical waveguides by the outside vapor deposition process," *Proceedings of the IEEE* **68**(10), pp. 1187–1190, 1980.

[2] T. Izawa, T. Miyashita, and F. Hanawa, "Continuous optical fiber perform fabrication method," *U. S. Patent* **4062665**, 1977.

[3] S. Nagel, J. B. MaChesney, and K. Walker, "An overview of the modified chemical vapour deposition process and performance," *IEEE Journal of Quantum Electronics* **18**, pp. 459–477, 1982.

[4] K. L. Walker, F. T. Geyling, and S. R. Nagel, "Thermophoretic deposition of small particles in the modified chemical vapour deposition (MCVD) process," *Journal of the American Ceramic Society* **63**, pp. 552–558, 1980.

[5] J. E. Townsend, S. B. Poole, and D. N. Payne, "Solution-doping technique for fabrication of rare-earth-doped optical fibers," *Electronics Letters* **23**(7), pp. 329–331, 1987.

[6] D. Wood, K. Walker, J. MacChesney, J. Simpson, and R. Csencsits, "Germanium chemistry in the MCVD process for optical fiber fabrication," *Journal of Lightwave Technology* **5**(2), pp. 277 – 285, 1987.

[7] T. Li, *Rare Earth Doped Fiber Lasers and Amplifiers*. Academic Press Inc., 1985.

[8] J. B. MacChesney and D. J. DiGiovanni, "Materials development of optical fiber," *Journal of the American Ceramic Society* **73**, p. 35373556, 1990.

[9] G. Blasse and A. Bril, "Investigations on Bi^{3+}-activated phosphors," *Journal of Chemical Physics* **48**(1), pp. 217–222, 1968.

[10] R. B. Lauer, "Photoluminescence in $Bi_{12}SiO_{20}$ and $Bi_{12}GeO_{20}$," *Applied Physics Letters* **17**(4), pp. 178–179, 1970.

[11] G. Blasse, "The ultraviolet absorption bands of Bi^{3+} and Eu^{3+} in oxides," *Journal of Solid State Chemistry* **4**(1), pp. 52 – 54, 1972.

[12] M. J. Weber and R. R. Monchamp, "Luminescence of Bi_4 Ge_3O_{12} : Spectral and decay properties," *Journal of Applied Physics* **44**(12), pp. 5495–5499, 1973.

[13] F. Kellendonk, T. van den Belt, and G. Blasse, "On the luminescence of bismuth, cerium, and chromium and yttrium aluminium borate," *Journal of Chemical Physics* **76**(3), pp. 1194–1201, 1982.

[14] R. Retoux, F. Studer, C. Michel, B. Raveau, A. Fontaine, and E. Dartyge, "Valence state for bismuth in the superconducting bismuth cuprates," *Phys. Rev. B* **41**(1), pp. 193–199, 1990.

[15] G. Blasse, A. Meijerink, M. Nomes, and J. Zuidema, "Unusual bismuth luminescence in strontium tetraborate (SrB_4O_7:Bi)," *Journal of Physics and Chemistry of Solids* **55**(2), pp. 171–174, 1994.

[16] M. A. Hamstra, H. F. Folkerts, and G. Blasse, "Red bismuth emission in alkaline-earth-metal sulfates," *Journal of Materials Chemistry* **4**(8), pp. 1349–1350, 1994.

[17] A. M. Srivastava, "Luminescence of divalent bismuth in M^{2+} BPO_5 (M^{2+} =Ba^{2+}, Sr^{2+} and Ca^{2+})," *Journal of Luminescence* **78**(4), pp. 239 – 243, 1998.

[18] S. Parke and R. S. Webb, "The optical properties of thallium, lead and bismuth in oxide glasses," *Journal of Physics and Chemistry of Solids* **34**(1), pp. 85 – 95, 1973.

[19] M. S. Chou and T. A. Cool, "Laser operation by dissociation of metal complexes: New transitions in As, Bi, Ga, Ge, Hg, In, Pb, Sb, and Tl," *Journal of Applied Physics* **47**(3), pp. 1055–1061, 1976.

[20] S. Drosch and G. Gerber, "Optically pumped cw molecular bismuth laser," *Journal of Chemical Physics* **77**(1), pp. 123–130, 1982.

[21] X. H. Zhu and J. B. Liu, "A hollow cathode bismuth ion laser," *Applied Physics B* **29**(4), pp. 291 –292, 1982.

[22] Y. Fujimoto and M. Nakatsuka, "Infrared luminescence from bismuth-doped silica glass," *Japanese Journal of Applied Physics* **40**(3B), pp. L279–L281, 2001.

[23] Y. Fujimoto and M. Nakatsuka, "Optical amplification in bismuth-doped silica glass," *Applied Physics Letters* **82**(19), pp. 3325–3326, 2003.

[24] M. Y. Peng, J. R. Qiu, D. P. Chen, X. G. Meng, I. Y. Yang, X. W. Jiang, and C. S. Zhu, "Bismuth- and aluminum-codoped germanium oxide glasses for super-broadband optical amplification," *Optics Letters* **29**(17), pp. 1998–2000, 2004.

[25] X. G. Meng, J. R. Qiu, M. Y. Peng, D. P. Chen, Q. Z. Zhao, X. W. Jiang, and C. S. Zhu, "Infrared broadband emission of bismuth-doped barium-aluminum-borate glasses," *Optics Express* **13**(5), pp. 1635–1642, 2005.

[26] X. G. Meng, J. R. Qiu, M. Y. Peng, D. P. Chen, Q. Z. Zhao, X. W. Jiang, and C. S. Zhu, "Near infrared broadband emission of bismuth-doped aluminophosphate glass," *Optics Express* **13**(5), pp. 1628–1634, 2005.

[27] M. Y. Peng, J. R. Qiu, D. P. Chen, X. G. Meng, and C. S. Zhu, "Broadband infrared luminescence from Li_2O-Al_2O_3-Z nO-SiO_2 glasses doped with Bi_2O_3," *Optics Express* **13**(18), pp. 6892–6898, 2005.

[28] M. Peng, J. Qiu, D. Chen, X. Meng, and C. Zhu, "Superbroadband 1310 nm emission from bismuth and tantalum codoped germanium oxide glasses," *Optics Letter* **30**(18), pp. 2433–2435, 2005.

[29] M. Y. Peng, D. P. Chen, J. R. Qiu, X. W. Jiang, and C. S. Zhu, "Bismuth-doped zinc aluminosilicate glasses and glass-ceramics with ultra-broadband infrared luminescence," *Optical Materials* **29**(5), pp. 556–561, 2007.

[30] J. J. Ren, L. Y. Yang, J. R. Qiu, D. P. Chen, X. W. Jiang, and C. S. Zhu, "Effect of various alkaline-earth metal oxides on the broadband infrared luminescence from bismuth-doped silicate glasses," *Solid State Communications* **140**(1), pp. 38–41, 2006.

[31] T. Suzuki and Y. Ohishi, "Ultrabroadband near-infrared emission from Bi-doped Li_2O–Al_2O_3–SiO_2 glass," *Applied Physics Letters* **88**(19), pp. 191912–3, 2006.

[32] J. J. Ren, H. F. Dong, H. P. Zeng, X. Hu, C. S. Zhu, and J. R. Qiu, "Ultrabroadband infrared luminescence and optical amplification in bismuth-doped germanosilicate glass," IEEE *Photonics Technology Letters* **19**, pp. 1395–1397, 2007.

[33] Y. Fujimoto, Y. Hirata, Y. Kuwada, T. Sato, and M. Nakatsuka, "Effect of GeO_2 additive on fluorescence intensity enhancement in bismuth-doped silica glass," *Journal of Materials Research* **22**(3), pp. 565–568, 2007.

[34] S. Zhou, H. Dong, H. Zeng, G. Feng, H. Yang, B. Zhu, and J. Qiu, "Broadband optical amplification in Bi-doped germanium silicate glass," *Applied Physics Letters* **91**(6), pp. 061919 –061919–3, 2007.

[35] M. Y. Peng, C. Wang, D. P. Chen, J. R. Qiu, X. W. Jiang, and C. S. Zhu, "Investigations on bismuth and aluminum co-doped germanium oxide glasses for ultra-broadband optical amplification," *Journal of Non-Crystalline Solids* **351**(30-32), pp. 2388–2393, 2005.

[36] J. J. Ren, J. R. Qiu, B. T. Wu, and D. P. Chen, "Ultrabroad infrared luminescences from Bi-doped alkaline earth metal germanate glasses," *Journal of Materials Research* **22**(6), pp. 1574–1578, 2007.

[37] M. Hughes, T. Suzuki, and Y. Ohishi, "Towards a high-performance optical gain medium based on bismuth and aluminum co-doped germanate glass," *Journal of Non-Crystalline Solids* **356**(6-8), pp. 407 – 418, 2010.

[38] B. Denker, B. Galagan, V. Osiko, S. Sverchkov, and E. Dianov, "Luminescent properties of Bi-doped boro-alumino-phosphate glasses," *Applied Physics B* **87**(1), pp. 135–137, 2007.

[39] T. Murata and T. Mouri, "Matrix effect on absorption and infrared fluorescence properties of Bi ions in oxide glasses," *Journal of Non-Crystalline Solids* **353**, pp. 2403–2407, 2007.

[40] M. Y. Peng, B. T. Wu, N. Da, C. Wang, D. P. Chen, C. S. Zhu, and J. R. Qiu, "Bismuth-activated luminescent materials for broadband optical amplifier in WDM system," *Journal of Non-Crystalline Solids* **354**(12-13), pp. 1221–1225, 2008.

[41] V. V. Dvoyrin, V. M. Mashinsky, E. M. Dianov, A. A. Umnikov, M. V. Yashkov, and A. N. Guryanov, "Absorption, fluorescence and optical amplification in MCVD bismuth-doped silica glass optical fibres," *31st European Conference on Optical Communication, (*ECOC *2005)* , pp. 949–50, 2005.

[42] V. V. Dvoyrin, V. M. Mashinsky, L. I. Bulatov, I. A. Bufetov, A. V. Shubin, M. A. Melkumov, E. F. Kustov, E. M. Dianov, A. A. Umnikov, V. F. Khopin, M. V. Yashkov, and A. N. Guryanov, "Bismuth-doped-glass optical fibers - a new active medium for lasers and amplifiers," *Optics Letters* **31**(20), pp. 2966–2968, 2006.

[43] E. M. Dianov, V. V. Dvoyrin, V. M. Mashinsky, A. A. Umnikov, M. V. Yashkov, and A. N. Gur'yanov, "CW bismuth fibre laser," *Quantum Electronics* **35**(12), pp. 1083–1084, 2005.

[44] E. M. Dianov, A. V. Shubin, M. A. Melkumov, O. I. Medvedkov, and I. A. Bufetov, "High-power cw bismuth-fiber lasers," *Journal of the Optical Society of America B* **24**, pp. 1749–1755, 2007.

[45] I. Razdobreev, L. Bigot, V. Pureur, A. Favre, G. Bouwmans, and M. Douay, "Efficient all-fiber bismuth-doped laser," *Applied Physics Letters* **90**(3), pp. 31103–1–3, 2007.

[46] A. B. Rulkov, A. A. Ferin, S. V. Popov, J. R. Taylor, I. Razdobreev, L. Bigot, and G. Bouwmans, "Narrow-line, 1178 nm CW bismuth-doped fiber laser with 6.4 W output for direct frequency doubling," *Optics Express* , pp. 408–11, 2007.

[47] V. V. Dvoyrin, V. M. Mashinsky, and E. M. Dianov, "Efficient bismuth-doped fiber lasers," IEEE *Journal of Quantum Electronics* **44**(9-10), pp. 834–840, 2008.

[48] V. V. Dvoyrin, V. M. Mashinsky, and E. M. Dianov, "Yb-Bi pulsed fiber lasers," *Optics Letters* **32**(5), pp. 451–453, 2007.

[49] E. M. Dianov, A. A. Krylov, V. V. Dvoyrin, V. M. Mashinsky, P. G. Kryukov, O. G. Okhotnikov, and M. Guina, "Mode-locked Bi-doped fiber laser," *Journal of the Optical Society of America B* **24**, pp. 1807–1808, 2007.

[50] S. Kivisto, J. Puustinen, M. Guina, O. G. Okhotnikov, and E. M. Dianov, "Tunable modelocked bismuth-doped soliton fibre laser," *Electronics Letters* **44**(25), pp. 1456–U119, 2008.

[51] V. V. Dvoyrin, O. I. Medvedkov, V. M. Mashinsky, A. A. Umnikov, A. N. Guryanov, and E. M. Dianov, "Optical amplification in 1430-1495 nm range

and laser action in Bi-doped fibers," *Optics Express* **16**(21), pp. 16971–16976, 2008.

[52] E. M. Dianov, S. V. Firstov, V. F. Khopin, A. N. Guryanov, and I. A. Bufetov, "Bi-doped fibre lasers and amplifiers emitting in a spectral region of 1.3 μm," *Quantum Electronics* **38**(7), pp. 615–617, 2008.

[53] I. A. Bufetov, S. V. Firstov, V. E. Khopin, O. I. Medvedkov, A. N. Guryanov, and E. M. Dianov, "Bi-doped fiber lasers and amplifiers for a spectral region of 1300-1470 nm," *Optics Letters* **33**(19), pp. 2227–2229, 2008.

[54] E. M. Dianov, S. V. Firstov, V. F. Khopin, O. I. Medvedkov, A. N. Guryanov, and I. A. Bufetov, "Bi-doped fibre lasers operating in the range 1470-1550 nm," *Quantum Electronics* **39**(4), pp. 299–301, 2009.

[55] M. Neff, V. Romano, and W. Lüthy, "Metal-doped fibres for broadband emission: Fabrication with granulated oxides," *Optical Materials* **31**(2), pp. 247 – 251, 2008.

[56] Y. Qiu and Y. Shen, "Investigation on the spectral characteristics of bismuth doped silica fibers," *Optical Materials* **31**(2), pp. 223 – 228, 2008.

[57] Y. S. Seo, Y. Fujimoto, and M. Nakatsuka, "Amplification in a bismuth-doped silica glass at second telecommunication windows," *Conference on Lasers and Electro-Optics/Quantum Electronics and Laser Science and Photonic Applications Systems Technologies* , pp. 1858–1860, 2005. Technical Digest (CD) (Optical Society of America, 2005), paper CThR6.

[58] Y. S. Seo, Y. Fujimoto, and M. Nakatsuka, "Optical amplification in a bismuth-doped silica glass at 1300 nm telecommunications window," *Optics Communications* **266**(1), pp. 169–171, 2006.

[59] J. J. Ren, Y. B. Qiao, C. S. Zhu, X. W. Jiang, and J. R. Qiu, "Optical amplification near 1300 nm in bismuth-doped strontium germanate glass," *Journal of the Optical Society of America B-Optical Physics* **24**, pp. 2597–2600, 2007.

[60] Y. S. Seo, C. Lim, Y. Fujimoto, and M. Nakatsuka, "9.6 db, gain at a 1310 nm wavelength for a bismuth-doped fiber amplifier," *Journal of the Optical Society of Korea* **11**(2), pp. 63–66, 2007.

[61] Y. S. Seo, R. Sasahara, Y. Fujimoto, C. Lim, S. K. Hong, and M. Nakatsuka, "10.6 db gain at a 1310 nm wavelength for a bismuth-doped silica fiber amplifier," *Conference on Lasers and Electro-Optics/Pacific Rim 2007* , 2007. (Optical Society of America, 2007), paper FE2_2.

[62] I. A. Bufetov, K. M. Golant, S. V. Firstov, A. V. Kholodkov, A. V. Shubin, and E. M. Dianov, "Bismuth activated alumosilicate optical fibers fabricated by surface-plasma chemical vapor deposition technology," *Applied Optics* **47**(27), pp. 4940–4944, 2008.

[63] V. G. Truong, L. Bigot, A. Lerouge, M. Douay, and I. Razdobreev, "Study of thermal stability and luminescence quenching properties of bismuth-doped silicate glasses for fiber laser applications," *Applied Physics Letters* **92**(4), 2008.

[64] J. J. Ren, J. R. Qiu, D. P. Chen, X. Hu, X. W. Jiang, and C. S. Zhu, "Ultrabroad infrared luminescence from Bi-doped aluminogermanate glasses," *Solid State Communications* **141**(10), pp. 559–562, 2007.

[65] S. Khonthon, S. Morimoto, Y. Arai, and Y. Ohishi, "Luminescence characteristics of Te- and Bi-doped glasses and glass-ceramics," *Journal of the Ceramic Society of Japan* **115**(1340), pp. 259–263, 2007.

[66] V. O. Sokolov, V. G. Plotnichenko, and E. M. Dianov, "Origin of broadband near-infrared luminescence in bismuth-doped glasses," *Optics Letters* **33**(13), pp. 1488–1490, 2008.

[67] E. F. Kustov, L. I. Bulatov, V. V. Dvoyrin, and V. M. Mashinsky, "Molecular orbital model of optical centers in bismuth-doped glasses," *Optics Letters* **34**(10), pp. 1549–1551, 2009.

[68] J. Duffy, "Redox equilibria in glass," *Journal of Non-Crystalline Solids* **196**, pp. 45 – 50, 1996.

[69] M. Hughes, T. Suzuki, and Y. Ohishi, "Advanced bismuth-doped lead-germanate glass for broadband optical gain devices," *Journal of Optical Society of America B* **25**(8), pp. 1380–1386, 2008.

[70] J. J. Ren, G. P. Dong, S. Q. Xu, R. Q. Bao, and J. R. Qiu, "Inhomogeneous broadening, luminescence origin and optical amplification in bismuth-doped glass," *Journal of Physical Chemistry A* **112**(14), pp. 3036–3039, 2008.

[71] I. Razdobreev, V. Y. Ivanov, L. Bigot, M. Godlewski, and E. F. Kustov, "Optically detected magnetic resonance in bismuth-doped silica glass," *Optics Letters* **34**(17), pp. 2691–2693, 2009.

[72] M. Y. Sharonov, A. B. Bykov, V. Petricevic, and R. R. Alfano, "Spectroscopic study of optical centers formed in Bi-, Pb-, Sb-, Sn-, Te-, and In- doped germanate glasses," *Optics Letters* **33**(18), pp. 2131–2133, 2008.

[73] G. Li, M. Nogami, and Y. Abe, "Defect formation and evolution in Teo_2-containing borosilicate glass films derived from a sol-gel process," *Physical Review B* **51**(21), pp. 14930–14935, 1995.

[74] Y. Jeong, J. K. Sahu, D. N. Payne, and J. Nilsson, "Ytterbium-doped large-core fiber laser with 1.36 kW continuous-wave output power," *Optics Express* **12**(25), pp. 6088–6092, 2004.

[75] A. T*ü*nnermann, T. Schreiber, F. R*ö*ser, A. Liem, S. H*ö*fer, H. Zellmer, S. Nolte, and J. Limpert, "The renaissance and bright future of fibre lasers," *Journal of Physics B: Atomic, Molecular and Optical Physics* **38**(9), p. S681, 2005.

[76] "IPG Photonics." `http://www.ipgphotonics.com`.

[77] H. Pask, R. Carman, D. Hanna, A. Tropper, C. Mackechnie, P. Barber, and J. Dawes, "Ytterbium-doped silica fiber lasers: versatile sources for the 1-1.2 μm region," IEEE *Journal of Selected Topics in Quantum Electronics* **1**(1), pp. 2 –13, 1995.

[78] S. Sinha, C. Langrock, M. J. F. Digonnet, M. M. Fejer, and R. L. Byer, "Efficient yellow-light generation by frequency doubling a narrow-linewidth 1150 nm ytterbium fiber oscillator," *Optics Letters* **31**(3), pp. 347–349, 2006.

[79] J. Ota, A. Shirakawa, and K. Ueda, "High-power Yb-doped double-clad fiber laser directly operating at 1178 nm," *Japanese Journal of Applied Physics* **45**(4-7), pp. L117–L119, 2006.

[80] A. S. Kurkov, V. M. Paramonov, and O. I. Medvedkov, "Ytterbium fiber laser emitting at 1160 nm," *Laser Physics Letters* **3**(10), pp. 503–506, 2006.

[81] A. S. Kurkov, "Oscillation spectral range of Yb-doped fiber lasers," *Laser Physics Letters* **4**(2), pp. 93–102, 2007.

[82] R. Goto, K. Takenaga, K. Okada, M. Kashiwagi, T. Kitabayashi, S. Tanigawa, K. Shima, S. Matsuo, and K. Himeno, "Cladding-pumped Yb-doped solid photonic bandgap fiber for ASE suppression in shorter wavelength region," in *Optical Fiber Communication Conference and Exposition and The National Fiber Optic Engineers Conference*, OSA Technical Digest (CD) (Optical Society of America, 2008), paper OTuJ5.

[83] A. Shirakawa, H. Maruyama, K. Ueda, C. B. Olausson, J. K. Lyngsϕ, and J. Broeng, "High-power Yb-doped photonic bandgap fiber amplifier at 1150-1200 nm," *Optics Express* **17**(2), pp. 447–454, 2009.

[84] R. Goto, E. C. Magi, and S. D. Jackson, "Narrow-linewidth, Yb^{3+}-doped, hybrid microstructured fibre laser operating at 1178 nm," *Electronics Letters* **45**(17), pp. 877–878, 2009.

[85] C. B. Olausson, A. Shirakawa, M. Chen, J. K. Lyngsϕ, J. Broeng, K. P. Hansen, A. Bjarklev, and K. Ueda, "167 W power scalable ytterbium-doped photonic bandgap fiber amplifier at 1178 nm," *Optics Express* **18**(16), pp. 16345–16352, 2010.

Chapter 3

Fabrication of Bi and Yb-doped optical fibres

3.1 Introduction

The purpose of this chapter is to describe briefly the methods used for the fabrication of the Bi and Yb-doped optical fibres used in this work. Efforts in making Bi-doped fibres using the conventional MCVD, along with the novel MCVD chemical-in-crucible deposition and powder-in-tube (PIT) technology are discussed.

The chemical-in-crucible deposition technique, based on the MCVD process, was developed for the high power rare earth doped fibre fabrication and also used for the fabrication of Bi-doped fibres. The PIT technology, which is significantly different from the MCVD process, was applied to study the fabrication dependance of Bi-doped fibre spectroscopy.

3.2 Fabrication of the Bi and Yb-doped optical fibres

3.2.1 MCVD and the solution doping technique

A series of Bi-doped preforms were fabricated by the MCVD and the solution doping method. The primary host investigated was silica, although other co-dopants such as Al, P and Ge were added, since the composition of the host can affect the properties of the Bi ion [1–3]. The preforms L30081 and L30082 were co-doped with Yb^{3+}, in an attempt to improve the pump absorption and ultimately to transfer their energy to the Bi ions through so-called "sensitization". It was anticipated that Yb ASE will act as a pump for Bi. Bi ($BiCl_3$, Sigma-Aldrich, 99.999% purity), Al ($AlCl_3$, Sigma-Aldrich, 99.9999% purity) and Yb ($YbCl_3$, Sigma-Aldrich, 99.9999% purity) were incorporated by solution doping technique and other dopants were deposited from the vapour phase.

Bi-doped fibres with cladding diameter 80 to 150 μm, with low (PC373 from Luvantix) and high (DSM314 from DSM Desotech) index coating, with respect to silica cladding, were drawn. The concentration and absorption as well as other characteristics of the MCVD based fabricated preforms and fibres are given in table 3.1.

Core glass composition	Preform ID	Bi concentration in 200 mL solution (gm)	Al concentration in 200 mL solution (gm)	Fibre ID	Core/Cladding Diameter(μm)	Core NA (average)
SiO_2:Al_2O_3	L30031	5.0	5.0	L3003101	6/80	0.11
				L3003102	10/125	—
				L3003103	15/150	—
				T0037	10/125	0.10
	L30201	5.0	10.0	T0312	10/125	—
	L30247	—	—	T0395	10/125	—
SiO_2:Al_2O_3:GeO_2	L30103	2.5	5.0	T0151	11/125	0.16
	L30117	2.5	7.5	T0175	8/100	0.14
				T0177	8/100	0.1
	L30123	2.5	4.0	T0184	10/125	—
				T0186	10/125	—
	L30150	2.5	5.0	T0189	10/125	—
SiO_2:Al_2O_3:GeO_2:P_2O_5	L30071	0.25	4.0	T0086	9/100	0.14
	L30124	2.5	4.0	T0185	10/125	—
SiO_2:GeO_2	L30190	0.8	—	T0298	5/125	—
SiO_2:GeO_2:P_2O_5	L30157	—	—	T0220	11/100	—
	L30235	—	—	T0372	—	—
SiO_2:Al_2O_3:Yb_2O_3	L30081	0.5	6.7	T0108	9/120	0.15
				T0110	9/120	0.15
SiO_2:Al_2O_3:P_2O_5:Yb_2O_3	L30082	1.0	6.7	T0107	10/120	0.14
				T0109	10/120	0.14

TABLE 3.1: List of Bi-doped fibres used in this work fabricated using the MCVD technique

3.2.2 MCVD chemical-in-crucible deposition technique

The main disadvantage of the solution doping process is that it is very difficult to employ for multiple core layers as it requires the process to be repeated for every single core layer and so is time consuming. However, lanthanide-based chelate complexes in conjunction with MCVD offer exciting opportunities to dope preforms in-line and to very high rare earth concentrations [4]. The high volatility, at moderately low temperature levels, for the lanthanide chelates, which are based on the compound 2,2,6,6-tetramethyl-3,5-heptandione (Tris) [5], allows for high concentrations of rare earth ions within the reaction zone during core fabrication.

The novel process, MCVD chemical-in-crucible deposition supports chelate heating directly within the MCVD preform structure. Thus, chelate delivery system is an addition to MCVD process, where special dopants and precursors are delivered into the deposition zone by direct evaporation of low vapour pressure precursors. This approach was developed initially for rare earth dopants but subsequently applied to bismuth as well, without further modification to the system [6].

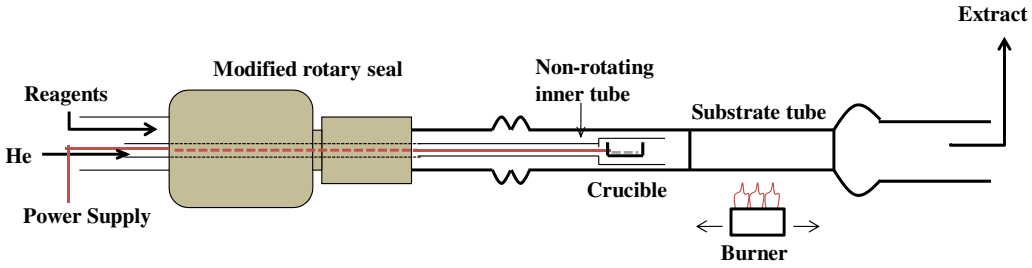

FIGURE 3.1: Schematic diagram of the setup designed for MCVD chemical-in-crucible deposition.

A schematic of the set up used for MCVD chemical-in-crucible deposition is shown in Fig. 3.1. In order to develop and integrate the chelate delivery system with MCVD, a commercial rotary seal is modified. The dopant source is situated in a crucible within the non-rotating inner tube and is heated directly, rather than by

Preform/Fibre ID	Core glass composition	Concentration (ppm-wt)	Core/ Cladding Diameter(μm)	Core NA (average)	Loss at 1285 nm (dB/km)	Laser Efficiency w.r.t. absorbed pump power (%)
L30083*	Al					
L30085*	Al					
L30094/T0124	Yb/P	3600(Yb)	12/125	0.11	26	69
L30101/T0145	Yb/P	Negligible	10/125	0.1		
L30104/T0169	F/Yb/P	Negligible	10/125	0.15		
L30105*	Yb/P			0.13		
L30106/T0156	Yb/P	4000(Yb)	11/125	0.13	106	
L30107/T0159	Yb/P	5500(Yb)	10/125	0.12	38	71
L30120/T0181	Yb/P	12000(Yb)	10/125		370	63
L30157/T0220	Bi/P/Ge	—	10/100	0.18	350	—

TABLE 3.2: Chemical-in-crucible preforms/fibres fabricated

an external burner. The design and shape of the crucible plays an important role in maintaining the uniform flow of vapour and therefore uniform deposition of the dopant ions. A quartz crucible was designed and developed for the purpose. For stable and accurate temperature control a heater was constructed using resistance wire made of nickel-chromium alloy, which was coiled around the crucible. Power was supplied externally from a high current source with the temperature calibrated using a thermocouple. For use with chelate compounds the crucible is heated in the range of 150 to 300^{o}C. An inert carrier gas (He, in this case) is preheated and passed over the crucible through the inner tube. This is achieved while maintaining the rotation of the outer tube with the delivery of all other gases and vapours through it, such as $SiCl_4$, $GeCl_4$ etc.

A number of preforms and fibres were fabricated in order to optimise the parameters involved in uniform deposition of high rare earth concentration preforms. Table 3.2 gives an outline of the preforms and corresponding fibres fabricated along with their basic characterisations. In the fabrication process, the core in

some preforms became whitish, which is marked * in the table. No fibres were pulled from such preforms.

In the development of a fibre fabrication technique the characterisation of fabricated fibres is one of the most important task. In order to optimise the chemical-in-crucible technique, basic fibre characterisation such as: refractive index profile, transmission spectrum, background loss, concentration of dopants in the core and laser efficiencies were carried out on the fabricated fibres.

After setting up the lathe for the chemical-in-crucible delivery, two preforms with Al Tris were fabricated. During fabrication, no significant vapour was seen from the crucible. Next preform was made with Yb Tris. It is easy to check the presence of Yb in the fibre core, as small amount of Yb can change the absorption in the fibre considerably. On the other hand, in order to check the presence of Al by refractive index profile, relatively higher concentration is required. The Yb-doped preform (L30094) was a success and fibre (T0124) drawn from this shows a laser efficiency of 69% with respect to absorbed pump power, at 1060 nm with a 65 m long fibre. The background loss was also considerably low ∼26 dB/km at 1285 nm measured using a high resolution optical time domain reflectometer (OTDR).

Figure 3.2 shows the refractive index profile of the fibre T0156 drawn from the preform L30106. The central dip is because of the evaporation of P_2O_5 during high temperature collapsing of the preform.

The concentration of rare earth ions in the fibres were measured based on the white light absorption. Figure 3.3 shows the absorption spectra for Yb in a fibre (T0159) fabricated by the chemical-in-crucible technique. Using the absorption cross section of Yb in phosphosilicate host from literature, the concentration of Yb was estimated to be ∼ 5500 ppm in this fibre.

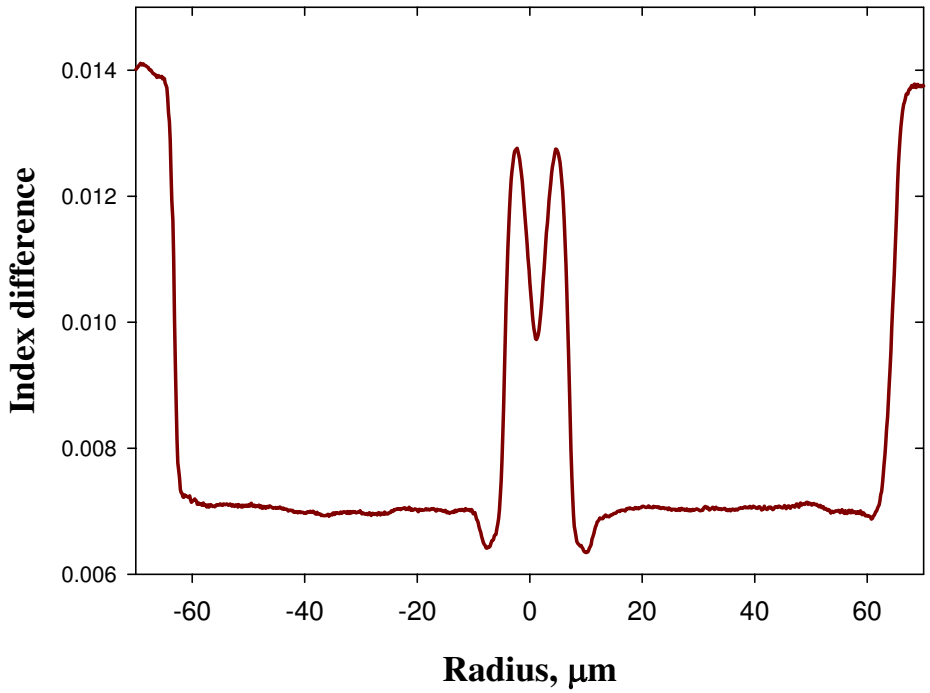

FIGURE 3.2: Refractive index profile of fibre T0156, fabricated by the chemical-in-crucible deposition technique.

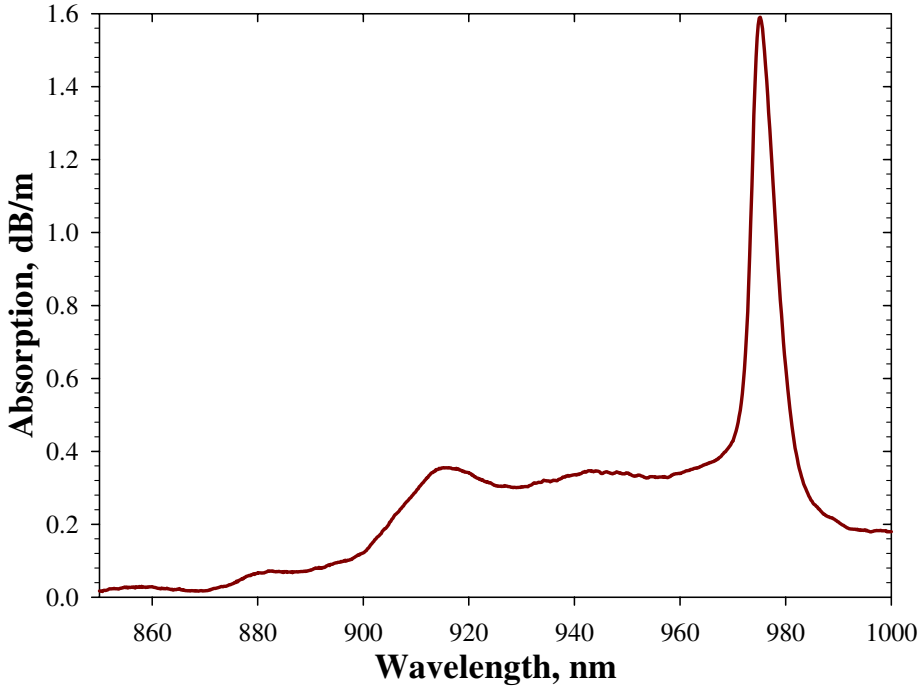

FIGURE 3.3: Absorption spectra of T0159 fabricated by the chemical-in-crucible deposition technique.

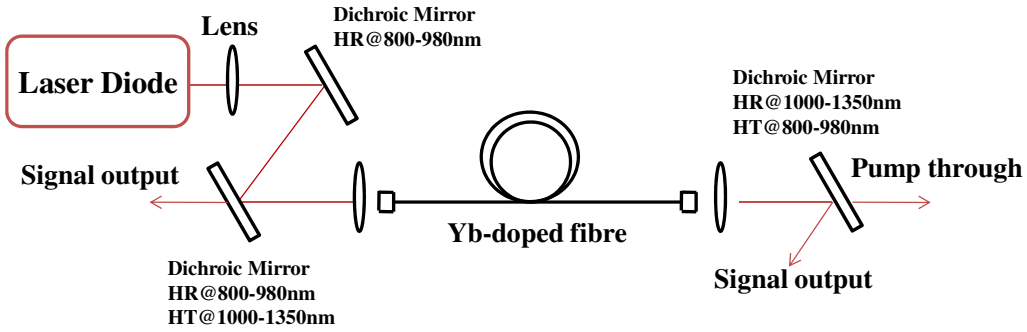

FIGURE 3.4: Schematic diagram for cladding pumped laser configuration.

The laser set up used for the efficiency measurement of the chemical-in-crucible fibres is shown in Fig. 3.4. The fibres were pumped by a 960 nm fibre pig-tailed, multi mode laser diode through a combination of collimating lenses and dichroic mirrors. A linear laser cavity was formed between perpendicularly cleaved end facets of the fibre, providing 4% Fresnel reflections. The laser characteristics are

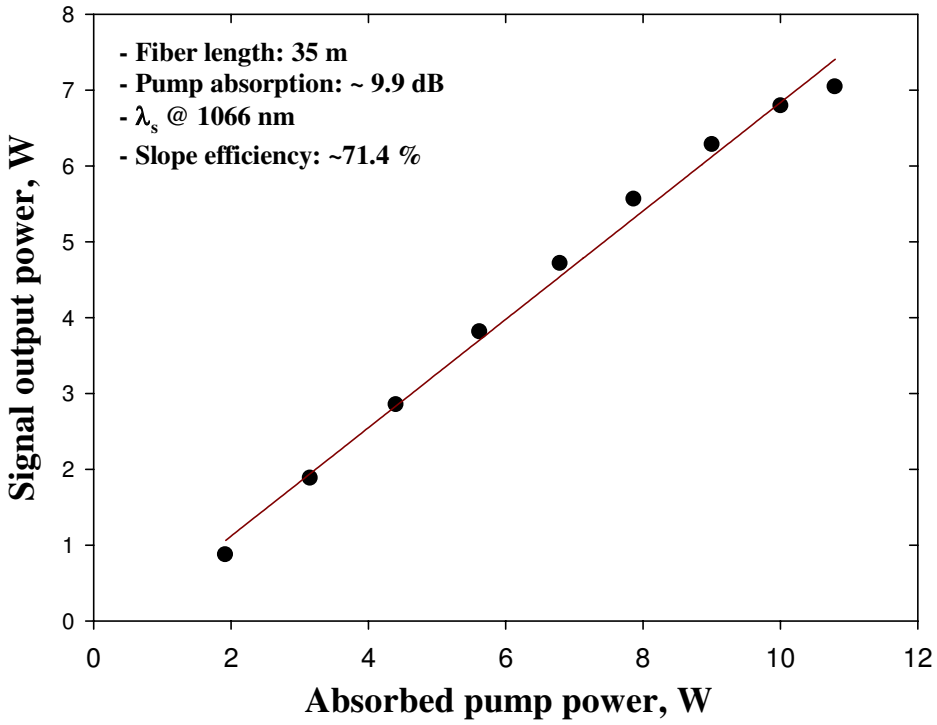

FIGURE 3.5: Laser characteristics of fibre T0159 cladding pumped at 960 nm.

shown in Fig. 3.5. The fibre showed more than 71% slope efficiency with respect

to the absorbed pump power, which is comparable to those fabricated by the standard MCVD process. Figure 3.6 shows a typical laser spectrum, which was taken by an optical spectrum analyser (OSA) with 1 nm resolution.

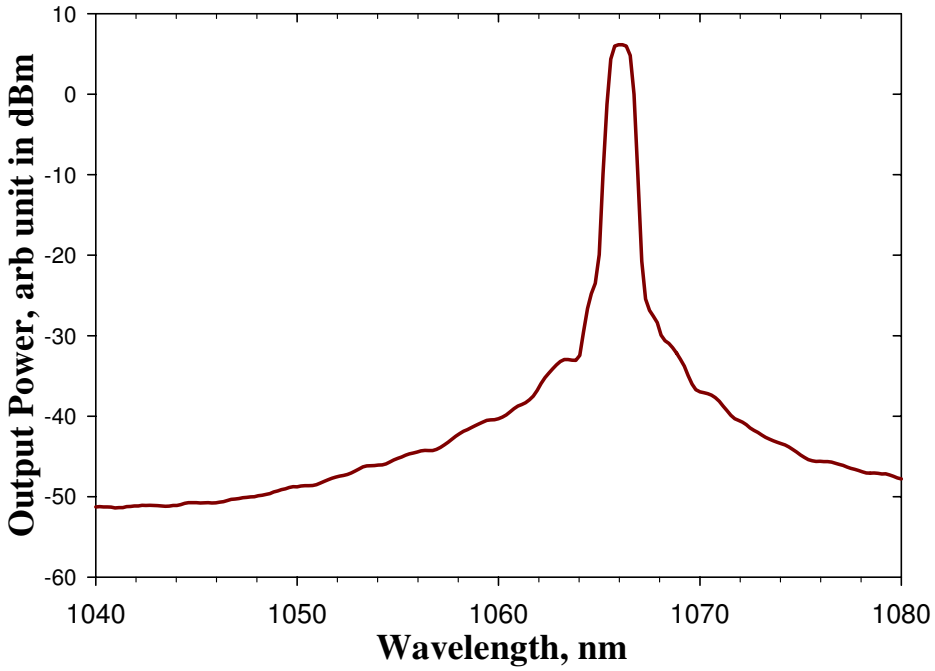

FIGURE 3.6: Spectrum from fibre T0159 cladding pumped at 960 nm.

Subsequently, a Bi-doped preform was also fabricated using $BiCl_3$ as precursor. The substrate tube was etched with SF_6 and polished, followed by the deposition of cladding layers. The crucible was filled with $BiCl_3$. Two core layers were deposited using a flow of 100 sccm of $SiCl_4$, 200 sccm of $POCl_3$ and 100 sccm of $GeCl_4$, whilst heating the crucible containing $BiCl_3$ to 400^{o}C. After core deposition, the tube was collapsed and sealed. The core looks pink during collapsing of the preform. The refractive index profile was measured along the length of the perform (Fig. 3.7). The complete characterisation of the fabricated fibre will be detailed in Chapter 4.

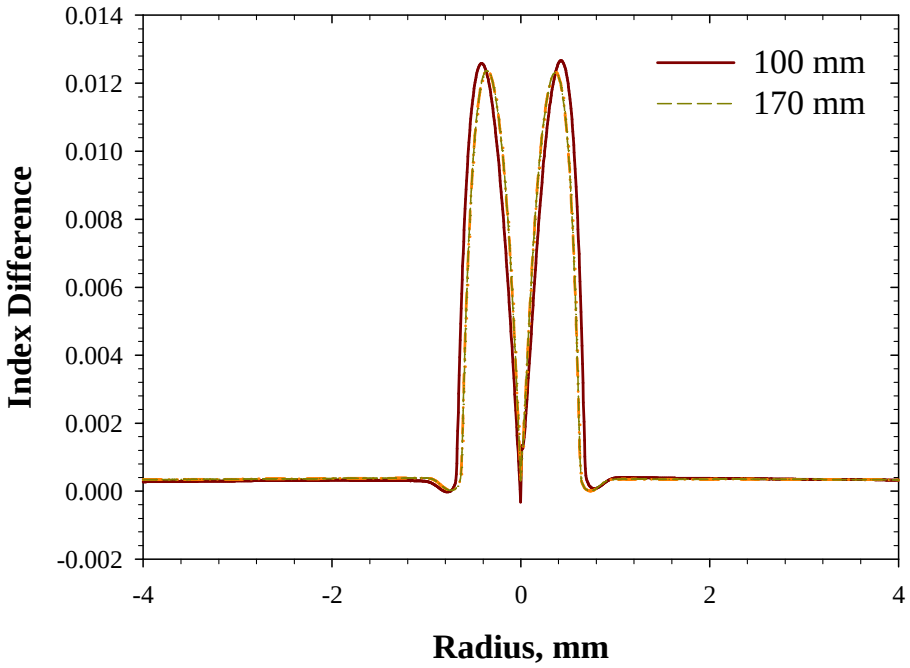

FIGURE 3.7: Refractive index profile of the Bi-doped chemical-in-crucible preform.

3.2.3 Powder-in-tube technique

The luminescence properties of Bi-doped fibre made using MCVD technique are often different from those observed in Bi-doped glasses. Also, it is reported that with the melting technique one can increase the Bi concentration in silica glass up to 1.0 mol% [7], whereas the reported concentration of Bi fabricated be MCVD is rather low [8]. Useful information can be extracted by studying Bi-doped fibres fabricated by technique that is significantly different from the MCVD. Powder-in-tube technology [9] is applied for Bi-doped fibre fabrication. It involves inserting the powder that act as a core material inside a silica cladding tube. The powder is then melted in a drawing furnace and subsequently drawn into fibre.

A schematic arrangement of the process is shown in Fig. 3.8. The material used for the fibre core was a powder consisting of 94.5 mol% SiO_2 (Sigma-Aldrich, 99.6% purity, 44 μm particle size), 5.0 mol% Al_2O_3 (Sigma-Aldrich, 99.7% purity, 10 μm

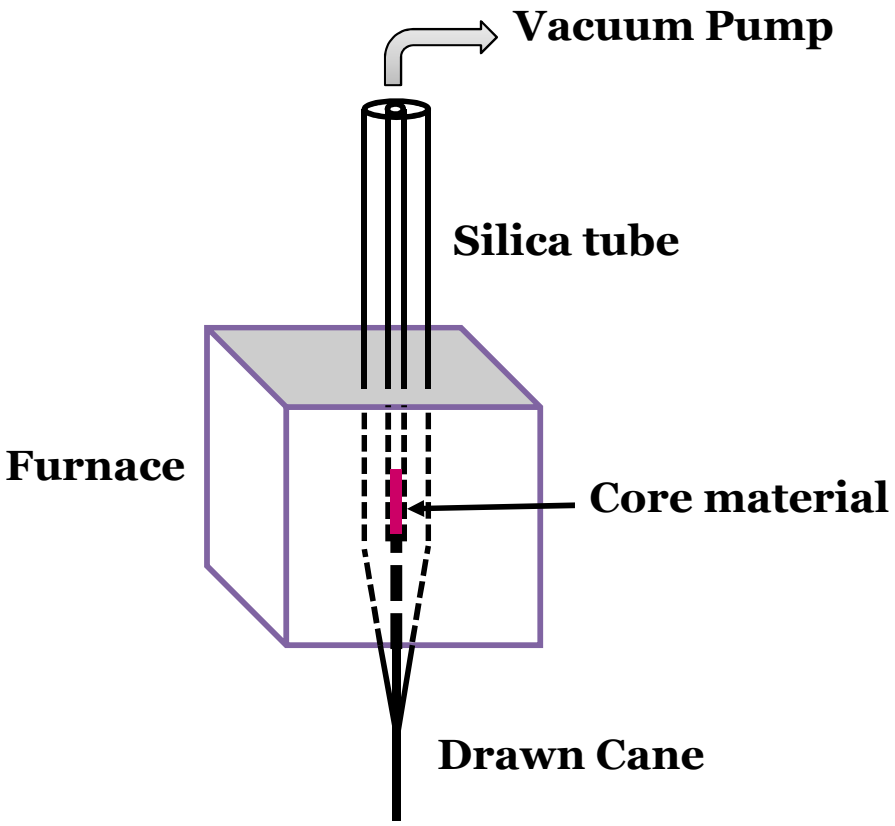

FIGURE 3.8: Schematic diagram of the setup designed for powder-in-tube technology.

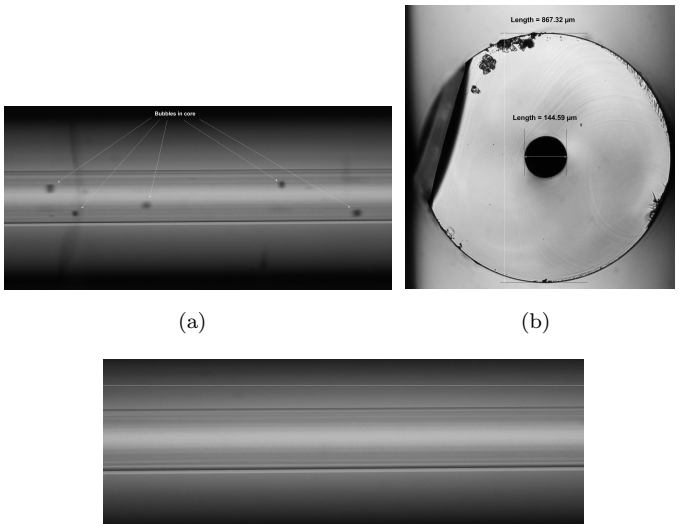

(a) (b)

(c)

FIGURE 3.9: Micrograph of Bi cane fabricated by the powder-in-tube technique (a) bubbles in the core, (b) cross sectional view and (c) clear section without bubbles.

particle size) and 0.5 mol% Bi_2O_3 (Sigma-Aldrich, 99.9% purity, 10 μm particle size). The powders were mixed in a mortar, and poured in to a silica substrate tube of 20 mm outer diameter by 16 mm inner diameter, which is sealed at one end, to a depth of 25 mm. The powder mix was then annealed in the furnace of a Heathway fibre drawing tower at 1750°C, for a total of 1 hour. During the anneal, the powder filled section of the substrate tube was moved up and down through the furnace hot zone to facilitate the removal of gas bubbles from the resulting glassy core. The tube was then drawn into a cane of 1 mm diameter. The resulting cane appeared to contain many tiny gas bubbles in the core. Several preforms were made with different annealing and drawing temperatures to optimise the process in order to get an uniform cane without gas bubbles. Examples of such canes are shown in Fig 3.9.

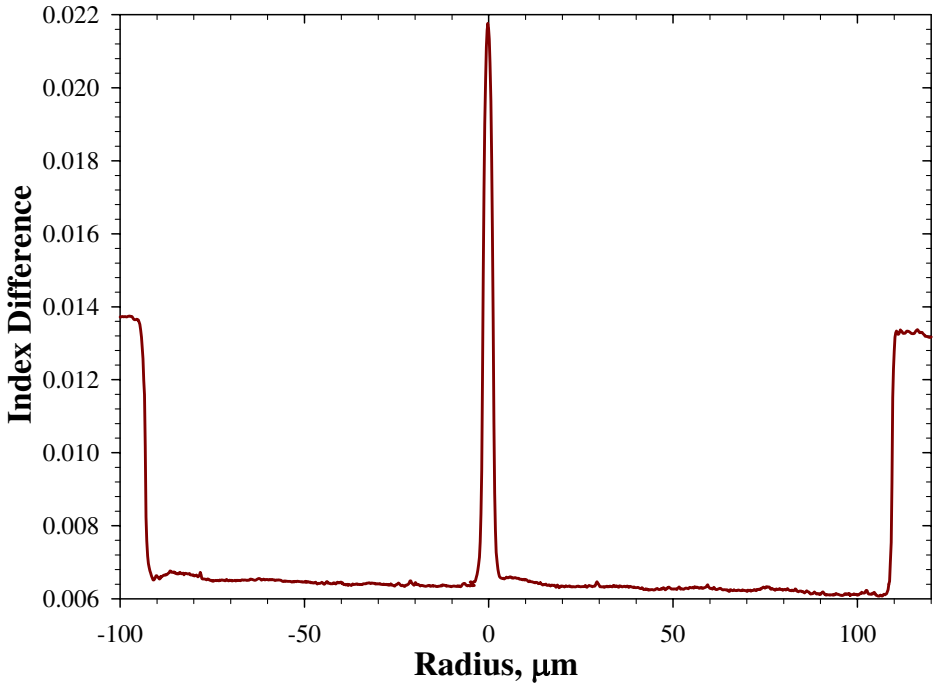

FIGURE 3.10: Refractive index profile of fibre T0226, fabricated by the PIT technique.

In the next preform, the same powder composition was then introduced in to a glass tube of dimensions 18 by 4 mm. A higher cladding-core ratio was used as

canes with smaller cladding-core ratio cracked or shattered during cooling. Canes drawn from this tube has less number of bubbles in the core. Figure 3.9(c) shows photographs of such a cane (Cane 2) used for the experimental work.

Fibre T0226 was drawn from Cane 11 with 3 μm core and 215 μm cladding, with a core NA of 0.25. Figure 3.10 shows the refractive index profile of the fibre. Due to low cut off the fibre was not used for experimental analysis.

3.3 Conclusions

A series of preform and fibres were fabricated using the conventional MCVD and the solution doping technique. A fabrication set up has been designed and developed for gas phase deposition of rare earth doped preforms using chelate compounds and successfully applied to Bi-doped fibre preform fabrication. The powder-in-tube technology has also been used to fabricate Bi-doped fibres.

References

[1] M. Y. Peng, D. P. Chen, J. R. Qiu, X. W. Jiang, and C. S. Zhu, "Bismuth-doped zinc aluminosilicate glasses and glass-ceramics with ultra-broadband infrared luminescence," *Optical Materials* **29**(5), pp. 556–561, 2007.

[2] X. G. Meng, J. R. Qiu, M. Y. Peng, D. P. Chen, Q. Z. Zhao, X. W. Jiang, and C. S. Zhu, "Near infrared broadband emission of bismuth-doped aluminophosphate glass," *Optics Express* **13**(5), pp. 1628–1634, 2005.

[3] Y. Fujimoto, Y. Hirata, Y. Kuwada, T. Sato, and M. Nakatsuka, "Effect of GeO_2 additive on fluorescence intensity enhancement in bismuth-doped silica glass," *Journal of Materials Research* **22**(3), pp. 565–568, 2007.

[4] R. P. Tumminelli, B. C. McCollum, and E. Snitzer, "Fabrication of high-concentration rare-earth doped optical fibers using chelates," *Journal of Lightwave Technology* **8**(11), 1990.

[5] J. E. Sicre, J. T. Duboise, K. J. Eisentraut, and R. E. Sievers, "Volatile lanthanide chelates. II. vapor pressures, heats of vaporization, and heats of sublimation," *Journal of American Chemical Society* **91**(13), pp. 3476–3481, 1969.

[6] A. J. Boyland, A. S. Webb, M. P. Kalita, S. Yoo, C. A. Codemard, R. J. Standish, J. Nilsson, and J. K. Sahu, "Rare earth doped optical fiber fabrication using novel gas phase deposition technique," in *Conference on Lasers and Electro-Optics*, 2010. OSA Technical Digest (CD) (Optical Society of America, 2010), paper CThV7.

[7] Y. Fujimoto and M. Nakatsuka, "Optical amplification in bismuth-doped silica glass," *Applied Physics Letters* **82**(19), pp. 3325–3326, 2003.

[8] A. B. Rulkov, A. A. Ferin, S. V. Popov, J. R. Taylor, I. Razdobreev, L. Bigot, and G. Bouwmans, "Narrow-line, 1178 nm CW bismuth-doped fiber laser with 6.4 W output for direct frequency doubling," *Optics Express* , pp. 408–11, 2007.

[9] J. Ballato and E. Snitzer, "Fabrication of fibers with high rare-earth concentrations for faraday isolator applications," *Applied Optics* **34**(30), pp. 6848–6854, 1995.

Chapter 4

Spectroscopic characterisation of Bi-doped fibre

4.1 Introduction

To assess the fabricated fibres and optimise the fabrication parameters for the construction of a Bi-doped fibre laser, a series of spectroscopic characterisation were carried out. A detailed knowledge of the spectroscopic properties, for example absorption and emission spectra, fluorescence lifetime and unsaturable loss, excited state absorption, is critical to optimise the Bi-doped fibres for device applications. It was observed that the spectroscopic properties of Bi-ions are considerably dependant of host materials and fabrication history.

This chapter presents the spectroscopy, basic characterisation and initial investigations of Bi-doped fibres with particular reference being made to fibres fabricated with different host glass compositions. Initially, Section 4.2 describes the chemical analysis of the Bi-doped preforms and fibres, in an attempt to reveal the content of Bi in the core. Section 4.3 then details the absorption characteristics of Bi-doped fibres with different host glass compositions. Bi luminescence and fluorescence

decay properties under different pumping wavelengths are presented in Section 4.4 and Section 4.5 respectively. The influence of unsaturable loss on laser performance is discussed in Section 4.6. The emission and absorption cross-section of Bi-doped fibres are presented in Section 4.7. Excited state absorption in Bi-doped alumino-germano-silicate fibre is reported in the 900-1300 nm wavelength range under 800 and 1047 nm pumping in Section 4.8. The feasibility of direct laser diode pumping of Bi-doped fibre lasers at the wavelengths of 915 and 975 nm was also examined through numerical simulations. Bi-doped fibre laser measurements were also performed, and are briefly described here, while detailed discussions are reserved for Chapter 5. Finally, characteristics of Bi-doped fibre under external influences like H_2-loading are compared to pristine fibre in Section 4.9.

4.2 Chemical analysis of Bi-doped fibres

The radial distribution of the chemical composition in the fibre core glass was determined by energy dispersive x-ray spectroscopy analysis (EDAX) and secondary ion mass spectrometry (SIMS) analysis. A Zeiss scanning electron microscope EVO 50 equipped with an Oxford Instruments energy dispersive x-ray analyser was used for the EDAX analysis. The concentration profiles of Al and Bi in Cane 2 (described in Chapter 3), fabricated by the PIT technology are shown in Fig. 4.1.

The SIMS analysis was performed by the Loughborough Surface Analysis Limited. The analysis was performed using primary ion bombardment and positive secondary ion detection. Luminescence measurement was carried out on the samples by stepping a 10 μm analysis area along the diameter of the preform (L30031) in 2 μm steps. Figure 4.2 shows the SIMS profile of the Bi-doped alumino-silicate preform L30031, which clearly displays the presence of Bi in the core. The two Si channels are 30_{Si} which is the minor isotope of Si and 28_{Si}, the major isotope was

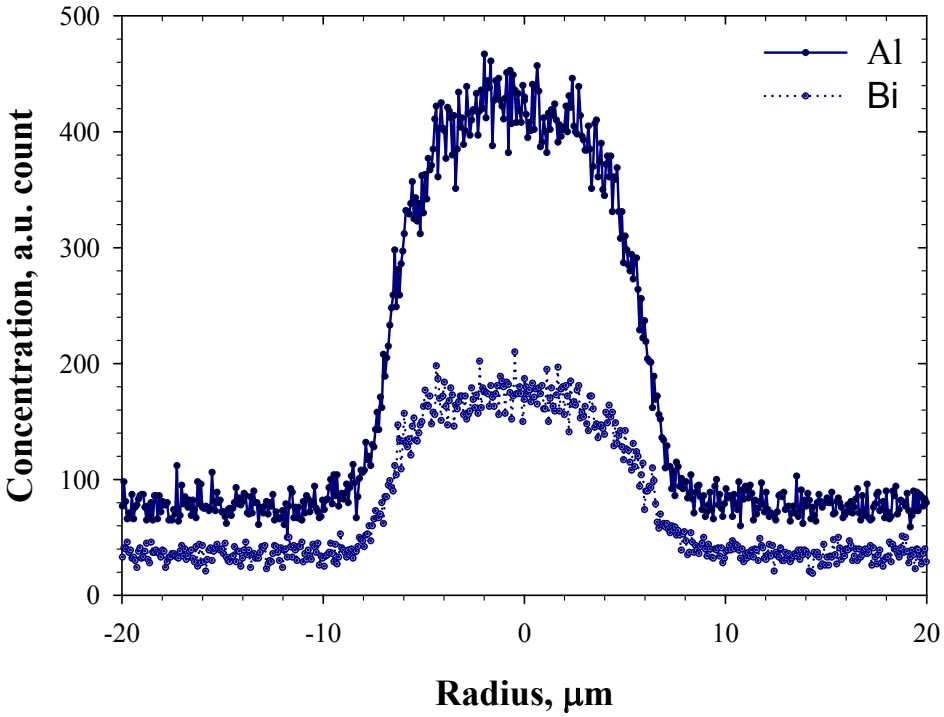

FIGURE 4.1: Radial distribution of Al and Bi across Cane 2, determined by EDAX analysis.

too intense to get on scale at the same time as the dopants. The calculation of Bi concentration from the SIMS measurement was not possible due to the absence of a standard profile for comparison.

4.3 Absorption spectra of Bi-doped fibres

Absorption spectroscopy is the most fundamental optical characterisation and was carried out both in the Bi-doped preforms and fibres. In Bi-doped preform, the absorption measurements were taken with a Varian Cary 500 spectro-photometer. The absorption was measured in the range of 200 to 1750 nm. The preform slices of 11 mm diameter were cut and polished on both sides with length of around 0.5 to 3 mm. Fig. 4.3 shows the Bi absorption bands at 500 and 700 nm of the alumino-germano-silicate preform L30117. The other absorption bands in the near

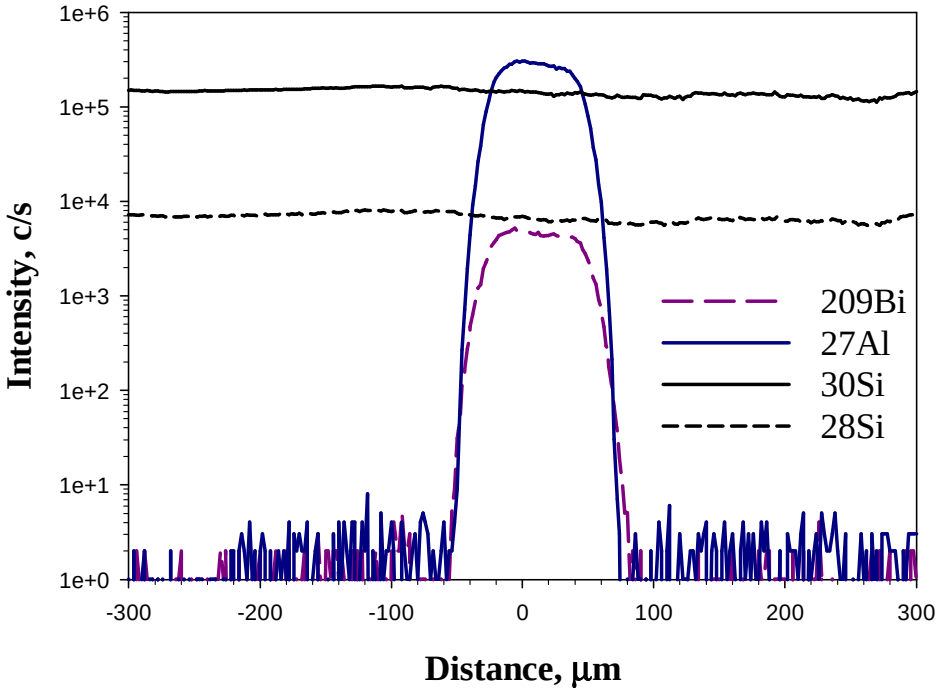

FIGURE 4.2: SIMS analysis of the preform L30031.

infra-red (NIR) regions was not distinct due to relatively low Bi concentration and short sample length.

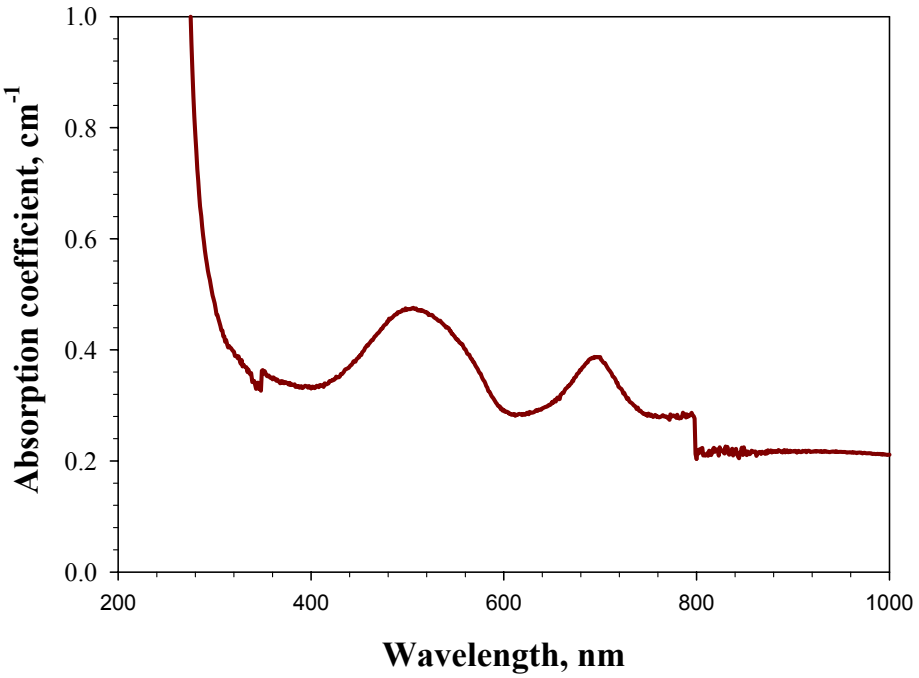

FIGURE 4.3: Absorption spectra of Bi-doped preform L30117.

Core glass composition	Fibre ID	Absorption at 1080 nm (dB/m)	Loss at 1285 nm (dB/km)
SiO_2:Al_2O_3	L3003102	0.65	>1000
	T0037	9.0	∼1000
	T0312	0.46	140
	T0395	2.89	—
SiO_2:Al_2O_3:GeO_2	T0151	1.2	40
	T0175	1.7	60
	T0177	3.5	<100
	T0184	0.02	—
	T0186	0.019	—
	T0189	0.08	—
SiO_2:Al_2O_3:GeO_2:P_2O_5	T0086	0.2	<50
	T0185	0.2	—
SiO_2:GeO_2	T0298	0.02	40
SiO_2:GeO_2:P_2O_5	T0220	2.2	350
	T0372	1.0	500

TABLE 4.1: Absorption and background loss in Bi-doped fibres

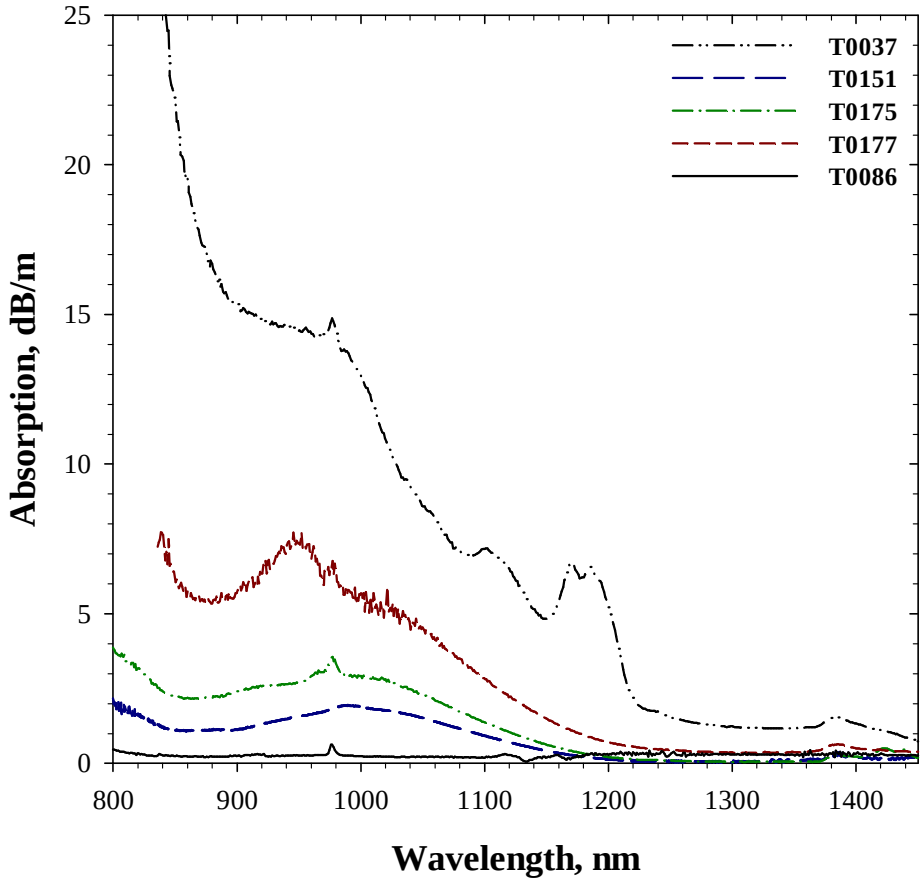

FIGURE 4.4: Absorption spectra of Bi-doped fibres.

The small signal absorption in the Bi-doped fibres were measured by the conventional cut-back technique, using a white light source and a Yokogawa AQ-6315A OSA with a resolution of 1 nm. Different fibre lengths were used depending on the Bi concentration and fibre loss. System dependence responses were minimized by repeating the measurement several times. Typical absorption bands of Bi at 500, 700 and 1000 nm and a shoulder at 800 nm were observed in all the fibres. Figure 4.4 shows the absorption spectrums of the fabricated Bi-doped fibres with different core glass compositions, in the spectral region of 800-1450 nm. The Bi absorptions at 1080 nm are summarised in table 4.1. It appears that the absorption depends on the Bi concentration and presence of other dopants in the fibre. The temperature dependance of absorption was also measured in the fibres and no noticeable change in the temperature range of 283 to 300 K were observed in the

800-1700 nm wavelength region. The background loss in the fibres were measured with a Sunrise Luciol OTDR at 1285 nm and presented in table 4.1.

4.4 Fluorescence spectra of Bi-doped fibres

Measurement of fluorescence spectrum of the Bi-doped fibres and preforms were carried out by different excitation sources. The fluorescence output was collected from the side of the preform with a 500 μm silica fibre and detected with an OSA. A PUMA 960 nm diode source was used to check the fluorescence in alumino-silicate preform L30031 and Yb co-doped alumino-phospho-silicate preform L30082. The fluorescence pattern from the preform L30031 has a peak around 1100 nm and in case of L30082 the Bi peak shifts to 1300 nm (Fig. 4.5). The emission bandwidth is seen to be broad, with a FWHM (@3 dB) of 170 nm in case of L30031 and 220 nm in case of L30082 preform. The alumino-germano-silicate preform L30103, when pumped with 1090 nm, showed a peak $\sim$ 1130 nm (Fig 4.6).

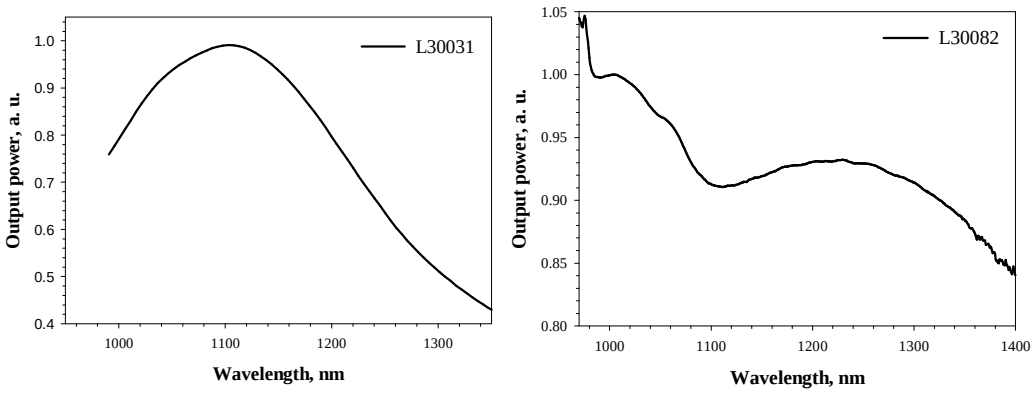

(a) (b)

FIGURE 4.5: Transverse fluorescence spectrum of the preform (a) L30031 and (b) L30082, when pumped with 960 nm, taken with an OSA with 1 nm resolution.

To investigate the pump wavelength dependance of fluorescence, different pump sources were employed to collect the fluorescence spectrum from Bi-doped fibres.

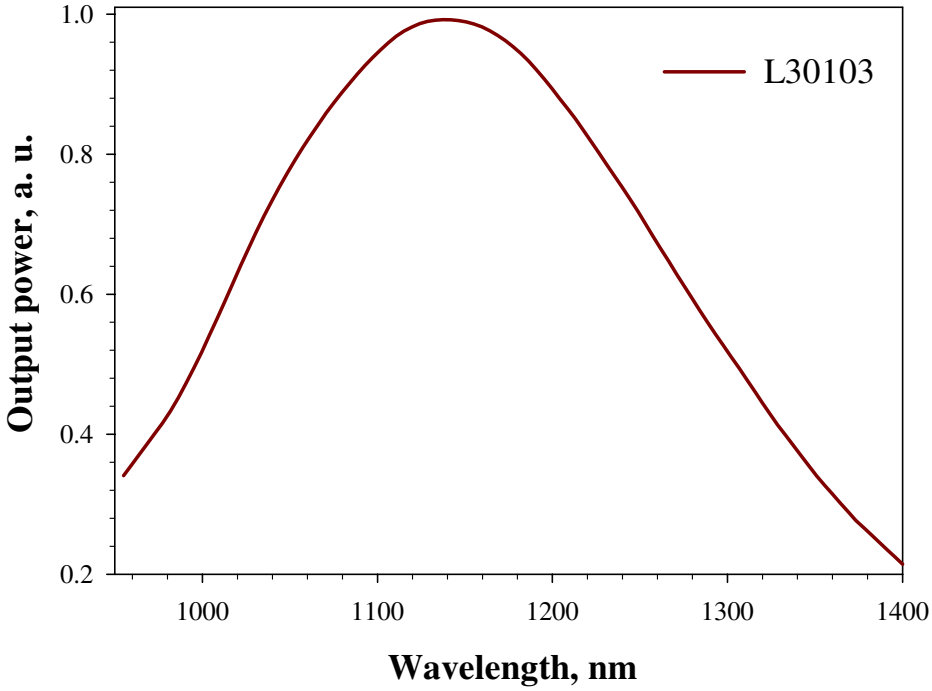

FIGURE 4.6: Transverse fluorescence spectrum of the preform L30103, when pumped with 1090 nm, taken with an OSA with 1 nm resolution.

Also, a variety of Bi-doped fibres, fabricated with different host glass compositions, were studied for their possible influence on Bi luminescence. Low pump power was used in the measurement to avoid ASE. To confirm that, the pump power level was reduced until a change in pump power does not affect the output spectrum. Also, signal was measured from the side of a short fibre to prevent re-absorption. In case of transverse measurement, the drawback of weak signal can be overcome by pumping harder as the scattered light is not subject to gain along the length of the fibre and so the output will be always free from ASE. The fluorescence spectrum was collected with various laser sources: a 915 nm Axcel Photonics laser diode, a JDS Uniphase laser diode at 976 nm, a fibre coupled Nd:YLF at 1047 nm and a 1090 nm GT Wave Yb fibre laser.

The luminescence spectra at 977 and 1090 nm excitation of fibres with different host glass compositions are shown in Fig. 4.7. In case of alumino-silicate and alumino-germano-silicate fibres (T0037 and T0151 in figure, respectively) the peak

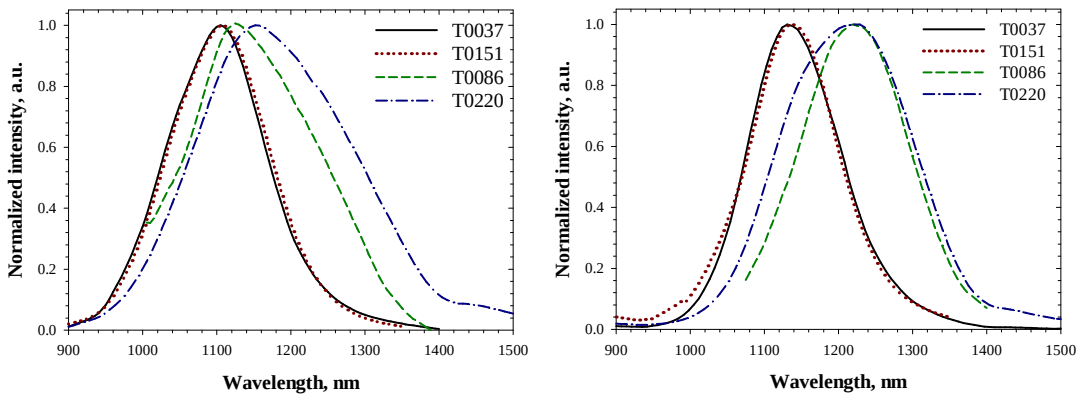

FIGURE 4.7: Scaled transverse fluorescence spectra of Bi-doped fibres with different hosts, when pumped with (a) 977 nm and (b) 1090 nm.

position is around 1100 nm at 977 nm and 1130 nm at 1090 nm. In case of phospho-alumino-germano-silicate and phospho-germano-silicate fibres (T0086 and T0220 respectively) the peak shifts to longer wavelengths of 1130 and 1150 nm respectively at 977 nm; while in case of 1090 nm pumping the peak position was 1220 nm. The peak position of the emission band shifts to longer wavelengths in presence of P in the core. Our results suggest that P also increases the bandwidth, as shown in Fig. 4.7. We further investigate the dependence of the luminescence band on the pump wavelengths. Figure 4.8 presents the measured fluorescent spectra for fibre T0151 at different pumping wavelengths from 915 to 1090 nm. The peaks were scaled to unity for comparison. The fluorescence peak shifts towards longer wavelengths and become narrower with longer pump wavelengths. We observed similar pump wavelength dependence of fluorescence in other fibres as well.

It was observed that the luminescence properties observed above are essentially different from the Bi-doped glasses described in Chapter 2, which shows in many cases a luminescence band near 1300 nm wavelength range. To study the possible influence of fabrication methods along with the host glass and pump wavelength, a Bi-doped cane was fabricated with the PIT technology and their luminescence properties, under different excitation sources, are compared to fibres fabricated

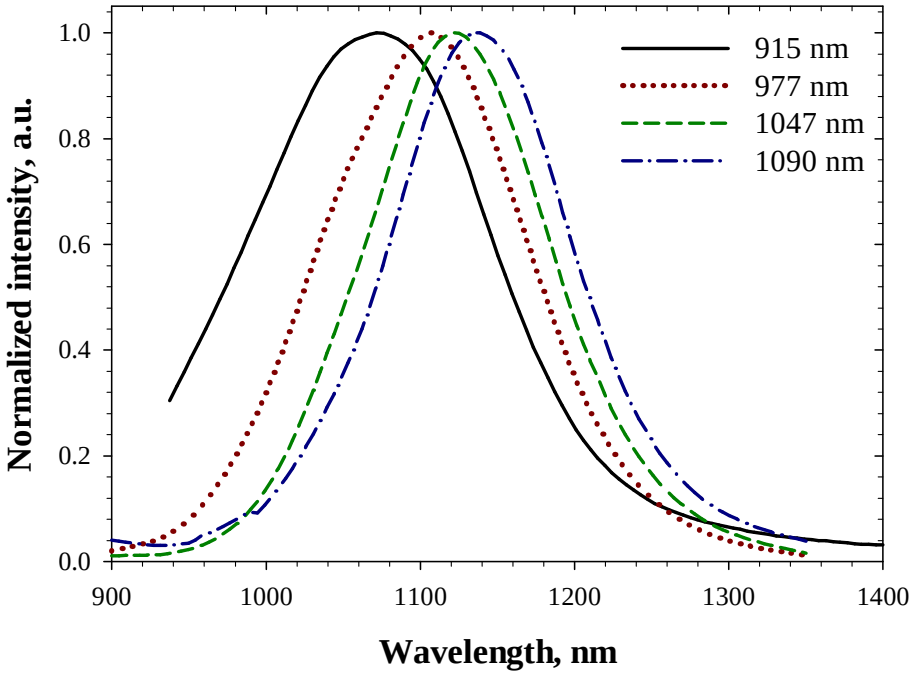

FIGURE 4.8: Scaled transverse fluorescence spectra of alumino-germano-silicate Bi fibre by different excitation sources.

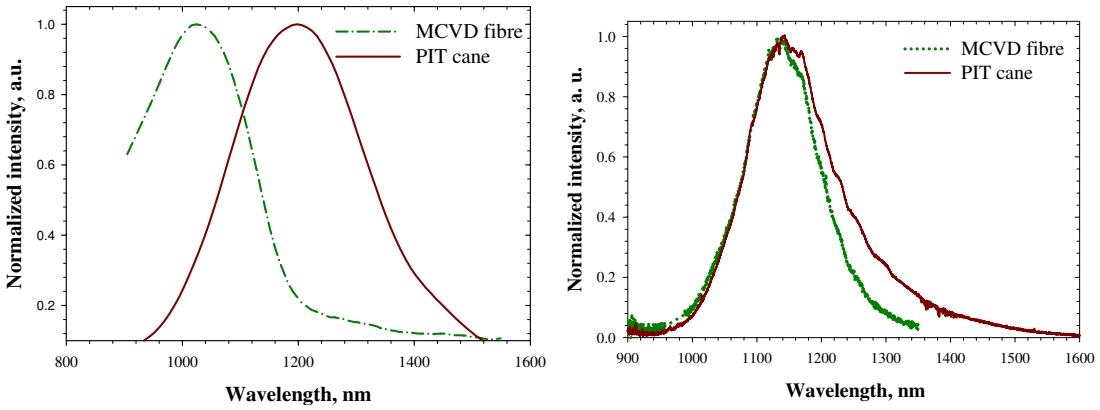

(a) 808 nm (b) 1090 nm

FIGURE 4.9: Normalised transverse emission spectra of Bi-doped cane and fibre fabricated by PIT and MCVD technique, at pump wavelength of (a) 808 nm and (b) 1090 nm.

by the MCVD technique. Figure 4.9 shows the fluorescence comparison spectra of the PIT cane and MCVD based alumino-silicate Bi-doped fibres. It is clearly shown that the emission is dependent of the fabrication method. The PIT cane showed broad fluorescence band centered at 1250 nm under 808 nm excitation

[Fig. 4.9(a)]. Its FWHM bandwidth is ∼270 nm. The fluorescence looks close to that of Bi-doped alumino-silicate glasses fabricated by the melt and quenching method [1]. However, in case of the MCVD Bi-doped fibre, the peak appeared in the shorter wavelength of 1000 nm with 200 nm of FWHM bandwidth. Under 1090 nm pumping, the peak position for both remains same, while the PIT cane shows broader fluorescence [Fig. 4.9(b)]. A more detailed analysis is needed to interpret the fabrication dependant behaviour of Bi-luminescence. Nonetheless, the PIT seems promising for the construction of broadband sources based on Bi-doped fibres.

4.5 Fluorescence lifetime

4.5.1 Experimental fluorescence lifetime

Fluorescence lifetime is defined as the time taken for the emission intensity to decay to $1/e \approx 0.368$ of its initial value. The fluorescence decay time measurements were obtained by exciting Bi-doped fibres with various excitation sources and the experimental setup is shown in Fig. 4.10. The excitation source was modulated using an IntraAction AOM 40R acousto-optic modulator (AOM). The modulation signal was generated by a Hewlett Packard 8112A pulse generator which then activated an IntraAction Corp. ME radio frequency generator. Pulsed pump light was launched into a short length of Bi-doped fibre so as to avoid re-absorption of fluorescence. In addition, lifetime shortening via stimulated emission was avoided by using low pump levels. It is also important that the input pulse separation is substantially greater than the emission decay time. Pulse period of 10 msec and temporal resolution of 2 μsec was used for the measurement. The fluorescence was detected with a Thorlab PDA10CS-EC InGaAs detector, which was set to a gain of

40-70 dB. The detector was in direct contact with the coiled fibre in the transverse measurement configuration. The life time of the excited level was recorded with a Tektronix DPO7254 oscilloscope with a 2.5 GHz bandwidth and a sampling rate of 40 GS/s. The signal was averaged for 512 times to improve signal to noise ratio in the measurement. The lifetime measurement was repeated several times to reduce random experimental error.

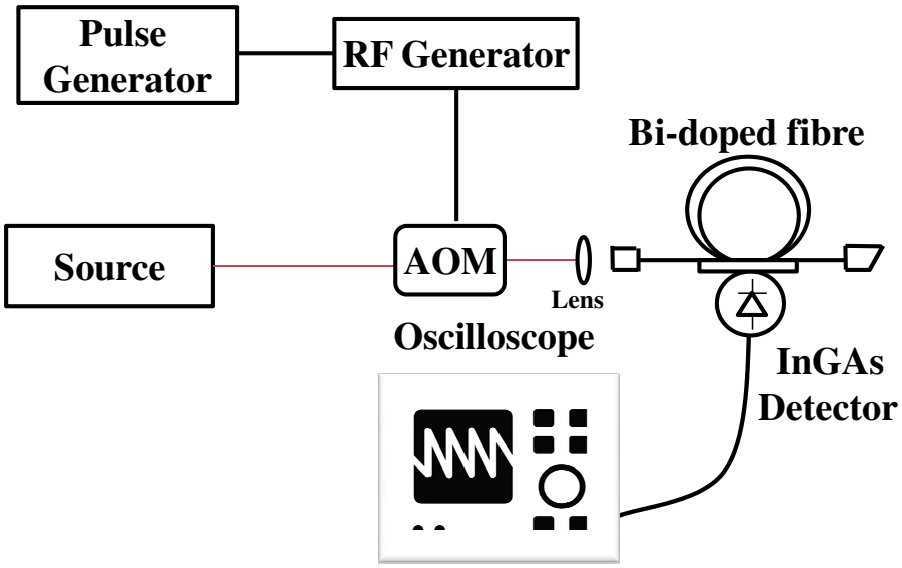

FIGURE 4.10: Experimental setup used to measure fluorescence lifetime.

The fluorescence decay time seems to depend on the pumping wavelengths and was measured at 915, 977, 1047 and 1090 nm for the alumino-germano-silicate fibre T0151. The recorded time was 750 μsec under 1090 nm pumping, but it reduced to 670 μsec under 915, 977 and 1047 nm pump (Fig. 4.11). The observed lifetimes of fibre T0175 and T0177 under 1090 nm pumping were 750 μsec, which reduced to 680 μsec under 977 nm pump wavelength. The lifetime values at different excitation wavelengths of the Bi-doped fibres measured are summarised in table 4.2.

Core glass composition	Fibre/cane ID	Excitation wavelength (nm)	Emission Peak (nm)	Lifetime (μsec)
SiO_2:Al_2O_3	L3003102	975	1100	—
	T0037	977	1100	647
		1090	1130	690
	Cane 2	808	1250	—
		1090	1130	—
	T0395	1090	1130	—
SiO_2:Al_2O_3:GeO_2	T0151	915	1070	670
		977	1100	670
		1047	1120	670
		1090	1130	750
	T0175	977	1100	680
		1090	1130	750
	T0177	977	1100	680
		1090	1130	750
SiO_2:Al_2O_3:GeO_2:P_2O_5	T0086	977	1130	740
		1090	1230	700
	T0185	977	1130	600
		1090	1230	650
SiO_2:GeO_2:P_2O_5	T0220	977	1160	470
		1090	1250	500
	T0372	1090	1250	—

TABLE 4.2: Fluorescence decay characteristics of Bi-doped fibres and cane.

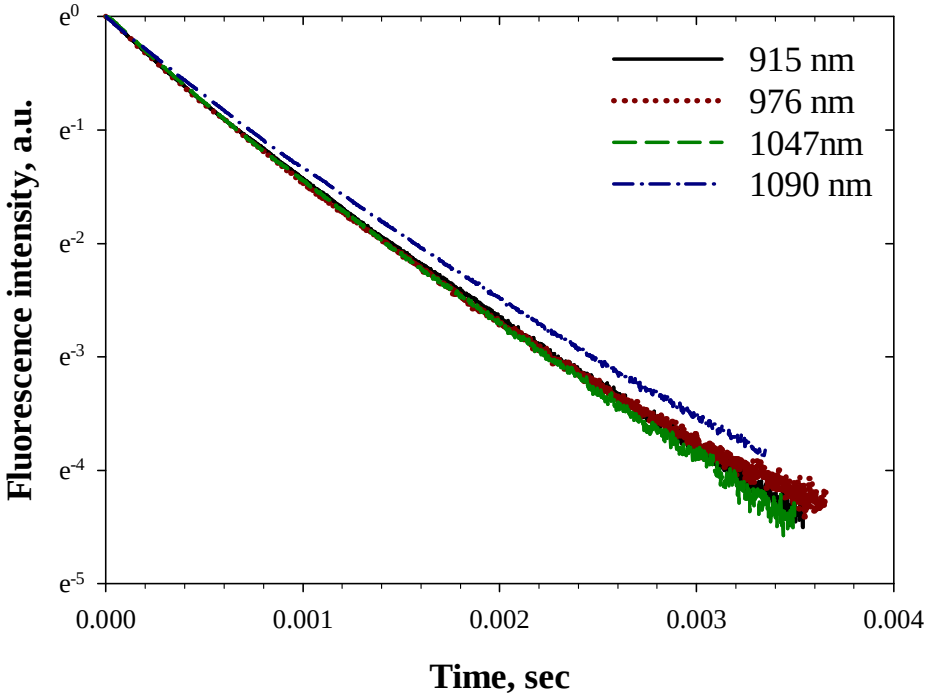

FIGURE 4.11: Fluorescence decay of alumino-germano-silicate fibre T0151 under different excitation.

4.5.2 Analysis of fluorescence lifetime

It was observed that the measured lifetime data deviates from single exponential behaviour. There can be a number of reasons why the measured lifetime data deviates from single exponential behaviour e.g. inhomogeneous broadening of spectral lines or the ions which are responsible for emission siting in different sites. In this section, the fluorescence emission from Bi-doped fibre is analysed using stretched exponential and continuous lifetime distribution model.

A suitable way of describing non-exponential decay is by fitting data to a stretched exponential [2],

$$I(t) = I(0)\exp\left(-\left(\frac{t}{\tau}\right)^{\beta}\right) \tag{4.1}$$

where $I(t)$ is the fluorescence intensity at time t, τ is a characteristic relaxation time and β is the stretched factor ranging from 0 to 1. The closer β is to 0 the more the function deviates from single exponential. The stretch factor is a measure of the deviation from exponential behaviour of the fluorescence decay.

The double exponential function is given by equation 4.2

$$I(t) = y_0 + I_1 \exp -\left(\frac{t}{\tau_1}\right) + I_2 \exp -\left(\frac{t}{\tau_2}\right) \tag{4.2}$$

where τ_1 and τ_2 are the two characteristic lifetimes and I_1 and I_2 are their respective coefficients.

Another approach is the continuous lifetime distribution used in chromium doped alumino-silicate and gahnite glasses [3–5], where the distribution of the luminescence decays are approximated by a continues function of decay constants $A(\tau)$. Hence, the luminescence decay is given by [4],

$$I(t) = \int \frac{A(\tau)}{\tau} e^{-\frac{t}{\tau}} d\tau \tag{4.3}$$

Which can be approximated by the discrete representation,

$$I(t) = \sum_i \frac{A_i}{\tau_i} e^{-\frac{t}{\tau_i}} \tag{4.4}$$

where the series of discrete coefficients, A_i, represents the continuous distribution of the decay constants, $A(\tau)$. It is common to use a logarithmic scale for the decay constant in order to represent the decay contribution over a wide variation of lifetime. So, Eq. 4.3 becomes,

$$I(t) = \int A(\tau) e^{-\frac{t}{\tau}} d(\ln \tau) \tag{4.5}$$

And Eq. 4.4 becomes,

$$I(t) = \sum_i A_i e^{-\frac{t}{\tau_i}} \tag{4.6}$$

The coefficient A_i enumerate the contributions of those sites that have a decay constant τ_i. Equation 4.6 was implemented in MatLab by Dr Seongwoo Yoo from the ORC and were used to recover all possible decay constants from the decay data by regression analysis. For the simulation, 125 logarithmically spaced lifetime values were chosen.

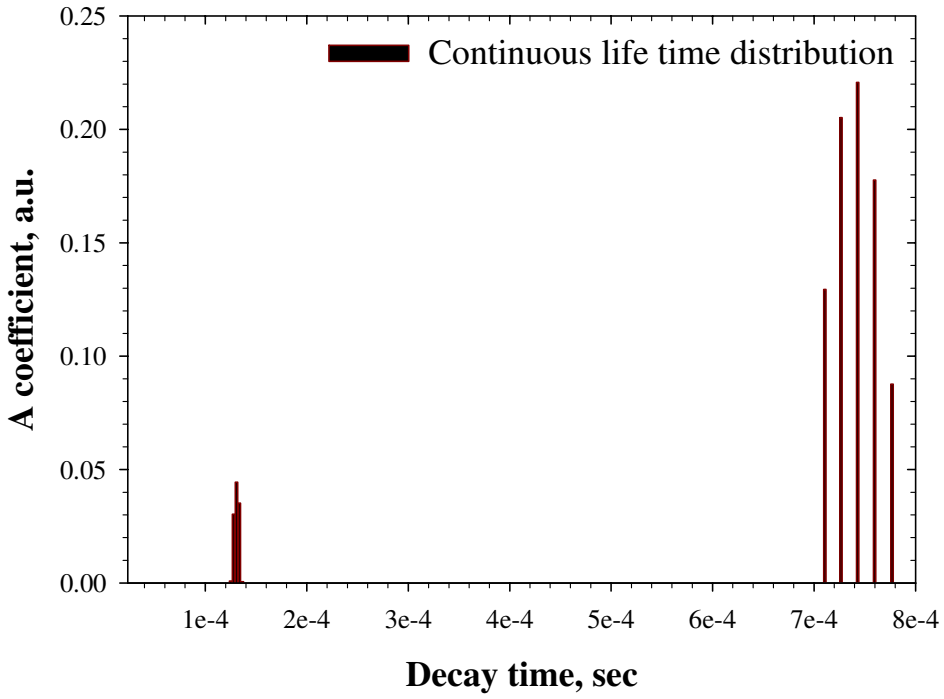

FIGURE 4.12: Recovered lifetime decay coefficients for T0151.

Figure 4.12 shows the distribution of lifetimes in fibre T0151. The figure shows two distribution peaks centred at 130 and 750 μsec.

Figure 4.13 shows the fluorescence decay of the alumino-silicate fibre T0151 at 1090 nm. The decay curves were fitted with single exponential, double exponential, stretched exponential and continuous life time distribution fit, and they were

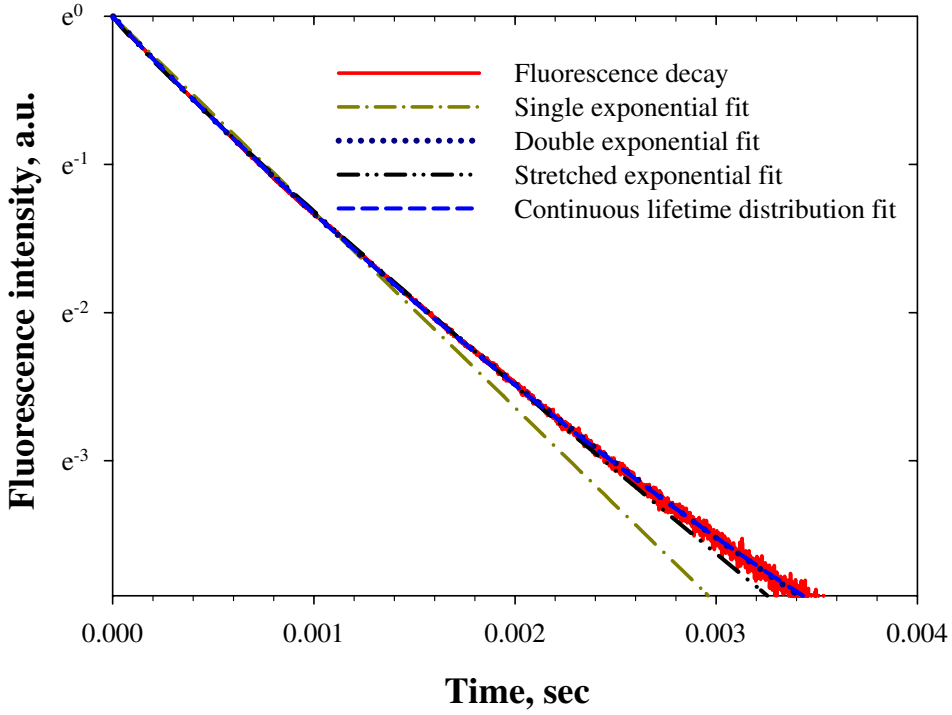

FIGURE 4.13: Fluorescence decay at 1090 nm fitted with single, double, stretched and continuous lifetime distribution of T0151.

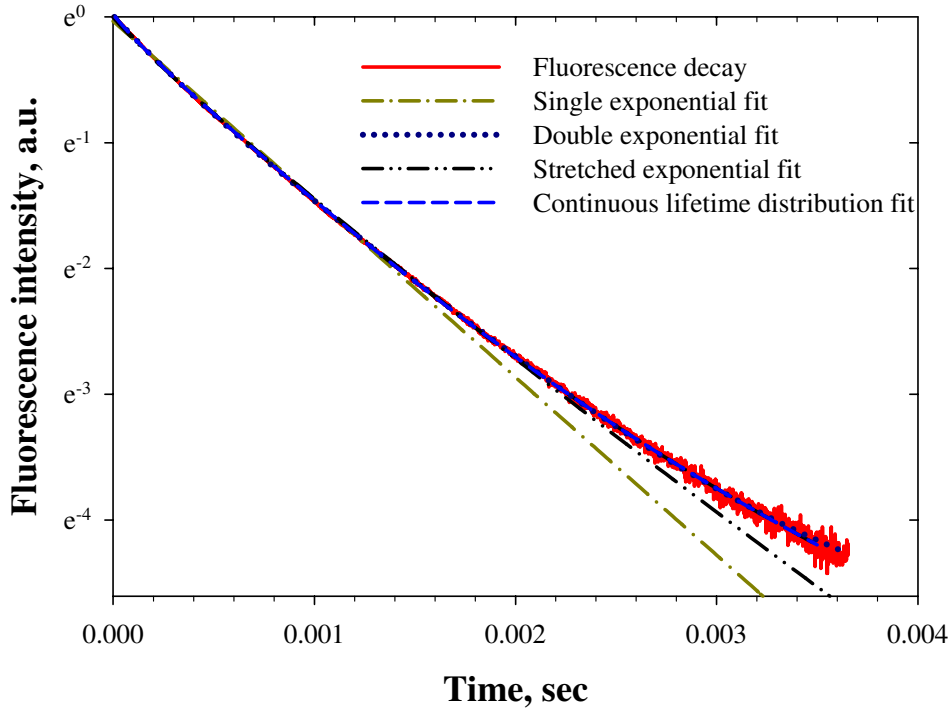

FIGURE 4.14: Fluorescence decay at 977 nm fitted with single, double, stretched and continuous lifetime distribution of T0151.

Excitation wavelength (nm)	Stretched exponential fit [β] (μsec)	Continuous lifetime distribution peak 1 (μsec)	Continuous lifetime distribution peak 2 (μsec)
977	668 [0.912]	645	130
1090	750 [0.924]	750	130

TABLE 4.3: Lifetime with stretched and continuous lifetime distribution of T0151

all best expressed by continuous exponential fitting. The deviation from the single exponential is evident from figure. The lifetimes for double exponential fit are 775μsec and 290μsec. With stretched fitting, lifetime of 750 μsec was obtained. Continuous lifetime distribution model revealed two different decay constants, short and long decay times of 130 μsec and 750 μsec respectively. Similar results were obtained in case of 977 nm excitation as well [Fig. 4.14]. Table 4.3 shows the lifetime calculated from stretched and continuous distribution model of the alumino-germano-silicate fibre under different pumping wavelengths. Thus, it seems to indicate that the Bi ions, which are responsible for 1160-1300 nm emission, do sit in different sites.

4.6 Unsaturable loss and saturation absorption mechanism

The measured value of the Bi fibre laser is lower than the efficiency of widely used fibre lasers. One possible cause of poor efficiency can be lifetime shortening due to quenching (e.g. via cross relaxation). However, quenching can also lead to unsaturable absorption (as background loss), again leading to poor efficiency [6, 7]. Unsaturable absorption can be caused by quenching-process such as cross-relaxation and upconversion, which prevent some of the Bi ions form being excited.

For example, clustered ions are subject to a fast cross relaxation that directly causes a loss of the population inversion. These ions will then practically always be in the ground state, and always absorb, and waste, pump energy. This is obviously detrimental in fibre lasers, and appears as an increase in threshold as well as a reduction in the conversion efficiency. It can be determined via laser efficiency measurements, or more directly, from absorption measurements with a high-power source [6].

The unsaturable absorption was determined by measuring transmission through the core from a Yb-doped fibre laser (GTWave) at 1080 nm. The measurement was carried out at different power levels. At high powers the absorption should bleach. Any remaining absorption can, ideally be taken as a direct measure of the unsaturable absorption. The fraction of unsaturable loss to the total small signal absorption is the important measure, and has a direct impact on the efficiency.

Experimentally, light from the laser was launched into one port of a fused fibre coupler (coupling ratio 80/20 at 1080 nm), which is single-moded at 1080 nm. One of the output ports (20 port) was used to monitor the launched power, whereas the other port was fusion spliced to the Bi-doped fibre. A short length of Bi-doped fibre was used in order to avoid any undesired gain at the signal band at around 1160 nm and to ensure that even the transmitted power would be large enough to bleach the fibre. The output spectrum was monitored on the optical spectrum analyser to check the power level in the signal band. In order to bleach the absorption, the power should be much higher than the intrinsic saturation power throughout the fibre. The intrinsic saturation power is given by $\frac{Ah\nu}{\Gamma(\sigma_a+\sigma_e)\tau}$, where A is the area of the Bi-doped region, $h\nu$ is the photon energy, Γ is the overlap between the excitation radiation and the doped region, σ_a and σ_e are the absorption and emission cross-sections respectively, and τ is the fluorescence lifetime. The maximum power launched into the Bi-doped fibre was around 3 W at

1080 nm, which is much higher than the saturation power of 13 mW. For accurate measurements, the power was varied over several orders of magnitude, to cover both small-signal and saturated absorption conditions.

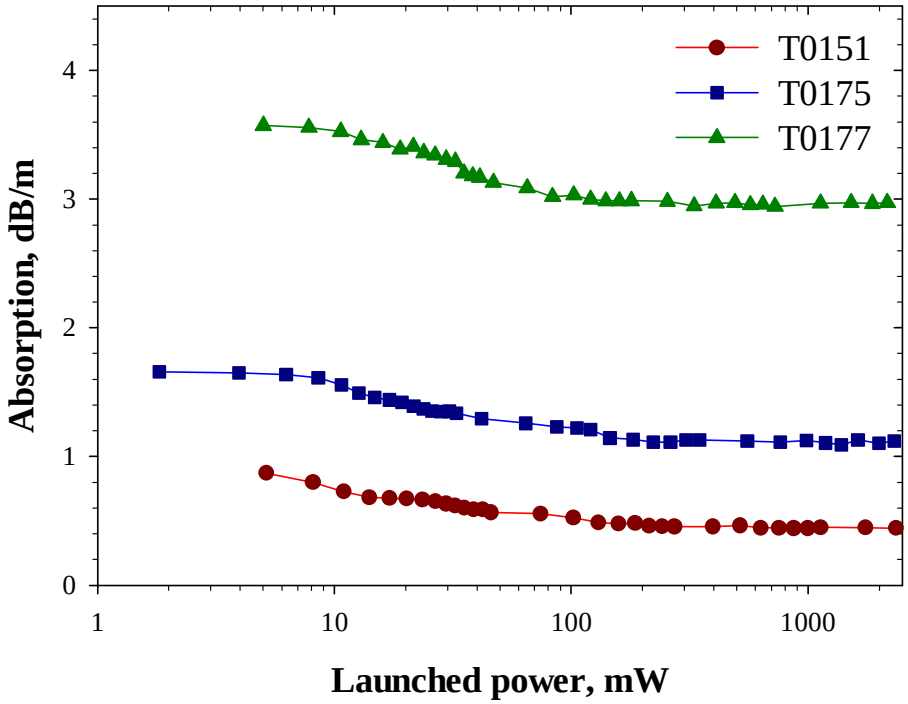

FIGURE 4.15: Averaged optical losses of Bi fibre against launched power at room temperature.

A Bi-doped fibre (T0177) with which laser experiments had failed (detailed in Chapter 5) was investigated, at room temperature. The fibre has a 0.1 NA, 8 μm diameter alumino-silicate core. The core absorption was 3.5 dB/m at 1080 nm. A 1.96 and 0.94 m long fibre was used for the measurement. The unsaturable loss in this fibre was found to be almost 2.9 dB/m at 1080 nm, which was actually 82% of the total Bi induced absorption measured at this wavelength. Such high unsaturable loss would certainly reduce laser performance. It would mean that at least 82% of the absorbed pump photons would fail to excite a Bi ion that would later relax, emitting a longer-wavelength photon, and thus fail to contribute to the generation of emission at 1160 nm. This amount of unsaturable absorption would well exceed that required to prevent us from reaching lasing with the pump

sources available. In conclusion, unsaturable absorption via Bi quenching or inhomogeneity seems to be the reason why this fibre did not operate in a laser configuration.

Another fibre (T0175), with 0.14 NA, 8 μm diameter alumino-silicate core, with lasing efficiency less than 1% was investigated. Core absorption at 1080 nm is 1.7 dB/m. The fibre revealed an unsaturable absorption of 1.1 dB/m which is 64% of the total small signal absorption measured. This number indeed leads to a fibre with poor laser performance.

Fibre T0151 had 0.16 NA, 11 μm core with 1.2 dB/m of core absorption. This fibre shows lower unsaturable absorption as well as background loss. The maximum pump power launched into the fibre was 2.5 W, which was sufficient to saturate the absorption. The unsaturable loss was found to be almost 0.4 dB/m, which is 33% of the total small signal absorption measured at this wavelength, as shown in Fig. 4.15. This fibre had a slope efficiency of 10% with respect to launched pump power in a core-pumped 1160 nm laser configuration. Nevertheless, a 33% unsaturable absorption fraction is not negligible and would contribute to significant background loss at least.

It was observed that the unsaturable loss in Bi-doped fibre decreases at longer wavelengths and at a lower temperature. The unsaturable loss was also measured at wavelength of 1047 and 1090 nm. The unsaturable loss increases at 1047 nm, while at 1090 nm its value decreases. Table 4.4 summarizes the results under different pumping. The unsaturable loss in T0151 at the pump wavelength of 1090 nm was also measured at different temperatures in an attempt to reveal the temperature dependance of unsaturable absorption. The fibre was dipped in water at various temperatures, so as to maintain the same temperature during the entire experiment. The unsaturable loss was proportional to the water temperature as

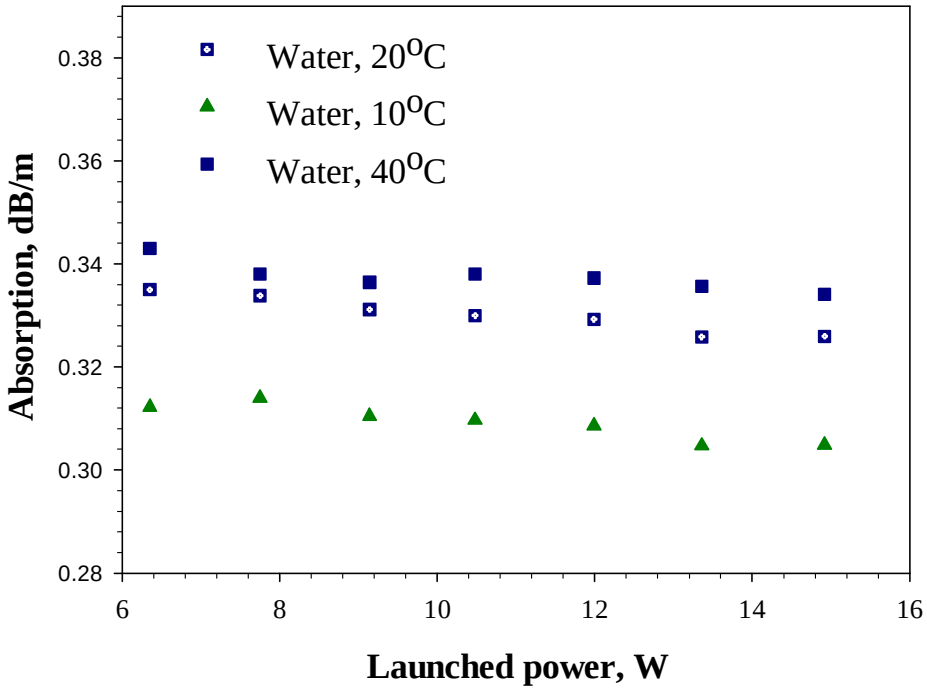

FIGURE 4.16: Measured unsaturable loss at different temperatures.

Core composition	Fibre ID	Wavelength (nm)	Small signal absorption (dB/m)	Unsaturable loss (dB/m)
SiO_2:Al_2O_3	T0037	1080	9.0	8.2
	T0312	1080	0.46	0.4
SiO_2:Al_2O_3:GeO_2	T0151	1047	1.55	1.03
		1080	1.2	0.4
		1090	1.0	0.3
	T0175	1047	2.36	1.99
		1080	1.7	1.1
		1090	1.54	0.86
	T0177	1080	3.5	2.9
		1090	3.2	2.7
SiO_2:GeO_2:P_2O_5	T0220	1080	2.2	2.1

TABLE 4.4: Unsaturable loss in Bi-doped fibres at room temperature

shown in Fig. 4.16. The ratio of unsaturable absorption to small signal absorption was measured as 33, 30 and 28% at 40^{o}C, 20^{o}C and 10^{o}C respectively. Note that no temperature dependence of the small signal absorption was observed, in the wavelength range investigated. This suggests that the reduction in unsaturable loss

at lower temperature can be viewed as a suppression of the unsaturable loss part, in the measured small signal absorption. At this stage, the exact reason of the origin of unsaturable loss and its temperature dependence in the Bi-doped fibre is not fully understood, and further investigation is required. Concentration quenching is unlikely to be the origin of the temperature dependence of unsaturable loss, as no life time shortening of the Bi fibre at different temperatures was observed in the experiment. Thus, the Bi laser efficiency would be improved with an externally forced heat sink, or by pumping the fibre with the wavelength possessing lower unsaturable loss.

4.7 Absorption and emission cross-sections of Bi-doped fibre

The measured values of fluorescence spectrum and decay time was used to determine the absorption (σ_a) and emission (σ_e) cross-sections in the aluminosilicate fibre T0151. The Füchtbauer-Ladenburg relation was used to evaluate emission cross-section spectrum [8]. It is worth noting that the analysis is based on several assumptions which makes it less accurate method for measuring cross sections. To relate absorption and emission cross sections, it assumes that the measured spectra are homogeneously broadened. It also assumes that all of the Stark components are equally populated, or the probability of all transitions between the levels are equal.

The emission cross-section spectra determined are shown in Fig. 4.17, for pump wavelengths of 915, 977 and 1090 nm. We see that the emission cross-sections strongly depend on the pump wavelength. The peak shifts to shorter wavelength and the linewidth becomes broader with shorter pump wavelength. Moreover, the

peak of the cross-sections becomes lower with shorter pump wavelengths. The observed fluorescence linewidth dependence on the pump wavelength indicates a wide site distribution of the active Bi ions. It is worth mentioning that such dependence was not observed in the pump region in 1064 - 1090 nm [9]. The measurement resolution was 1 nm.

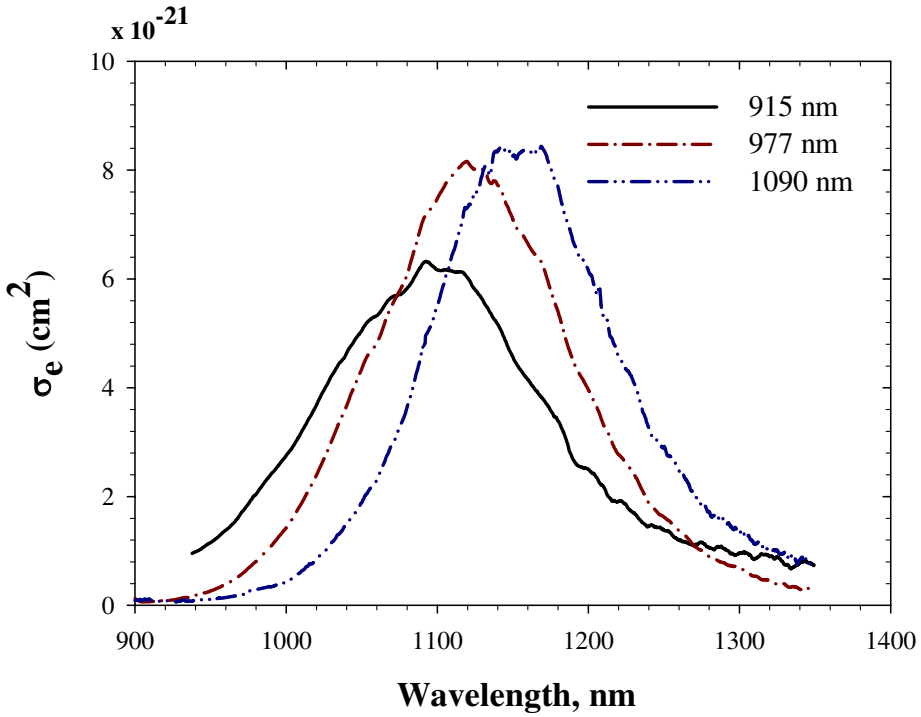

FIGURE 4.17: Measured emission cross-section spectra for T0151.

To determine the absorption cross-section, the saturation intensity, I_{sat}, in the Bi-doped fibre T0151, under 1090 nm pumping was measured. A uniform pump intensity and uniform distribution of active Bi ion across the fibre core was assumed. The saturation in the fluorescence was observed at I_{sat} of $\sim 36\,\mathrm{kW/cm^2}$. Note that the same ratio of unsaturable absorption to the grounds state absorption was assumed in the whole wavelength range for the σ_a calculation. The unsaturable absorption is wavelength dependent. Nonetheless, it was believed that, it would still be instructive to determine σ_a despite the uncertainty. The results are shown in Fig. 4.18.

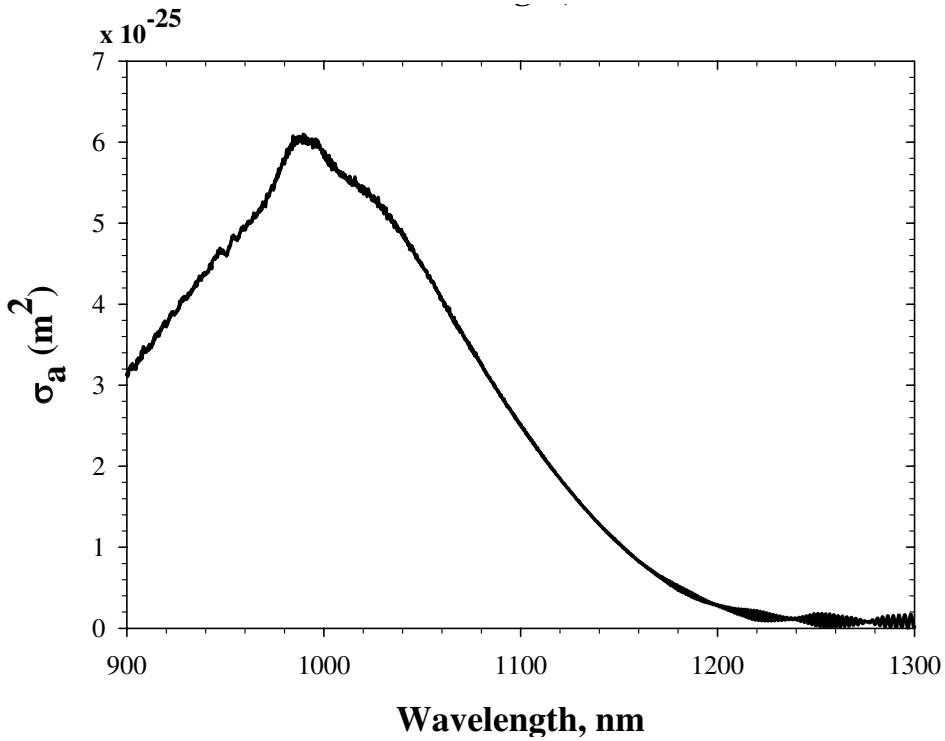

FIGURE 4.18: Measured absorption cross-section spectra for T0151.

4.8 Pump excited state absorption in Bi-doped fibre

Bi-doped fibre lasers operating at 1.15 - 1.21 μm, utilise diode pumped Yb-doped fibre lasers for pumping at the 1080 nm pumping band. However, silicate-based Bi-doped fibres exhibit broad and intense absorption bands, as discussed in section 4.3, which suggest the use of various other pumping wavelengths, in addition to 1080 nm. In particular, high power laser diodes emitting at 808, 915 and 975 nm have good overlap with the absorption bands of Bi-doped fibres. Direct laser diode pumping would make Bi-doped fibres more compact and cost-effective, which makes these wavelengths particularly attractive for pumping. At these wavelengths, laser diodes are commercially available with more than 100 W of output power and with unmatched brightness. However, it was observed that in case of 915 and 975 nm pumping, the fibre did not lase with sufficiently long fibre length

to absorb essentially all the pump power. Detailed characteristics of Bi-doped fibre under 915 and 975 nm pump will be given in Chapter 4. It seems there are problems to be overcome to allow efficient operation at those wavelengths. The performance of fibre lasers and amplifiers can be considerably impaired by undesired effects such as unsaturable absorption and excited state absorption (ESA) [6, 10]. In fact, the unsaturable absorption at the pump wavelength of 1080 nm has been revealed as a main limitation of the efficiency of Bi-doped fibre lasers, as described in section 4.6. ESA at pump wavelengths is also detrimental because it typically absorbs the pump power without exciting any ions into the meta-stable state. Hence, pump-ESA should be avoided (as should ESA at the emission wavelength).

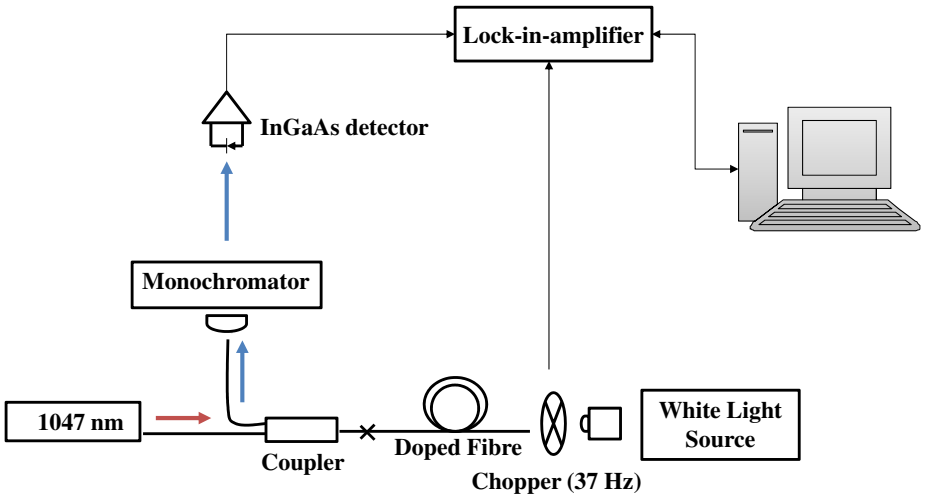

FIGURE 4.19: Experimental arrangement for ESA measurement.

Fibre T0151 was chosen to reveal the existence of the ESA by measuring change in transmission with and without bleaching the ground state population. The fibre was fabricated by the modified chemical vapor deposition and solution doping technique in an alumino-germano-silicate host. The properties of a Bi-doped fibre critically depend on the fibre compositions or fabrication processes, and fibre with different host materials by different fabrication process would show different properties. However the compositions of the fibre under investigation are close to

other Bi-doped fibres used for laser operations. The fibre lased at 1160 nm with 10% of slope efficiency with respect to the launched pump power in a linear cavity with 100% and 4% feedback in its two ends. The detailed results will be discussed in Chapter 4. The ESA in the 900 - 1250 nm wavelength range for the fibre, under 808 and 1047 nm pumping was investigated.

The experimental arrangement is shown in Fig. 4.19. The change in transmission in the Bi-doped fibre was measured, as the 1047 nm pump was switched on and off. For this, a probe beam from a white light source was chopped at 37 Hz and launched into the Bi-doped fibre. Following transmission through the Bi-doped fibre, the probe beam was passed through a monochromator with 2 nm resolution and collected by an InGaAs detector. A lock-in amplifier was used to select only the probe component at the 37 Hz modulation frequency. For pumping, CW light at 1047 nm from a fibre-coupled Nd:YLF laser, was injected into the Bi-doped fibre at the probe output end, through a wavelength-selective fused fibre coupler.

Initially, to verify the experimental set up, a standard single mode fibre (SMF28) was tested in both pumped and un-pumped condition. It was observed that the transmission was identical for the two cases (Figure 4.20).

The transmission through the Bi-doped fibre between 900 and 1300 nm was measured both pumped and un-pumped condition to obtain the ESA. When pumped, the power of the transmitted probe changed, with a larger change for a larger pump power. Above 100 mW of launched pump power, saturation in the transmitted probe power was observed.

Furthermore, the small signal ground state absorption (GSA) spectrum was determined by cutting back the fibre from 2.7 m to 1 m, and measuring the transmission with the pump off. The measured GSA well agreed with the same measurement done with an optical spectrum analyser and a white light source configuration

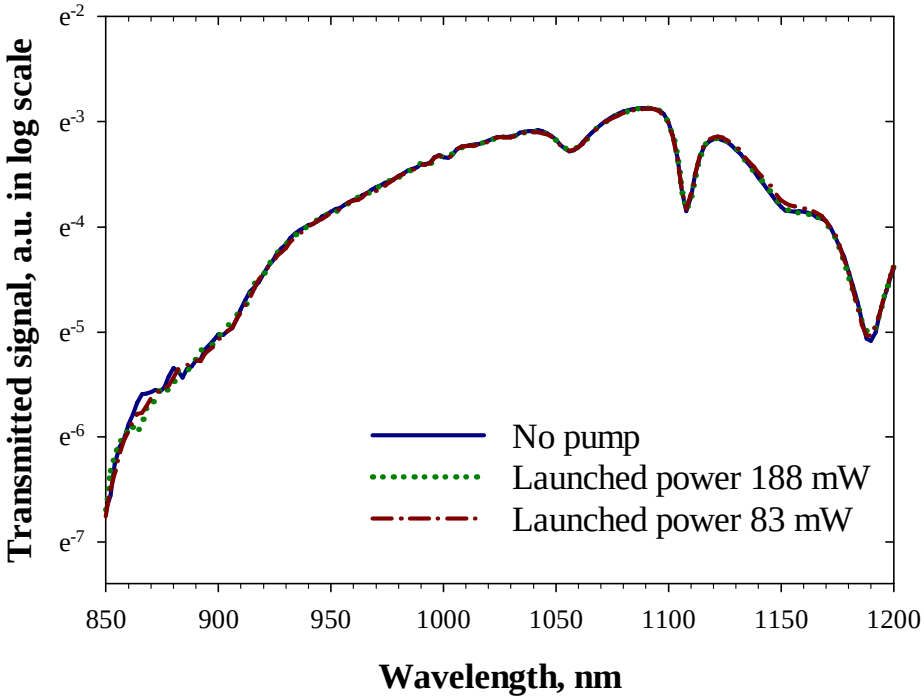

FIGURE 4.20: Changes in transmitted signal with and without pump in a SMF28 fibre.

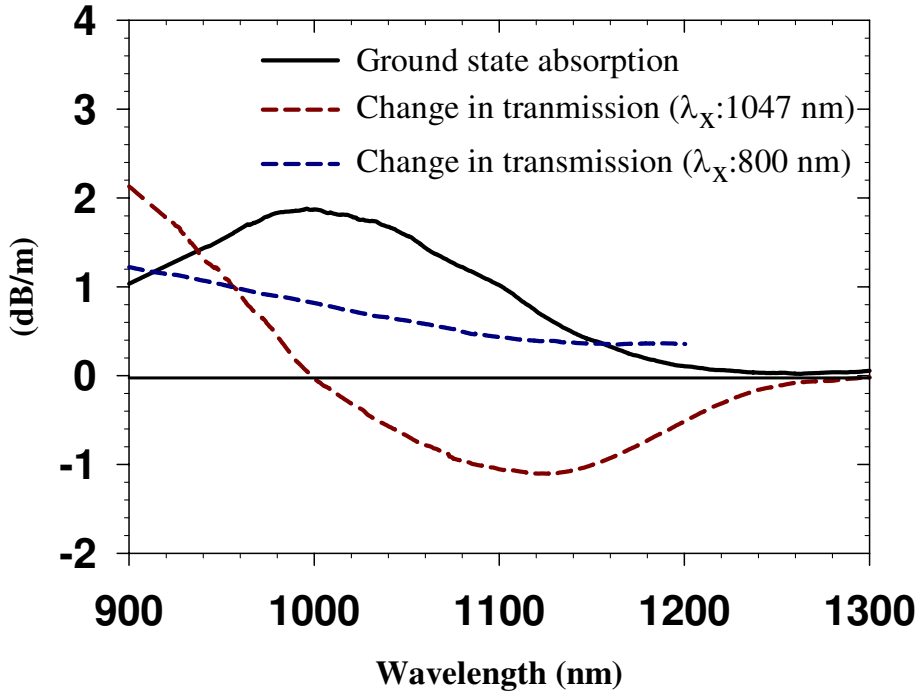

FIGURE 4.21: Measured ground state absorption and changes in transmission in Bi-doped fibre.

within 5% difference in dBm. The GSA and change in the transmission are shown in Fig. 4.21. The change in the transmission can be expressed in logarithmic units per unit length as [11]:

$$\Delta\alpha = -\frac{1}{L}\ln\left(\frac{T_{on}}{T_{off}}\right) = N'(\sigma_{esa} - (\sigma_{gsa} + \sigma_e)) \tag{4.7}$$

where L is a fibre length, T_{on} and T_{off} are white light transmission (linear units) with pump on and off, respectively, N' is a constant accounting for the overlap between the signal and the population in the excited state, and σ_{esa}, σ_{gsa}, and σ_e are cross-sections of excited state absorption, ground state absorption, and emission, respectively. Equation 4.7 suggests that the ESA is dominant over the sum of σ_{gsa} and σ_e when the change is negative, i.e., when the transmission decreases when the pump is turned on. Strong ESA is observed in the 900 - 1000 nm range, growing towards shorter wavelengths, as shown in Fig. 4.21. On the contrary, the pumping band at $\sim$ 1080 nm as well as the Bi emission band, $\sim$ 1160 nm, shows a negative change, i.e., the transmission increases with larger pump powers. A ratio of ESA to GSA cross-section (σ_{esa}/ σ_{gsa}) was calculated at 915 and 976 nm from the figure. Comparing the spectral shapes of ((σ_{gsa}+ σ_e)- σ_{esa}) and (σ_{gsa}+ σ_e), there is no significant distortion around the fluorescence peak, which indicates negligible ESA at the peak emission wavelength. The N' in equation 4.7 was then calculated at the peak wavelength and finally the cross-section spectrum for excited state absorption (Fig. 4.22) was determined. The ratio of the ESA to GSA cross-sections becomes 7.97 and 2.48 at 915 nm and 975 nm, respectively, while the ESA is nearly negligible at 1080 nm and in the laser emission band of the Bi-doped fibre laser. No change in ESA at lower temperature, when water cooled at 15^{o}C, was observed as shown in Fig. 4.23. It is worth mentioning here that, unlike ESA, unsaturable loss depends on the external temperature.

The influence of the pump ESA at 915 and 975 nm on the performance of the

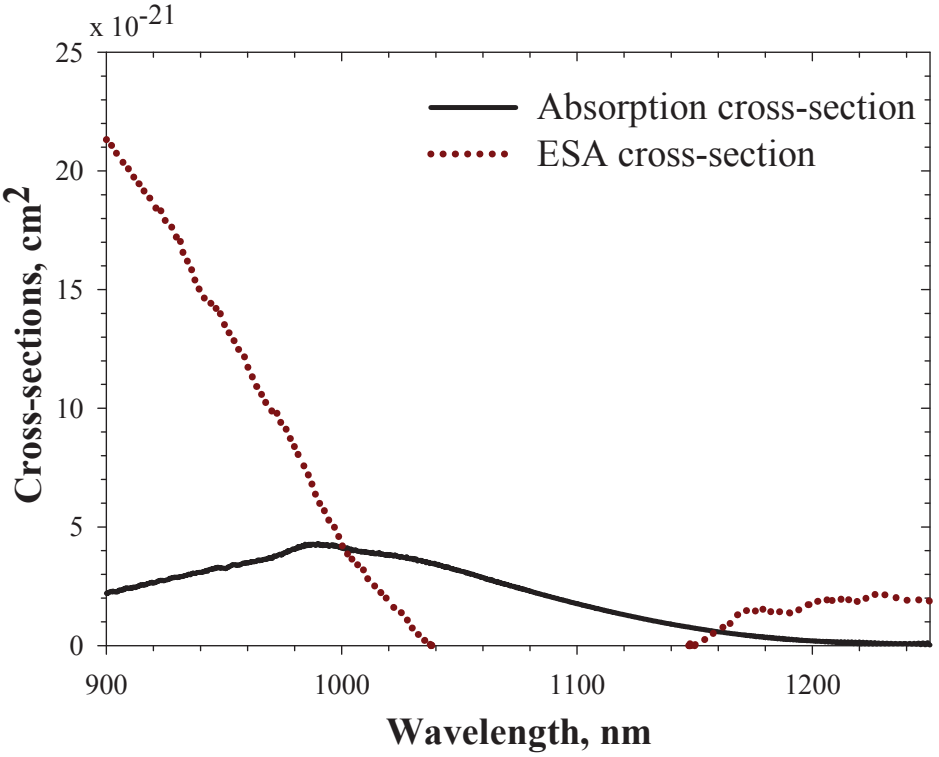

FIGURE 4.22: Measured GSA and ESA cross-section spectra.

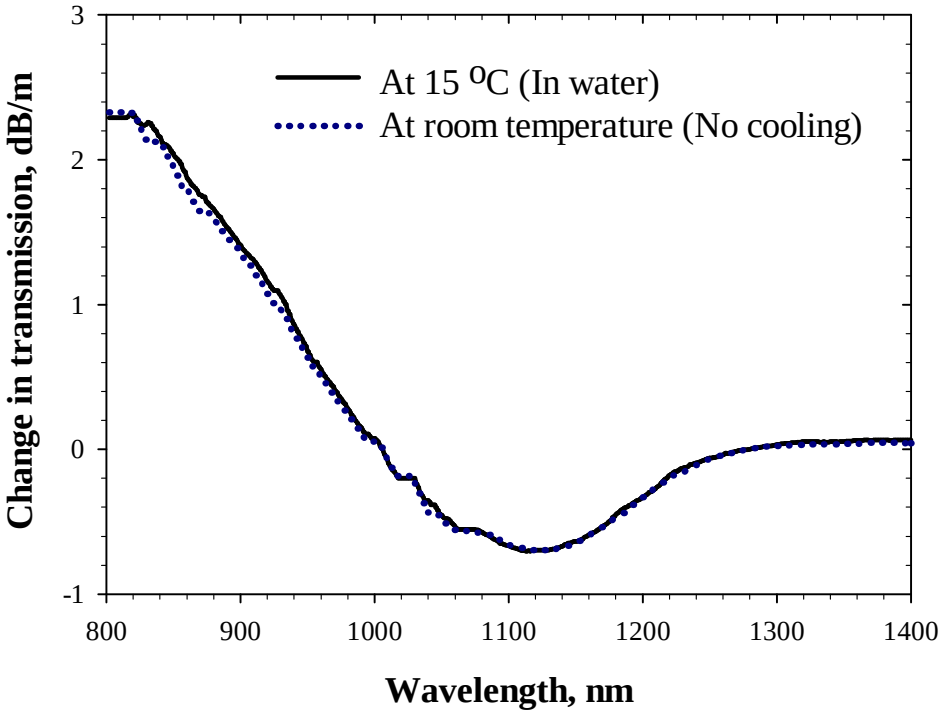

FIGURE 4.23: Dependance of ESA on temperature.

1160 nm Bi-doped fibre laser was estimated using simulation. The energy transitions between pump and signal was assumed as those of Yb^{3+} in a glass [12], with an additional upper excited state level accounting for the ESA. It was also assumed that the population in the upper excited state level is negligible due to rapid decaying to the meta-stable level and signal ESA was ignored. The rate equations become:

$$\frac{dn_2}{dt} = -\frac{dn_1}{dt} = \left(\frac{\sigma^p_{gsa} I_p}{h\nu_p} + \frac{\sigma^s_{gsa} I_s}{h\nu_s}\right) n_1 - \left(\frac{\sigma^p_e I_p}{h\nu_p} + \frac{\sigma^s_e I_s}{h\nu_s} + \frac{1}{\tau}\right) n_2 \tag{4.8}$$

where n_1 and n_2 are the populations in the ground state and meta-stable state, and the total population, n, is equivalent to $(n_1{+}n_2)$. Furthermore, σ^p_{gsa} and σ^p_e are ground state absorption and emission cross-sections for the pump wavelength, σ^s_{gsa} and σ^s_e are the corresponding values for the signal wavelength. In addition, I_p and I_s are pump and signal intensities, h is Planck's constant, ν_p and ν_s are pump and signal frequencies, and τ is the lifetime of the meta-stable state. For simplicity, it was assumed that the pump and signal propagate in the fundamental mode of the fibre. Furthermore, I_p and I_s are simplified as $I_p = \Gamma_p(P_p/A)$, $I_s = \Gamma_s(P_s/A)$, where P_p and P_s are pump and signal powers, A is the area of doped region in the core, and Γ_p and Γ_s are pump and signal overlap factors.

The signal and pump power propagation through the fibre in the presence of the pump ESA will be given by:

$$\begin{aligned} \frac{dP^{\pm}_p}{dz} &= \Gamma_p\left((\sigma^p_e - \sigma^p_{esa})n_2 - \sigma^p_a n_1\right) P^{\pm}_p - \alpha_p P^{\pm}_p \\ \frac{dP^{\pm}_s}{dz} &= \Gamma_s\left(\sigma^s_e n_2 - \sigma^s_a n_2\right) P^{\pm}_s - \alpha_s P^{\pm}_s \end{aligned} \tag{4.9}$$

where α_p and α_s are the loss at pump and signal wavelengths. The signs depend on the direction of propagation. A linear laser cavity with feedback of 100% in one end and 4% in the other, out-coupling end, was assumed. The pump

was launched to the 4% feedback end. The unsaturable absorption was treated as a background loss. The concentration of active Bi ions was calculated to ∼ 8.3X10^{24} m^{-3} from the measured GSA and cross-section. The fibre lengths were optimized for the maximum output signal power. For 1080 nm pumping, 25 m length was used to match the experimental results (Chapter 4), however, the 25 m fibre length is close to the optimised length (22 m). The output signal power was calculated for up to 2.1 W of pump power according to the laser experiments. In addition, 1 dB of signal and 2 dB of pump losses were included for the calculation of 1080 nm pumping to match the experimental condition. These additional losses arose from imperfection of the wavelength division multiplexing (WDM) coupler. For comparison, the laser performance under 975 nm pumping without ESA was also calculated. Figure 4.24 shows the calculated laser performances. The model well describes the experimental results by 1080 nm pumping. Thus, the ESA at specific wavelength is independent of the excitation wavelength as long as they excite to the same meta-stable level. In addition, the laser efficiency is indeed under the influence of the pump ESA ($\sigma_{esa}/\sigma_{gsa}$). Under 975 nm pumping, the signal output power, limited to ∼ 0.02 W due to the pump ESA, could otherwise be more than 0.5 W. The high ESA strength together with low emission cross-section did not allow the Bi-doped fibre to oscillate under 915 nm pumping within the given pump power level. It should be noted that the impact of the pump ESA can be mitigated by reducing a population inversion factor. An average population inversion factor for the 975 nm pumping is ∼ 0.6 when 2.1 W of pump power is launched to 8 m Bi-doped fibre, but it can be reduced to ∼0.3 by replacing the 4% feedback end with 50%. Consequently, the output power can reach ∼0.13 W at the maximum pump power (See Fig. 4.24). It should be noted that cladding pumping usually generates lower inversion. In addition, for Bi-doped fibre amplifiers, bi-directional pumping would be more efficient than co-directional pumping for the ESA pumping band as found in the Er-doped fibre amplifiers at 800 nm pumping

band [10]. No other pump loss mechanism was considered in the calculation such as cooperative upconversion.

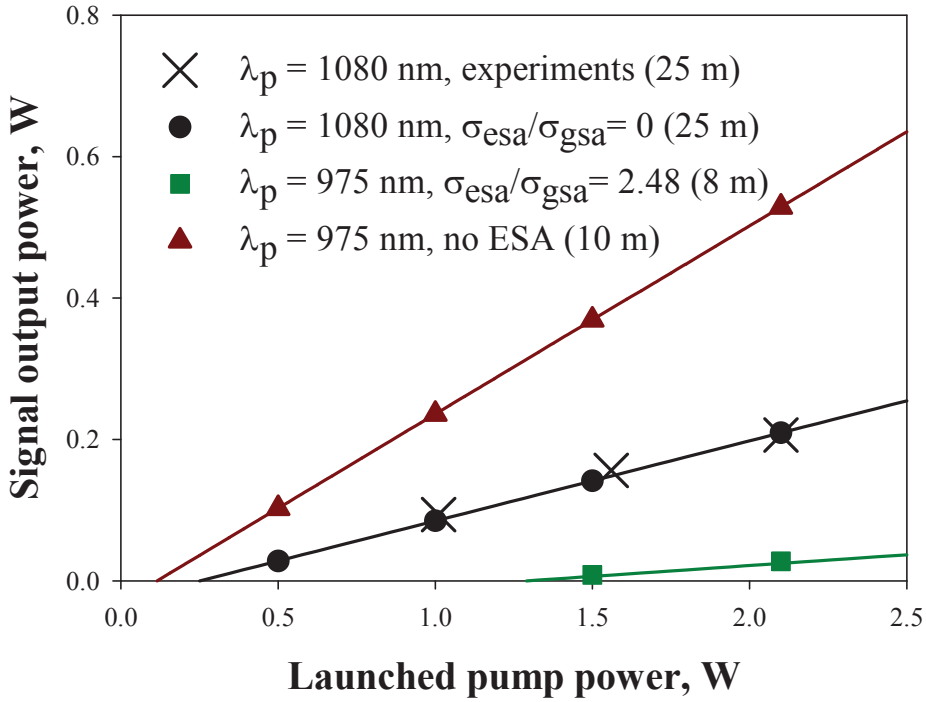

FIGURE 4.24: Influence of pump ESA on Bi-doped fibre laser performance (Numbers in parenthesis are fibre lengths used for the calculation).

ESA under 800 nm pumping was also measured with the same Bi-doped fibre used before. The fibre coupler in Fig. 4.19 was replaced with a dichroic mirror (DM). The DM has high reflection at 900-1200 nm and high transmission at 800 nm. A 800 nm Ti:Sapphire laser was used as a pump source. It seems that the signal saturates over 144 mW of launched power. The change in the transmission is shown in Fig. 4.21. Under 800 nm pumping, the ESA is seen to be dominant all over the wavelengths investigated including the Bi emission band. Although the curve of transmission change did not extend to 800 nm, because of the limitation in the DM that covers the 900 nm to 1200 nm range, an increase in absorption at stronger pump power suggested the presence of ESA at 800 nm. The signal ESA on top of the pump ESA makes 800 nm pumping less promising.

In conclusion, pump ESA has been measured in the 900 - 1300 nm range under 1047 nm pumping. A strong ESA was observed at 915 and 975 nm, whereas no significant ESA was found in the 1080 nm pumping band nor in the primary emission band of Bi-doped fibre lasers. The ratio of the ESA to GSA cross-sections at 915 nm and 975 nm becomes 7.97 and 2.48 respectively, while the ESA is nearly negligible at 1080 nm pump band. The measurement under 800 nm pumping revealed strong ESA from 900 - 1200 nm. The pump ESA together with the observed signal ESA would limit the efficiency of the Bi-doped fibre laser under 800 nm pumping. From these results, it can be concluded that 1080 nm is the ideal pump band for Bi-doped silicate fibre lasers and amplifiers.

4.9 Post fabrication treatment of Bi-doped fibres

In recent years, significant research has been carried out on the spectroscopic properties of Bi-doped fibre fabricated by the MCVD technique, with various glass compositions. However, the origin of the luminescent center responsible for the Bi-emission is still unclear. In addition, improvement in the lasing efficiency of the Bi-doped fibre laser is necessary for possible practical applications. It is therefore interesting to investigate the dependence of the luminescence properties of Bi-doped fibre on external influences. A recent study on the influence of high temperature annealing and hydrogen-loading then annealing showed that Bi-related luminescence is very sensitive to the annealing process [13]. Peng et al. reported an increase in absorption and emission intensities with increasing average pulse energies in bismuthate glass by femtosecond laser irradiation at 800,nm [14].

In this section, the spectroscopy of Bi doped pristine, H_2-loaded, ultra violet (UV)-irradiated and H_2-loaded UV-irradiated preforms will be discussed. Also, the influence of H_2-loading on the spectroscopic properties of a Bi-doped fibre will be compared to pristine fibre.

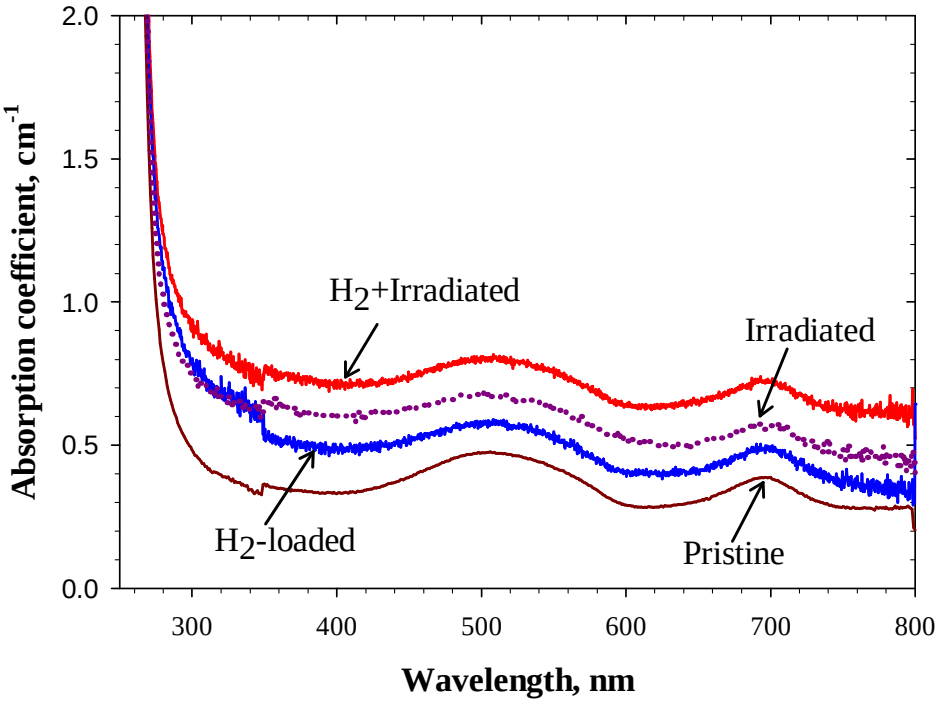

FIGURE 4.25: Absorption measurement for pristine, H_2-loaded, UV irradiated and H_2-loaded UV irradiated Bi prefrom.

The preform under investigation was fabricated by MCVD and the solution doping technique with a core glass composition of Al:SiO_2. The preform was hydrogen loaded following typical condition for the fibre Bragg grating fabrication and was kept in H_2 atmosphere at 70^{o}C for four days, under the pressure of 190 atm. A fluence of 10 kJ/cm^2 for 244 nm UV exposure was used for the measurement. The absorption in the preform was measured following the procedure outlined in section 4.3. Fig. 4.25 shows the absorption dependance of the Bi preform L30117 on different external conditions: H_2-loaded, UV irradiated and H_2-loaded UV irradiated. It was observed that absorption increases for H_2-loaded, irradiated and H_2-loaded irradiated samples respectively.

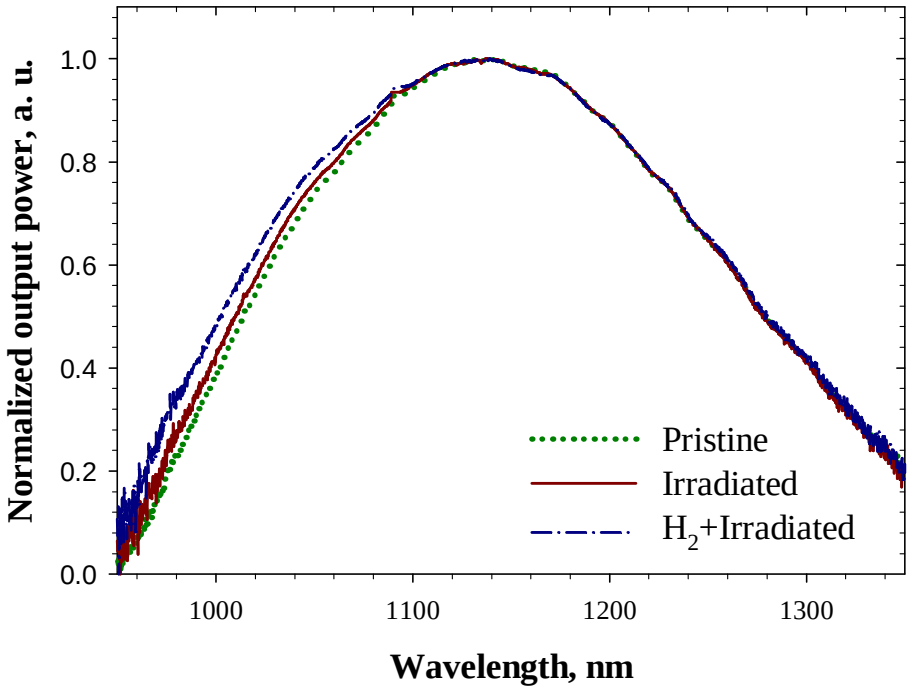

FIGURE 4.26: Fluorescence measurement for pristine, UV irradiated and H_2-loaded UV irradiated Bi preform.

The fluorescence for the preform samples were also measured. The plot (Fig 4.26) shows the normalised fluorescence curve. The fluorescence was slightly broader in case of H_2-loaded fibre.

Fibre T0175 drawn from the same preform was H_2-loaded using similar conditions. No index change was observed due to H_2-loading of the fibre. The small signal absorption in the fibre was measured by the standard cut-back technique, using a white light source and an optical spectrum analyser and the background loss was measured at 1285 nm. The measured absorption spectra in the wavelength region of 800 - 1400 nm, for the pristine and H_2-loaded fibre are shown in Fig. 4.27. The small signal absorption at 1090 nm for the pristine and H_2-loaded fibre was 1.5 and 2.2 dB/m respectively. The peak around 900 nm in the hydrogen loaded fibre accounts for water peak. A small peak around 980 nm indicates possible contamination from Yb ion. The corresponding background loss at 1285 nm was 60 and 90 dB/km for the pristine and H_2-loaded fibre. The unsaturable losses in both

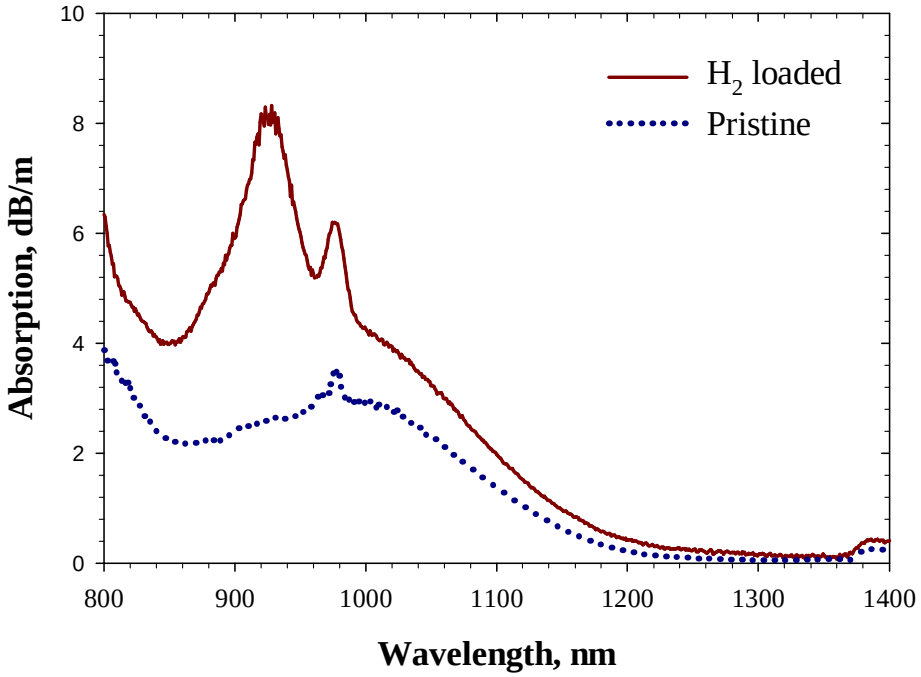

FIGURE 4.27: Absorption spectrum of H_2-loaded and pristine Bi-doped Al:SiO_2 fibre.

the fibres were measured at the pump wavelength of 1090 nm. The unsaturable loss remains unchanged after the H_2-loading. Thus, the ratio of unsaturable absorption to small signal absorption reduced from 64 to 45% after the H_2-loading.

The fluorescence spectrum was collected from the side of the fibre using a multi-mode fibre and measured with an OSA. A 1090 nm GT Wave Yb-doped fibre laser was used as an excitation source. All measurement was carried out at room temperature. No change in fluorescence shape, under 1090 nm pump wavelength, was observed due to H_2-loading. However, enhancement of emission after the H_2-loading was reported in [15]. The fluorescence decay time from the fibres were also measured. The decay time became significantly shorter after the H_2-loading. The measured decaying times are shown in Fig. 4.28. The decay times are $\sim 750\,\mu$sec in the pristine fibre, but it drops to $\sim 290\mu$sec in the H_2-loaded fibre. It appears that the active Bi ions are quenched by the loaded hydrogen [16]. The laser performances of the fibres were tested in a ring cavity with 2% output coupling. With a

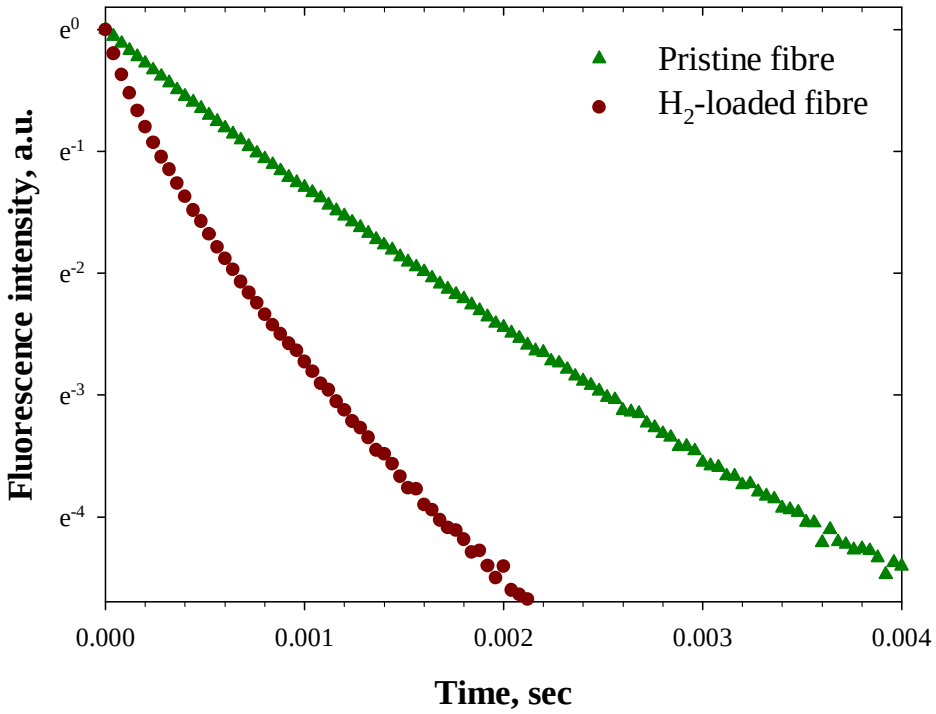

FIGURE 4.28: Fluorescence decay in a pristine fibre and H_2-loaded fibre.

15 m long pristine fibre, when pumped at 1090 nm, the oscillation at 1178 nm was observed, but the efficiency was less than 1%, due to high unsaturable loss present in the fibre. The detailed results will be described in Chapter 5. The H_2-loaded fibre, when tested in the same setup, failed to lase, with 6 W of available pump power. The fibre length was 12 to 15 m, allowing 15 to 20 dB pump absorption, in laser configuration. Hence, the results suggest that although the H_2-loading may increase the fluorescence intensity [15], the quenching of the Bi ions by the hydrogen eventually limits the laser performance. The H_2-loaded fibre was then placed in an oven at 100^{o}C for 24 hrs to outgas the excess H_2 from the loaded fibre. The post-annealed fibre showed lasing action at 1179 nm, with slope efficiency approximately the same as the untreated fibre. The inhibition of laser action can be attributed to the quenching of Bi ions by molecular hydrogen that shortens the radiative lifetime. It was observed that the post annealed fibre recovers the lifetime of pristine fibre and restore the laser device performance.

4.10 Conclusions

In this chapter basic characterisation and spectroscopic properties have been presented for Bi-doped preform and fibre in various silica based hosts. Absorption and fluorescence characteristics of the Bi-doped fibre have been examined and found to be strongly dependent on the pump wavelength and host material. The use of silica doped with P seems to shift the luminescence spectra to a longer wavelength. The Bi-doped fibre fabricated by PIT technology, which is a non chemical vapor deposition process, shows significant change in luminescence, as compared to Bi-doped fibres fabricated by the MCVD process. Emission decay lifetimes were measured in Bi-doped fibres. The deviation from single exponential in Bi-doped fibre suggests that the Bi ions responsible for emission sits on different sites. Presence of unsaturable loss and its temperature dependance was revealed and investigated. The ESA in Bi-doped fibres were measured in the 900 - 1300 nm range under 1047 nm pumping. A strong ESA appeared at 915 and 975 nm, whereas no significant ESA was found in the 1080 nm pumping band nor in the primary emission band of Bi-doped silicate fibre lasers. The strength of the ratio of the ESA to the GSA was stronger in 915 nm than in 976 nm. The measurement under 800 nm pumping revealed strong ESA from 900 - 1200 nm. The presence of ESA at 800 nm was inferred. The pump ESA together with the observed signal ESA would limit the efficiency of the Bi-doped fibre laser under 800 nm pumping. The spectral shape of the emission cross-section depends on the pump wavelength, and the emission cross-section peak reduced under 915 and 975 nm pumping. Thus, the pump ESA together with the weak emission cross-section would limit the efficiency of the Bi-doped fibre laser under 915 and 975 nm pumping. It was also suggested to reduce the population inversion factor to mitigate the impact of the pump ESA. The dependence of spectral characteristics in Bi alumino-silicate preform and fibre on different external treatment was investigated. The absorption in

H_2-loaded fibre seems to increase but the excess molecular hydrogen can result in fluorescence quenching and a shortening of the radiative lifetime, which adversely affects the laser performance.

To conclude, the behaviour of Bi-doped fibre is found to be strongly dependant on their host material. The emission characteristics including fluorescence spectra and lifetimes are dependant on the wavelength of excitation. In addition, the deleterious effects of unsaturable loss and excited state absorption can be controlled by careful choice of pumping wavelength. Unsaturable loss can also be controlled by external cooling of the fibre as unsaturable loss decreases at lower temperature.

References

[1] Y. Fujimoto and M. Nakatsuka, "Infrared luminescence from bismuth-doped silica glass," *Japanese Journal of Applied Physics* **40**(3B), pp. L279–L281, 2001.

[2] J. C. Phillips, "Stretched exponential relaxation in molecular and electronic glasses," *Reports on Progress in Physics* **59**(9), pp. 1133–1207, 1996.

[3] M. Grinberg and K. Holliday, "Luminescence kinetics and emission lifetime distribution of Cr^{3+}-doped aluminosilicate glass," *Journal of Luminescence* **92**(4), pp. 277 – 286, 2001.

[4] M. Grinberg, D. L. Russell, K. Holliday, K. Wisniewski, and C. Koepke, "Continuous function decay analysis of a multisite impurity activated solid," *Optics Communications* **156**(4-6), pp. 409 – 418, 1998.

[5] M. Grinberg, K. Wisniewski, C. Koepke, D. L. Russell, and K. Holliday, "Luminescence and luminescence kinetics of chromium doped gahnite glass ceramics," *Spectrochimica Acta Part A: Molecular and Biomolecular Spectroscopy* **54**(11), pp. 1735 – 1739, 1998.

[6] R. Paschotta, J. Nilsson, A. Tropper, and D. Hanna, "Ytterbium-doped fiber amplifiers," IEEE *Journal of Quantum Electronics,* **33**(7), pp. 1049 –1056, 1997.

[7] M. K. Davis, M. J. F. Digonnet, and R. H. Pantell, "Characterization of clusters in rare-earth-doped fibers by transmission measurements," *Journal of Lightwave Technology* **13**(2), pp. 120–126, 1995.

[8] W. Barnes, R. Laming, E. Tarbox, and P. Morkel, "Absorption and emission cross section of Er^{3+} doped silica fibers," IEEE *Journal of Quantum Electronics* **27**, pp. 1004 –1010, apr 1991.

[9] V. V. Dvoyrin, V. M. Mashinsky, and E. M. Dianov, "Efficient bismuth-doped fiber lasers," IEEE *Journal of Quantum Electronics* **44**(9-10), pp. 834–840, 2008.

[10] S. Zemon, B. Pedersen, G. Lambert, W. Miniscalco, L. Andrews, R. Davies, and T. Wei, "Excited-state absorption cross sections in the 800-nm band for

Er-doped, Al/P-silica fibers: Measurements and amplifier modeling," IEEE *Photonics Technology Letters* **3**(7), pp. 621 –624, 1991.

[11] J. E. Román, M. Hempstead, C. Ye, S. Nouh, P. Camy, P. Laborde, and C. Lerminiaux, "1.7 μm excited state absorption measurement in erbium-doped glasses," *Applied Physics Letters* **67**(4), pp. 470 –472, 1995.

[12] E. M. Dianov, A. V. Shubin, M. A. Melkumov, O. I. Medvedkov, and I. A. Bufetov, "High-power cw bismuth-fiber lasers," *Journal of the Optical Society of America B* **24**, pp. 1749–1755, 2007.

[13] V. G. Truong, L. Bigot, A. Lerouge, M. Douay, and I. Razdobreev, "Study of thermal stability and luminescence quenching properties of bismuth-doped silicate glasses for fiber laser applications," *Applied Physics Letters* **92**(4), 2008.

[14] M. Y. Peng, Q. Z. Zhao, J. R. Qiu, and L. Wondraczek, "Generation of emission centers for broadband nir luminescence in bismuthate glass by femtosecond laser irradiation," *Journal of the American Ceramic Society* **92**(2), pp. 542–544, 2009.

[15] C. Ban, L. Bulatov, V. Dvoyrin, V. Mashinsky, H. Limberger, and E. Dianov, "Infrared luminescence enhancement by UV-irradiation of H_2-loaded Bi-Al-doped fiber," in *35th European Conference on Optical Communication,* ECOC *2009*, pp. 1 –2, 20-24 2009.

[16] J. D. Prohaska, D. P. Machewirth, and E. Snitzer, "Quenching of neodymium fluorescence by molecular hydrogen," *Optics Letter* **20**(7), pp. 719–721, 1995.

Chapter 5

Bi-doped fibre laser and amplifier

5.1 Introduction

Fibre lasers and amplifiers are very attractive candidates for many practical applications due to its compactness, robustness, well controlled beam shape, thermal management and simplicity. In recent years these outstanding properties of fibre laser has been exploited by incorporating various rare earth dopants such as Yb, Nd, Er and Tm to develop sources with broad wavelength tunability and multi-watt to kilo-watt level performance in the 1, 1.5 and 2 μm spectral regimes [1]. However, the development of high power fibre based sources in wavelengths outside these spectral bands is quite demanding. Particularly, there is a growing interest in finding efficient laser sources or amplifiers in the wavelength region of 1100 - 1500 nm, in order to extend the usable spectral range to the second telecommunication window, which is also the zero dispersion wavelength region of silica fibre. The creation of fibre laser and amplifier at this spectral region is important for many applications such as optical communications, medicine and astrophysics etc. Moreover, a fibre amplifier operating around 1179 nm is attractive for applications

requiring narrow line width, such as coherent beam combination and efficient frequency doubling to yellow. This chapter presents the development of a Bi-doped fibre sources at the wavelength region of 1179 nm.

Laser action in Bi-doped fibre is challenging to achieve both from a fabrication and a spectroscopic point of view. In order to investigate the underlying mechanism and to modify the fibre design to improve the fibres and fibre lasers, a study was initiated. At the same time, improvements in the fabrication process and an investigation of the influence of host compositions has also been carried out. This is indeed one of the important processes in a fibre laser development project, and is also followed in the development of Bi-doped fibre laser.

Chapter 3 shows that Bi has a large number of absorption bands in the visible and near infrared regions of the spectrum. This allows a variety of pump sources to be employed in the study of Bi-doped fibre. This work includes a 915 nm Axcel Photonics laser diode, a JDS Uniphase laser diode at 977 nm with a maximum output power of 200 and 450 mW respectively. A 1080 nm Yb-doped fibre laser (GTWave) with an output power of 3 W was also used for core pumping. For cladding pumping the pump sources were 915 and 960 nm fibre pigtailed PUMA with a maximum output power of 25 and 15 W respectively. An 808 nm laser diode from Apollo Instruments Inc., with a pump power of 20 W was also used.

In this Chapter, laser experiments with fibres of different compositions are discussed in detail. In sec. 5.2 initial investigation on Bi-doped fibre laser were carried out either in cladding-pumping or core-pumping schemes. Fibres were tested with different pump sources to assess the influence of pump wavelength. In sec. 5.3, continuous wave lasing operation at 1160 and 1179 nm with 25 m long Bi-doped fibre is described; when core pumped at 1080 nm wavelength band. The impact of unsaturable loss on Bi laser performances and the intricacy of increasing Bi

concentration for reducing fibre length is discussed. Furthermore, an opportunity to extend the pump band for the Bi-doped fibre laser was investigated by measuring the emission at 977 nm pump wavelength. The fibre laser dependance on different cooling arrangements are discussed in sec. 5.4. Effective heat extraction can reduce the temperature dependant unsaturable loss in the fibre, resulting in increased laser performance. In sec. 5.5 the operation of Bi-doped fibre amplifier at 1179 nm, in both low and high input signal regime, was examined. The amplifier efficiency and the saturation power both depend on the effective fibre cooling.

5.2 Initial investigation of Bi-doped fibre lasers

The first preform was fabricated with 5 gm of $BiCl_3$ in a 200 ml solution with a host glass composition of Al_2O_3:SiO_2. The NA of the core is 0.10. It was pulled into four different fibres, two with high index coating L3003101 and T0037, and the other two with low index coating L3003102 and L3003103 respectively. L3003101 and L3003103 show poor luminescence possibly due to high background loss and were abandoned.

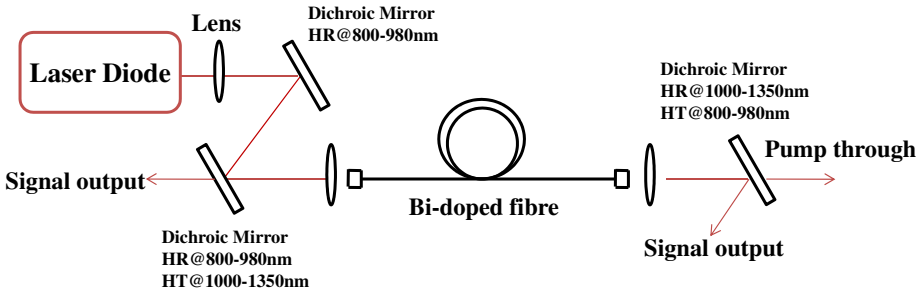

FIGURE 5.1: Schematic diagram of the cladding pumped laser configuration.

The laser setup used for basic laser characterisation in the cladding pumped regime is shown in figure 5.1. Fibre L3003102 was pumped with a 960 nm fibre pig-tailed, multi mode laser diode through a combination of collimating lenses and dichroic

mirrors such that 77% of the pump power could be launched into the fibre. A linear laser cavity was formed between perpendicularly cleaved end facets of the fibre, providing 4% Fresnel reflections. Two types of dichroic mirrors were used for separating the pump from the signal. The efficiencies of the Bi-doped fibre with different lengths were measured in order to find an optimum length. The signal output was measured at both ends of the fibre, and the pump throughput was also measured. In Fig. 5.2 the emission from a 20 m long fibre with an absorbed pump power of 9 W is presented. The 4% - 4% cleaved-bare facet configuration failed to overcome the threshold of the fibre, possibly due to high background loss(>1000 dB/km at 1100 nm). In order to achieve lasing, the throughput end was butt coupled to a high reflecting dichroic mirror in order to decrease the cavity loss. Still, however, threshold could not be reached.

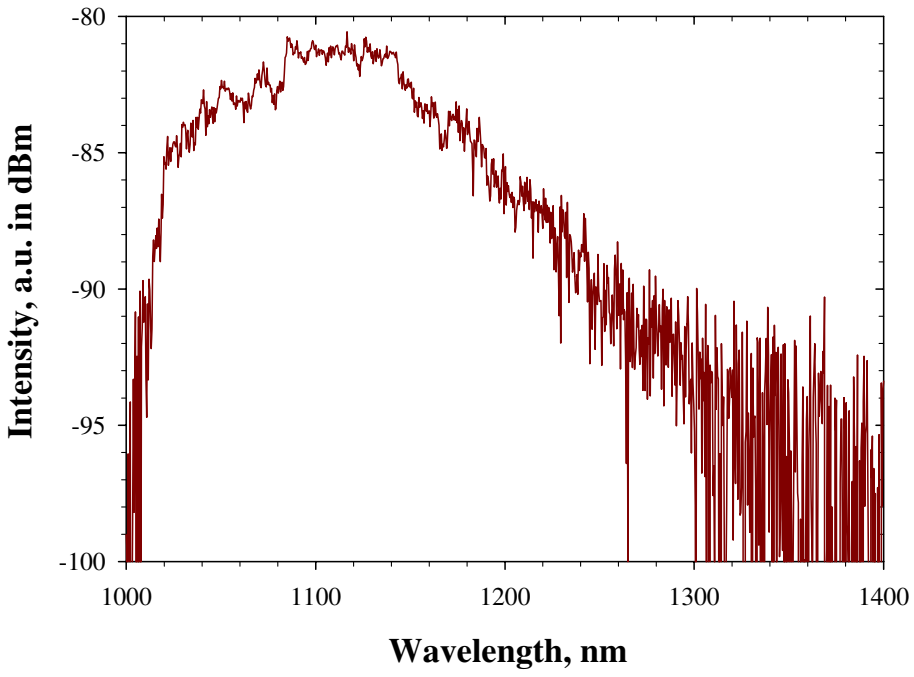

FIGURE 5.2: Longitudinal emission spectrum from fibre L3003102 cladding-pumped at 960 nm (Fibre length: 20 m, pump power: 15 W).

The same fibre was also tested using an 808 nm laser diode. Fresnel reflections from the cleaved ends of the fibre form the laser cavity and dichroic mirrors were

used to separate the pump light from the signal. Figure 5.3 shows the output spectra obtained from a 20 m long fibre with an absorbed pump power of 10 W. The fibre exhibits a broadband luminescence spectrum, with the maximum in the region of 1000 to 1200 nm.

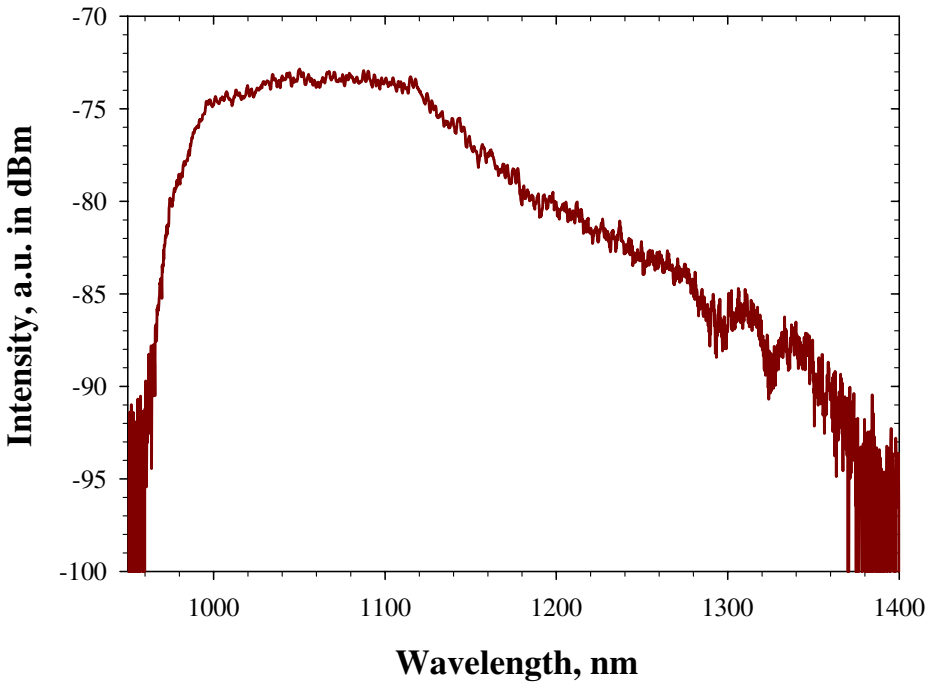

FIGURE 5.3: Longitudinal emission spectrum from fibre L3003102 cladding-pumped at 808 nm (Fibre length: 20 m, pump power: 20 W).

Fibre T0037, when core pumped by 915 nm single mode laser diode, shows emission peak around 1100 nm. Unfortunately there was no sign of any gain, possibly because of high concentration of Bi which increases the signal background loss.

Another preform (L30071) with a relatively lower Bi concentration, 0.25 gm of $BiCl_3$ in a 200 ml solution was fabricated with a host glass composition of Al_2O_3:GeO_2:P_2O_5:SiO_2. Ge was added in this preform to enhance the Bi luminescence [2]. P was added in an attempt to shift the emission band towards longer wavelength [3]. Unfortunately, the fibre (T0086) drawn from this preform showed poor luminescence, possibly due to low Bi concentration. Figure 5.4 shows the luminescence from the

fibre with 976 nm and 1060 nm pumping. It is worth mentioning here that this fibre showed broad emission peak at 1250 nm with a 3 dB bandwidth of 150 nm, for both pump wavelengths of 976 and 1060 nm.

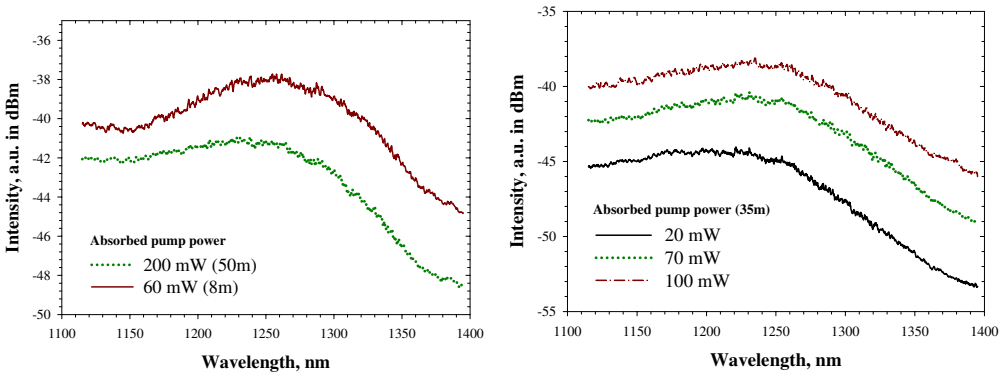

(a) (b)

FIGURE 5.4: Longitudinal emission spectrum of fibre T0086, when core pumped at (a) 977 nm and (b) 1060 nm.

Two new preforms were subsequently fabricated with slightly higher Bi concentration than the previous one. Preform L30081 with 0.5 gm of $BiCl_3$ in a 200 ml solution, with host glass composition of Al_2O_3:SiO_2 was made. The fibre was co-doped with Yb^{3+}, in an attempt to improve the pump absorption and ultimately energy transfer through so-called "sensitisation". Yb^{3+} has an intense absorption band at the emission wavelength of high power laser diodes and has been used as an excellent sensitiser for rare earth ions such as Er, Pr and Tm. It was expected that the spectral overlap between Yb^{3+} emission and absorption of Bi ions results in an efficient energy transfer between them and thus widening the choice of pumping schemes by offering an extended absorption spectrum. Double clad fibre T0110 with core NA 0.15 and inner cladding diameter 120 μm were pulled from the co-doped preform. This fibre when tested under the same cladding pumped setup with 960 nm laser diode, started lasing at two wavelengths, 1080 and 1120 nm where 1120 nm lasing is considerably stronger. Fibre length was 90 m with a pump absorption of 8.8 W. The Raman gain peak for 1080 nm pumping wavelength, in silica host should be around 1133 nm. So the 1120 nm peak may not be attributed

to Raman but due to the long length used for the experiment. Figure 5.5 shows the output spectrum from this fibre with a comparison to standard Yb alumino-silicate fibre of comparable pump absorption.

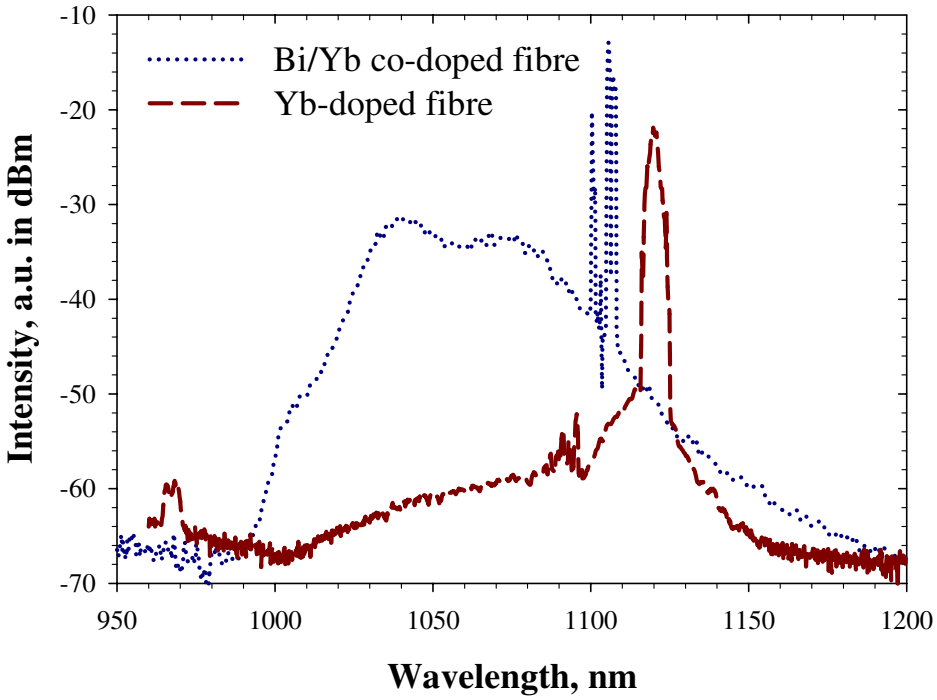

FIGURE 5.5: Longitudinal emission spectrum from Bi/Yb co-doped fibre T0110, in alumino-silicate host, when cladding-pumped at 960 nm (Fibre length: 90 m, pump power: 15 W). A spectrum from a similar Bi-free fibre is also shown for comparison.

Another preform L30082 with $BiCl_3$ concentration of 1.0 gm in a 200 ml solution and host glass composition of Al_2O_3:P_2O_5:SiO_2 was fabricated. This preform was also co-doped with Yb^{3+}. Fibre T0109 with inner cladding diameter of 120 μm was drawn and tested under the same setup. The excitation at wavelengths 808, 915 and 960 nm of the fibre results in two luminescence bands at about 1060 nm corresponds to Yb and 1300 nm related to Bi. The luminescence is dominated by emission from the Yb-ions at around 1060 nm.

When pumped at 960 nm, the fibre lased at 1060 nm. This is possibly due to the Yb ions rather than the Bi ions. However there is also a broad secondary peak

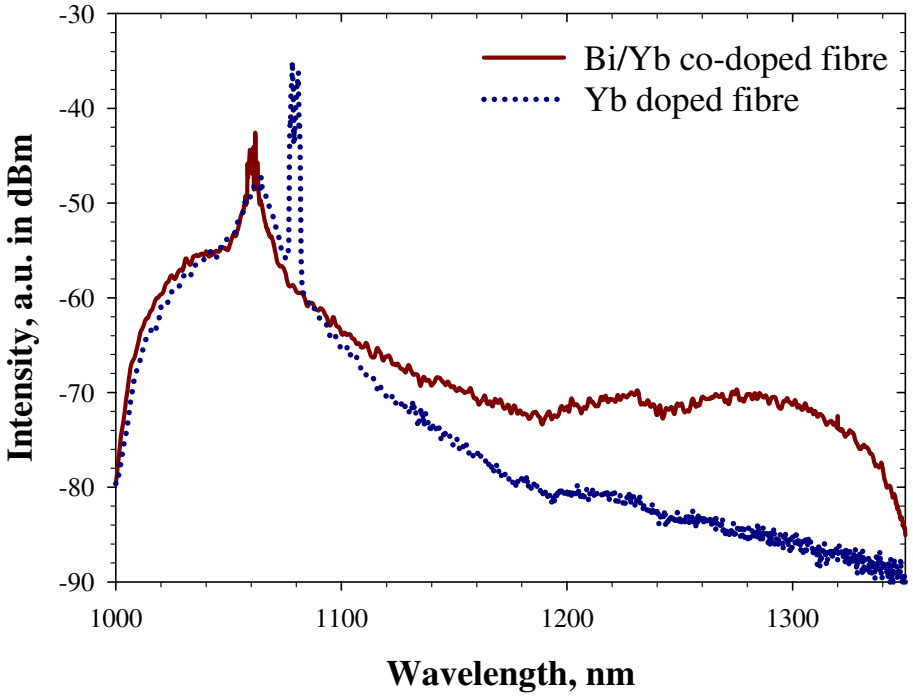

FIGURE 5.6: Longitudinal emission spectrum from Bi/Yb co-doped fibre T0109, in alumino-phospho-silicate host, when cladding-pumped at 960 nm (Fibre length: 90 m, pump power: 15 W). A spectrum from a similar Bi-free fibre is also shown for comparison.

extending out to 1300 nm, which is attributed to the Bi ions. It was not possible to get lasing on the Bi ions in a laser cavity with 4%-4% feedback. Figure 5.6 shows the output spectrum from a 90 m long fibre, measured with an optical spectrum analyser with a resolution bandwidth of 1 nm. To check that the ASE is coming from Bi and not from Yb, a standard Yb phospho-alumino-silicate fibre of the same length was tested using the above mentioned setup. No 1300 nm peak was observed this time. The results are compared in Fig. 5.6. It is concluded that the 1300 nm peak is indeed coming from Bi and not from Yb.

Pumping at 808 nm showed two luminescence peaks at 1060 and 1300 nm. The 1060 nm peak is attributed to Yb and the 1300 nm peak can be attributed to Bi (Fig. 5.7). It was observed again that the presence of P shifts the emission peak

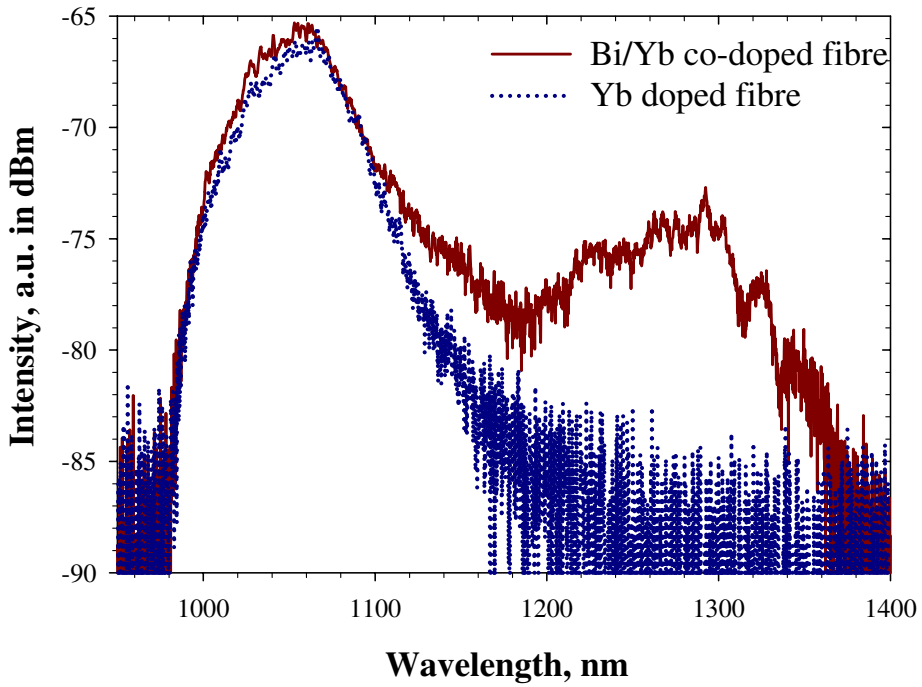

FIGURE 5.7: Longitudinal emission spectrum from Bi/Yb co-doped fibre T0109, in alumino-phospho-silicate host, when cladding-pumped at 808 nm (Fibre length: 90 m, pump power: 20 W). A spectrum from a similar Bi-free fibre is also shown for comparison.

towards longer wavelengths. The broad emission characteristics of Bi-Yb co-doped phosphate fibre indicates that the fibre might be promising for broadband sources.

5.3 Bi-doped fibre laser at 1179 nm

The focus was then shifted to construct an efficient core-pumped Bi-doped fibre laser with optimum Bi concentration and suitable host material. Core-pumped laser systems are easier to understand than cladding-pumped ones, due to a lower number of parameters and uncertainties to deal with. Since it was realized that the background loss caused by Bi ion itself, is one of the barriers in constructing Bi-doped fibre lasers and as it increases drastically with Bi concentrations, it is better to choose a core-pumping approach, with much lower Bi concentrations.

This is because, background loss becomes much higher in cladding pumped lasers than in a core pumped lasers.

Another preform was made with a concentration of 2.5 gm of $BiCl_3$ in a 200 ml solution. The glass composition was Al_2O_3:GeO_2:SiO_2. A fibre with a core diameter of 11 μm and NA of ~0.16, with high index coating was pulled from this preform. The Bi-doped fibre was tested in a laser configuration as shown in Fig. 5.8. Core pumping of the laser cavity was organized by using a 3 W Yb-doped fibre laser (GTWave) at 1080 nm. The Bi fibre was spliced to the 80% port (80% transmission at 1080 nm) of a WDM (1090/1150 nm). A linear 4%-100% reflecting cavity was formed by a perpendicularly cleaved end facet in the signal output port of the WDM and a high reflecting broadband mirror butted to the fibre on the other end of the cavity. As the WDM was not perfect, 20% signal output was propagating in the backward direction into the pump source. Lasing at 1160 nm was achieved with this setup. It is worth mentioning that the reported Bi-doped fibre laser has used the optimum cavity as 100%-50% [4]. The fibre length was varied from 50 to 20 m to maximize the signal output power.

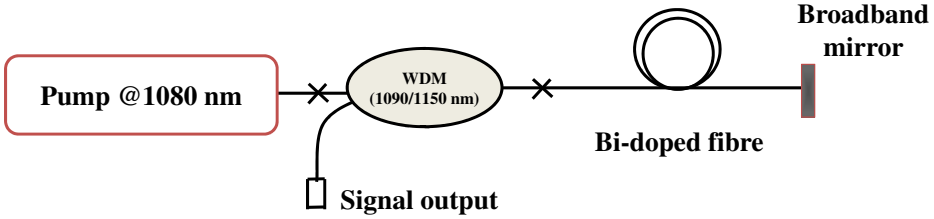

FIGURE 5.8: Experimental arrangement for Bi-doped fibre laser.

The dependence of output laser power on the launched pump power is shown in Fig. 5.9(a). A 10% of slope efficiency was achieved with respect to launched pump power at 1.16 μm with a 25 m long fibre. The 10% slope efficiency compares well with other reported fibre lasers at low pump powers [4]. The lasing threshold was around 200 mW. We observed no pulsing in a 25 m Bi-doped fibre lasers.

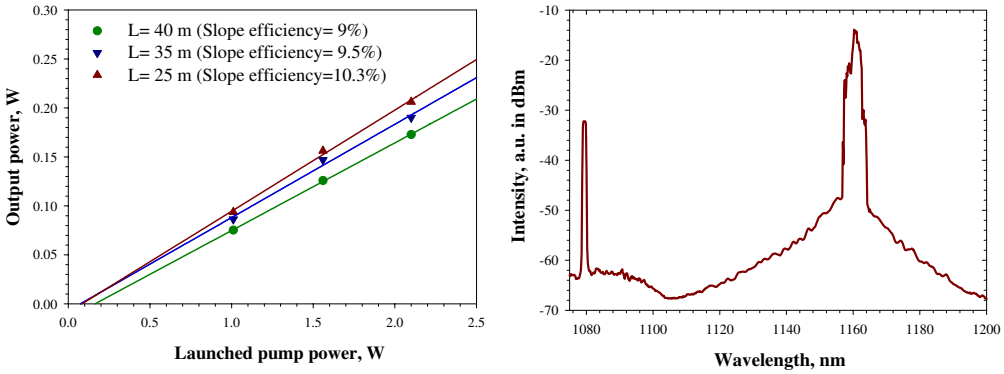

(a) (b)

FIGURE 5.9: Output power and output spectrum of Bi-doped fibre laser at 1160 nm.

Figure 5.9(b) shows a typical spectrum of 1160 nm Bi-doped fibre laser with a linewidth of 3 nm, which was taken by an optical spectrum analyser with 1 nm resolution. The broad linewidth is due to the free running laser configuration.

Fibre T0151 was also tested with a 15 W Yb-doped fibre laser (SPI Laser) at 1090 nm, using a similar set up, as in Fig. 5.8. Here the 1090/1150 nm WDM was replaced with a 1090/1179 nm WDM. In addition, a fibre Bragg grating (FBG) at 1179 nm with 11% reflectivity was used for the signal output coupling. The laser efficiency was slightly improved with 1090 nm, compared to the efficiency under 1080 nm pumping, at room temperature. However, the efficiency reached 15% when we dropped the environmental temperature to 10^{o}C. The response of the laser performance to the different pump wavelengths and the different external temperatures appears to be in accordance with the observed unsaturable absorption. The maximum signal output power at 1179 nm was 1.4 W at 22^{o}C, which increases up to 2 W at 10^{o}C [See Fig. 5.10(a)]. The narrow linewidth of 0.4 nm could be suitable for successive frequency doubling to yellow [Fig. 5.10(b)].

After characterising and analysing fibres with different compositions, it was apparent that the Bi concentration and composition of host material are important parameters in realising Bi doped fibre lasers. So to investigate the effect of host

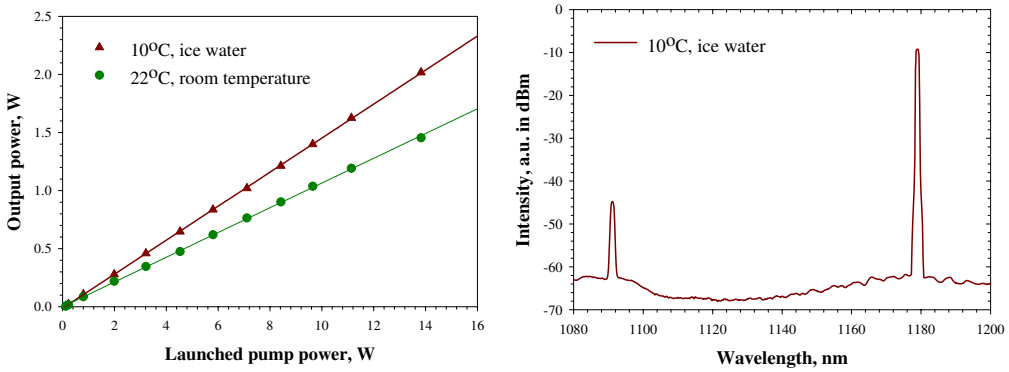

(a) (b)

FIGURE 5.10: Output power and output spectrum of 25 m long Bi-doped fibre laser at 1179 nm.

materials, particularly Ge and Al two more preforms were fabricated with the same Bi content as the previous one (L30103) but with different Ge and Al concentrations.

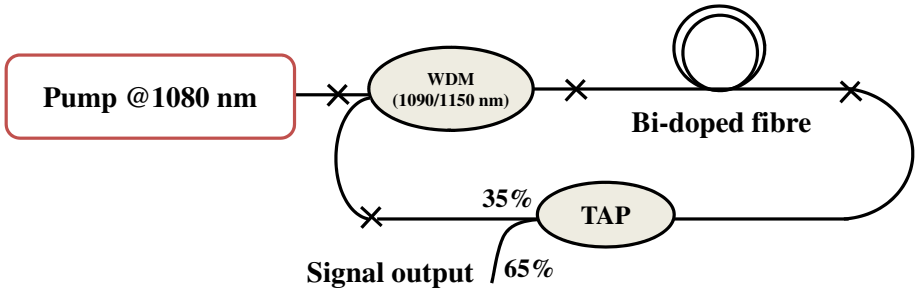

FIGURE 5.11: Ring cavity for 1080 nm pumping investigation.

Fibre T0175 was pulled from L30117, with high index coating with a core diameter of 8 μm and has the same Bi and Al concentration as T0151 but has lower Ge content. The fibre failed to lase in the 100%-4% linear cavity at room temperature and was tested in a ring cavity with 65% output coupling, as shown in the Fig. 5.11. With a 20 m long fibre, when pumped by 1080 nm, the oscillation at 1160 nm was observed, but the efficiency was quite limited to 1%. The threshold was 510 mW. The laser characteristics and spectrum are shown in Fig. 5.12(a) and 5.12(b) respectively.

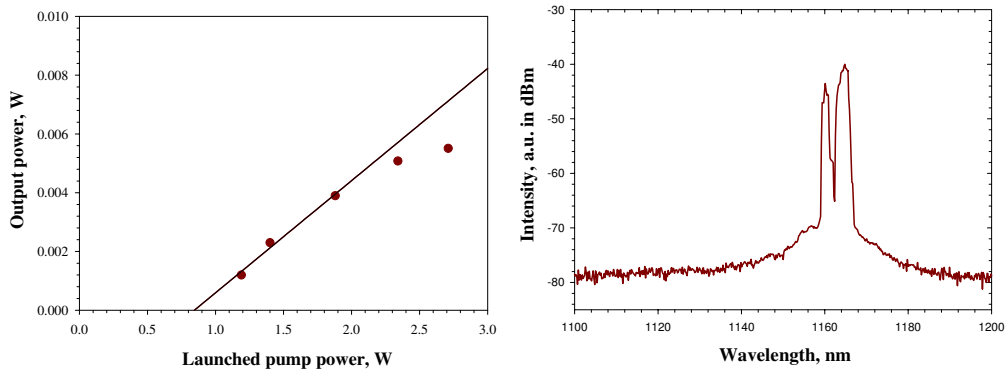

(a) (b)

FIGURE 5.12: Output power and output spectrum of Bi-doped fibre laser at 1160 nm.

Another fibre T0177 was made, further reducing the Ge concentration. This has the same Bi in solution but higher Al content than T0175. This fibre was tested in a strong ring cavity with 1% output coupling, but it failed to lase with the available pump power.

Bi-doped fibre lasers discussed so far, utilize laser diode pumped Yb-doped fibre lasers for pumping at the 1080 nm pumping band. However, Bi-doped fibres exhibit broad and intense absorption bands, which suggest the use of various other pumping wavelengths, in addition to 1080 nm. In particular, it is useful to use commercially available laser diodes emitting at 808, 915 and 975 nm as pumping sources which have good overlap with the absorption bands of Bi-doped fibres.

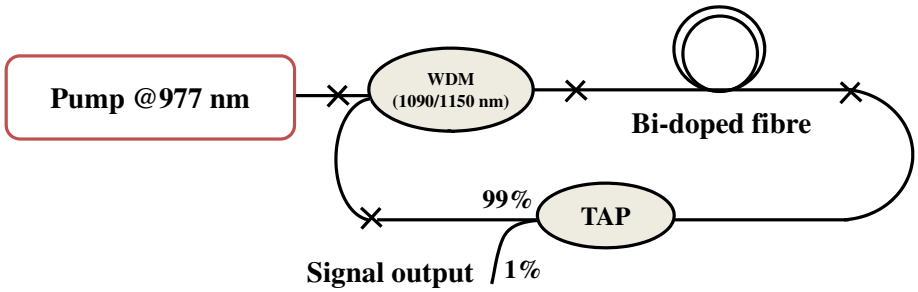

FIGURE 5.13: Ring cavity for 977 nm pumping investigation of Bi-doped fibre T0151.

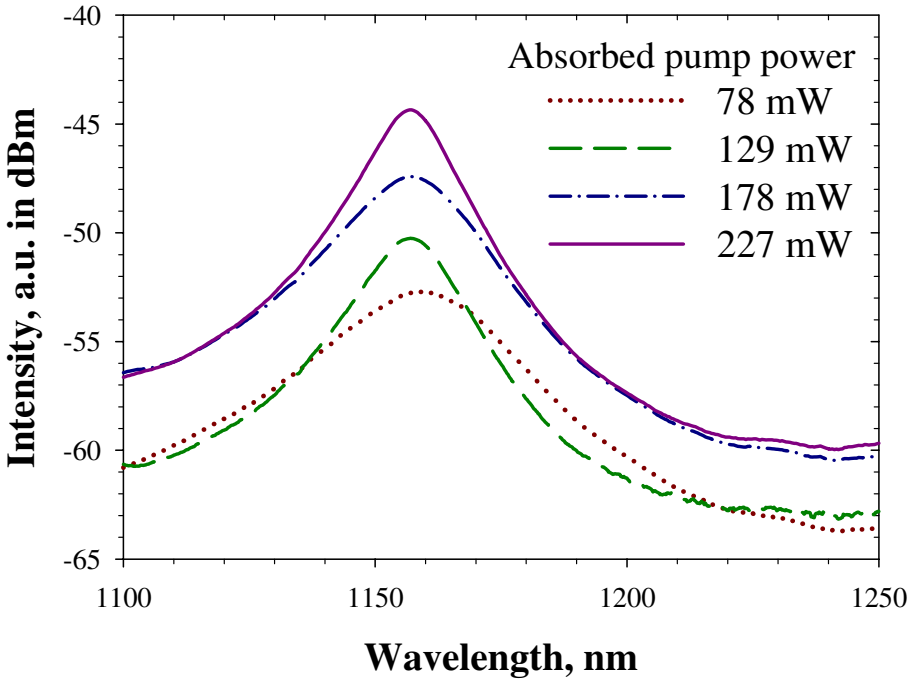

FIGURE 5.14: Emission spectra of Bi-doped fibre T0151, when core pumped at 977 nm.

To check the feasibility of 977 nm, fibre T0151 was investigated under 977 nm pumping. The fibre failed to reach threshold in the 4%-100% laser configuration, with the available pump power at 977 nm. The fibre could not cross the threshold even in a ring cavity with 1% output coupling (Fig. 5.13). The fibre length was 6 m, permitting 10 dB pump absorption. With maximum available pump power of 250 mW, the fibre failed to oscillate, but exhibited growth of ASE at 1160 nm (Fig. 5.14). Similar behavior was observed under 915 nm pumping, i.e. growth of ASE but no lasing with the available pump power. The poor efficiency under 915 and 977 nm pumping is somewhat explained by the excited state absorption present in the Bi fibre at these pump wavelengths and also the low emission cross-sections at signal wavelengths compared to that by 1090 nm pumping, as already been discussed in Chapter 4. The ASE was found to peak at longer wavelengths compared to the fluorescence peak under 976 nm pumping. This difference in peak wavelengths relies on the interplay of emission cross-section and absorption

cross-section, as observed in Yb-doped fibres as well [5].

5.4 Influence of cooling on Bi-doped fibre laser

The measured value of the Bi-doped fibre laser efficiency, even with the most efficient fibre, is lower than the conventional rare-earth doped fibre lasers. Also, in literature, the record efficiencies so far are 28% in the 1160-1200 nm [6] and 3% in the 1300-1500 nm wavelength range [7]. Further investigation of the Bi-doped fibre spectroscopy is necessary to increase the efficiency in the Bi-doped fibre laser. One possible reason that can impair the laser efficiency at the 1090 nm pump band is the presence of high unsaturable absorption in the fibre, which is temperature dependent. Unsaturable absorption is a loss mechanism which can be caused by quenching-process such as cross-relaxation and upconversion in case of rare earth ions [8]. This results in waste of pump energy, increase in laser threshold and also reduced conversion efficiency. It should be noted that the laser efficiency indeed relies on the strength of the ratio of unsaturable loss to the small signal absorption. Temperature rise in the Bi-doped fibre under strong pumping condition can increase the unsaturable loss in the fibre and thus can be one of the limiting factors for such laser systems. Increasing Bi concentration is certainly the way forward to make the cavity shorter, however it is believed that the higher Bi concentration builds more wrong-valanced or ill-coordinated Bi ions, which restricts the amount of Bi concentration. The unsaturable part in the absorption could be somewhat suppressed by a proper heat sink, as reflected in the Bi-doped fibre laser efficiency in Fig. 5.10(a). In addition, modification of compositions in host material or different fabrication process may be helpful to reduce the unsaturable loss in Bi-doped fibres. Here, the dependence of Bi-doped fibre laser efficiency on effective cooling of the fibre is reported.

A Fabry-Perot cavity to test laser performance of the Bi-doped fibre was composed. The experimental arrangement was similar to one described in figure 5.8, while the pump was replaced with a 15 W Yb-doped fibre laser at 1090 nm. The fibre length used for the experiment was 30 m. Figure 5.15 shows the Bi-doped fibre laser output power at various heat sink arrangements. It was found that at high pump powers the laser efficiency decreased when the fibre was cooled by natural convection. The rollover in output power was prominent at approximately 6 W of pump power at 24^{o}C in air. Thus it seems that the laser efficiency degrades at higher temperature. To verify the proposition, the fibre was heated at 40^{o}C by placing the fibre on a hot plate. A similar rollover was observed and the efficiency could not go beyond 2%. To provide more effective heat removal from the fibre, the fibre spool was then placed in a water bath at 20^{o}C. An increase in efficiency around 7.8%, compared to that measured at room temperature, was observed with water cooling. Moreover, no rollover in the output power was noticed, as the heat was efficiently extracted. On further cooling the fibre to 10^{o}C in water, an increase in efficiency up to 10% was observed, without any rollover of the output power. The water temperature was also raised to 40 and 50^{o}C, and the efficiency dropped down to 4.8 and 3.4% respectively, but no rollover was observed in the output power even at the maximum pump power. It is interesting to see that the output power in 24^{o}C air becomes lower than that in 40^{o}C water when the pump power goes beyond 8 W, which strongly suggests that the fibre temperature gets higher when cooled naturally. The results clearly indicate that proper heat extraction from the fibre is important to improve the laser performance.

The temperature dependence of the Bi-doped fibre laser can be explained on the basis of unsaturable loss present in the fibre at 1090 nm, as discussed in the previous chapter. The unsaturable loss was proportional to the water temperature and the ratio of unsaturable absorption to small signal absorption was measured as 33,

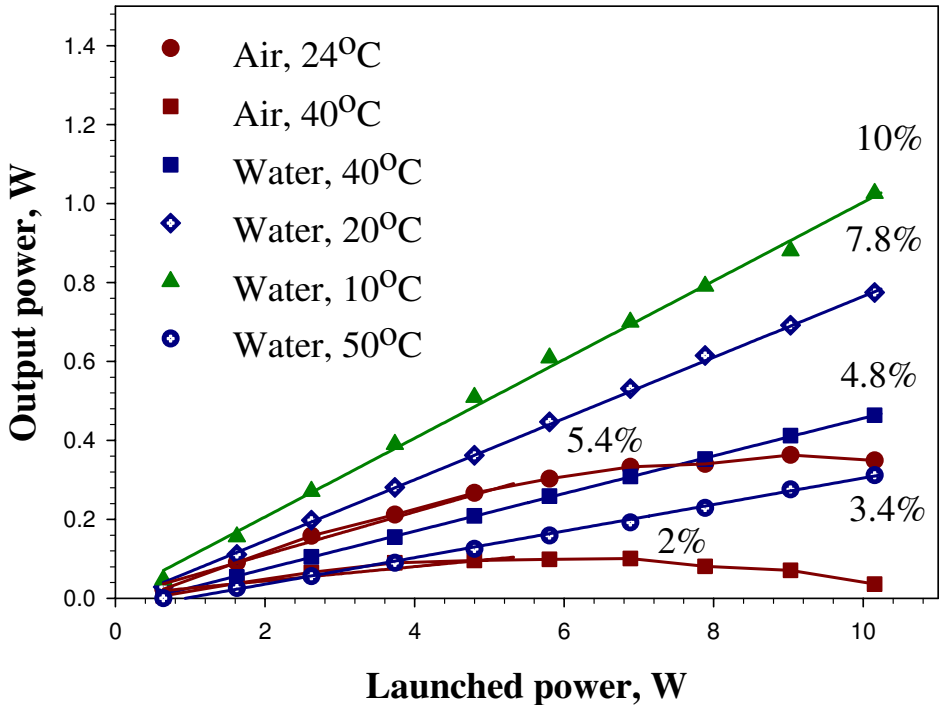

FIGURE 5.15: Bi-doped fibre laser performance at different heat sink arrangements.

30 and 28% at 40^{o}C, 20^{o}C and 10^{o}C respectively. Thus, it seems that the gradual increase in fibre temperature with the pump power, in absence of effective heat extraction [Air 24^{o}C and Air 40^{o}C; both in Fig. 5.15], leads to a rise in unsaturable loss in the Bi-doped fibre, contributing to rollover in the 1179 nm output power. So the increase in unsaturable loss at higher temperature is one of the reasons behind the lower efficiencies in Bi-doped fibre laser systems. At this stage, the exact reason of the origin of unsaturable loss and its temperature dependence in the Bi-doped fibre is not fully understood, and further investigation is required.

5.5 Bi-doped fibre amplifier at 1179 nm

The amplifier performance of the Bi-doped fibre T0151 was examined at 1179 nm. A signal wave at 1179 nm and pump wave at 1090 nm counter-propagated in the

fibre. The amplifier configuration is illustrated in Fig. 5.16. A 9 W Yb-doped fibre laser at 1090 nm was used as a pump source, and an Yb-doped fibre laser operating at longer wavelengths of 1179 nm, with an output power up to 3 W served as the seed source. The construction of the Yb-doped fibre laser at 1179 nm will be discussed in chapter 5. The Bi-doped fibre was spliced to two identical WDM couplers at both ends to separate signal and pump waves, and the signal output port and the unused port of the couplers were angle cleaved to suppress feedback. The seed power was varied from 2.5 mW to 2.2 W and the signal gain was recorded at each seed power level. The fibre length was not optimised for each seed power level. Rather, the fibre length was fixed at 30 m.

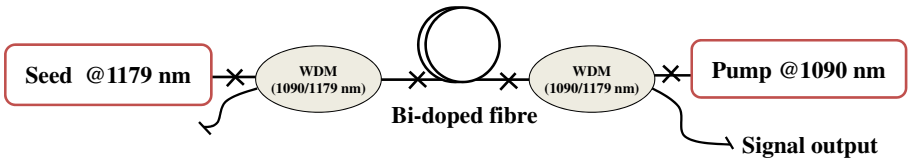

FIGURE 5.16: Schematic of Bi-doped fibre amplifier experimental setup.

Figure 5.17 shows the measured gain of the Bi-doped fibre amplifier in different heat sink arrangements for various input signal powers. The gain starts to saturate over 2 W of launched pump power. The influence of fibre temperature on the amplifier performance is directly compared in the saturated gain, at 25 mW seed power. It is clear, as shown in Fig 5.17, that just by cooling the fibre in the water bath, we could extract 2 dB more gain. The maximum gain achieved with water cooling was 19 dB at a signal seed power of 2.5 mW, which reduced to 7 dB at 250 mW of seed power. The maximum saturated output of 1 W was obtained for 6 W of pump power (250 mW signal input), at 20^{o}C in water. Also, the saturation output power dependence on the temperature was investigated further. Figure 5.18 shows the signal output power vs. gain at different pump power levels. The

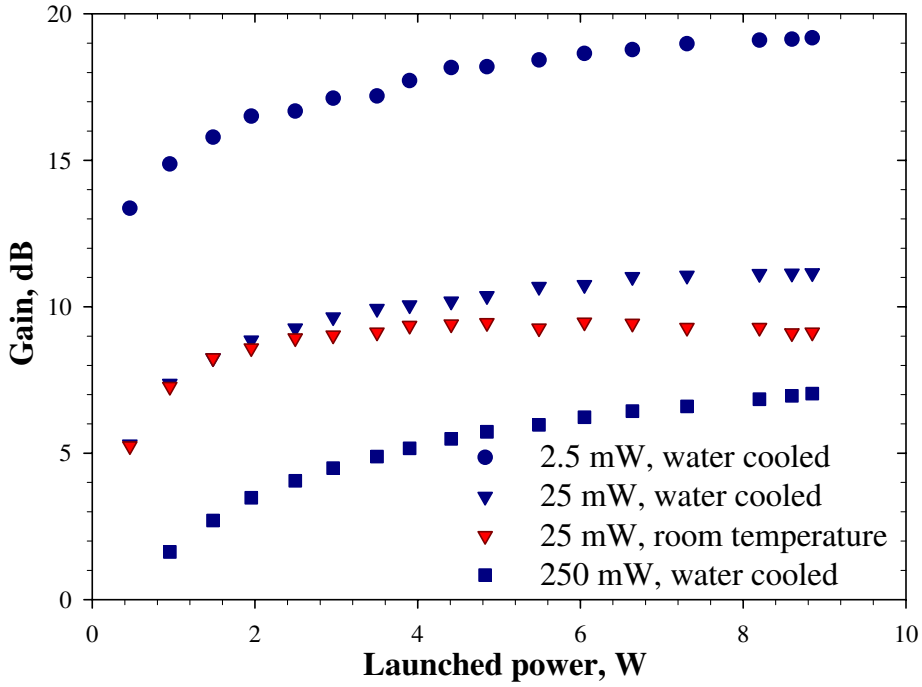

FIGURE 5.17: Dependence of gain on pump power for different seed powers with water cooling, 20^{o}C and room temperature.

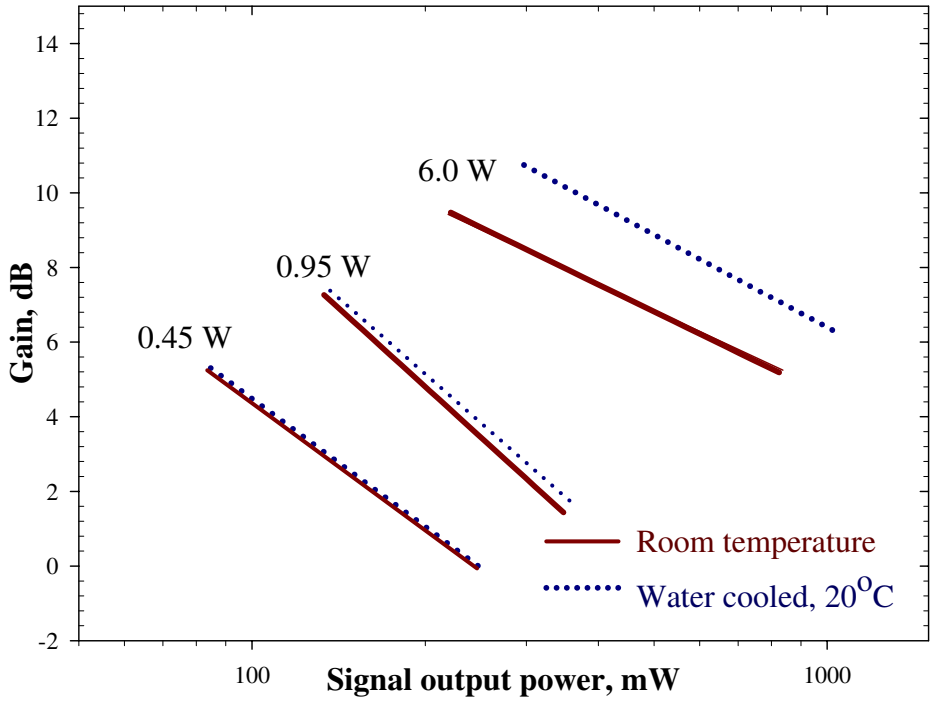

FIGURE 5.18: Gain versus signal output power at different pump powers (labeled in figure) with water cooling, 20^{o}C and room temperature.

saturation signal output power increases with pump power, as observed in Er-doped fibre amplifiers [9]. Furthermore, the saturation power becomes higher at low temperature for the pump power above 2 W. Thus, our results indicate that effective cooling can shift the saturation towards higher power, and help to increase the extractable output power from the Bi-doped fibre amplifier.

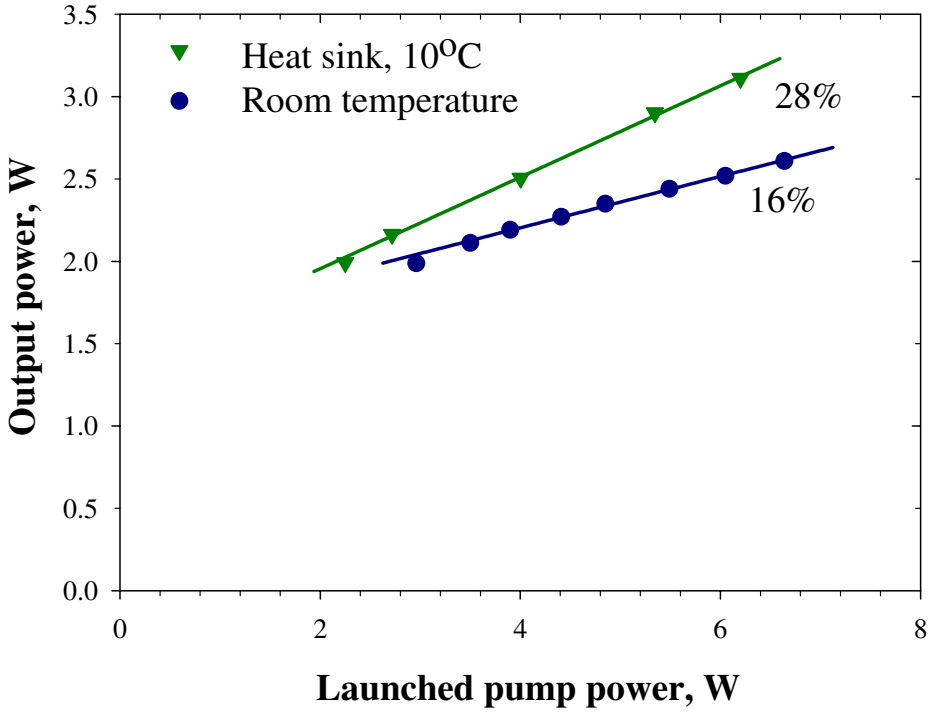

FIGURE 5.19: Output power with and without heat sink at seed power of 2.2 W.

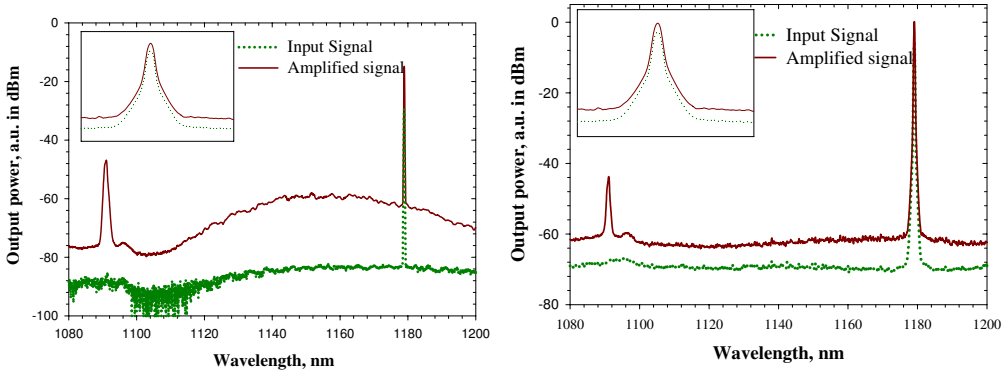

(a) Near threshold

(b) Maximum output power of 3.2 W

FIGURE 5.20: Output spectrum taken with an optical spectrum analyser with 0.2 nm resolution at different output power, at room temperature.

The Bi-doped fibre power amplifier characteristics, at a high seed power of 2.2 W, are shown in Fig. 5.19. The slope efficiency of the fibre at 24^{o}C was 16%. By dipping the fibre in water at 10^{o}C, the efficiency increased to 28%, giving an output power of more than 3 W. Although the gain is small, it is still interesting to observe that heat extraction strongly influences the amplifier performance even at such high seed power level. Figure 5.20 shows the measured signal spectrum at the different output power level at room temperature (OSA resolution 0.2 nm). It is worth noting that the line width of 0.28 nm was obtained even at the maximum output power. The fibre amplifier maintains the seed line width at all seed power levels.

The higher saturation power and higher efficiency at low temperature could be explained on the basis of low unsaturable loss at lower temperature in Bi-doped fibre at 1090 nm pump wavelength. The increase in saturation power with lower temperature is helpful in increasing the output power from Bi-doped fibre amplifier.

5.6 Conclusion

Experiments were carried out on Bi-doped fibre lasers emitting at wavelengths around 1160 nm. A 25 m Bi-doped fibre laser at 1160 nm was demonstrated. The laser efficiency was impaired when unsaturable loss was high. The host dependency of the Bi doped fibre laser has also been investigated. The low laser efficiency of 15% of the Bi-doped fibre laser may be attributed to unsaturable losses and ESA present at the pump as well as signal wavelengths. The temperature dependence of unsaturable loss and its influence on the efficiency of Bi-doped fibre laser operation was investigated. It was observed that effective heat removal can boost

the laser performance in Bi system by reducing the temperature dependant unsaturable loss in the fibre. Optical amplification in a Bi-doped fibre at 1179 nm was demonstrated, with various seed power levels, when pumped at 1090 nm. It is observed that an efficient heat sink is helpful in enhancing the gain as well as the saturation output power in the Bi-doped fibre amplifier.

References

[1] J. Nilsson, W. A. Clarkson, R. Selvas, J. K. Sahu, P. W. Turner, S. U. Alam, and A. B. Grudinin, "High-power wavelength-tunable cladding-pumped rare-earth-doped silica fiber lasers," *Optical Fiber Technology* **10**(1), pp. 5–30, 2004.

[2] Y. Fujimoto, Y. Hirata, Y. Kuwada, T. Sato, and M. Nakatsuka, "Effect of GeO_2 additive on fluorescence intensity enhancement in bismuth-doped silica glass," *Journal of Materials Research* **22**(3), pp. 565–568, 2007.

[3] X. G. Meng, J. R. Qiu, M. Y. Peng, D. P. Chen, Q. Z. Zhao, X. W. Jiang, and C. S. Zhu, "Near infrared broadband emission of bismuth-doped aluminophosphate glass," *Optics Express* **13**(5), pp. 1628–1634, 2005.

[4] E. M. Dianov, A. V. Shubin, M. A. Melkumov, O. I. Medvedkov, and I. A. Bufetov, "High-power cw bismuth-fiber lasers," *Journal of the Optical Society of America B* **24**, pp. 1749–1755, 2007.

[5] A. S. Kurkov, "Oscillation spectral range of Yb-doped fiber lasers," *Laser Physics Letters* **4**(2), pp. 93–102, 2007.

[6] V. V. Dvoyrin, V. M. Mashinsky, and E. M. Dianov, "Efficient bismuth-doped fiber lasers," IEEE *Journal of Quantum Electronics* **44**(9-10), pp. 834–840, 2008.

[7] E. M. Dianov, S. V. Firstov, O. I. Medvedkov, I. A. Bufetov, V. F. Khopin, and A. N. Guryanov, "Luminescence and laser generation in Bi-doped fibers in a spectral region of 1300-1520 nm," *Optical Fiber Communication Conference* , 2009. OSA Technical Digest (CD) (Optical Society of America, 2009), paper OWT3.

[8] M. K. Davis, M. J. F. Digonnet, and R. H. Pantell, "Characterization of clusters in rare-earth-doped fibers by transmission measurements," *Journal of Lightwave Technology* **13**(2), pp. 120–126, 1995.

[9] N. O. P.C. Becker and J. Simpson, *Erbium Doped Fiber Amplifiers: Fundamentals and Technology*, Academic Press, 1999.

Chapter 6

Long wavelength operation of Yb-doped fibre lasers

6.1 Introduction

In this chapter, an all-fibre, high power, narrow-linewidth Yb-doped silica fibre laser operating at 1179 nm is described; when core pumped at 1090 nm. The fibre was heated at 125^{o}C. The content of the chapter is arranged as follows. In Section 6.2, an overview of the basic spectroscopic properties of Yb^{3+} ion and its temperature dependance are discussed. In Section 6.3, a detailed description of the experimental set-up and results of Yb-doped fibre laser at 1179 nm is outlined. Optimisation of the laser cavity using numerical simulation is presented in Section 6.4. The results described in this chapter are particularly important for efficient frequency doubling for suitable laser guide star applications.

6.2 Properties of Yb^{3+} ions in glass

The spectroscopic properties of Yb^{3+} ions are simple compared to other rare earth ions. The energy level structure consists of two manifolds, the ground manifold $^2F_{7/2}$ splits into four Stark sub-levels as labeled from a to d, and the excited manifold splits into three Stark sub-levels as labeled from e to g in the Fig. 6.1 [1]. The electronic structure of Yb^{3+} ions presents an absorption peak at 910 nm which corresponds to transitions from sub-level a to sub-levels f and g, while the peak at 976 nm corresponds to transition of sub-level a to e. The absorption at longer wavelengths is formed by the transitions from the population above sub-level b. Pertaining to the emission transitions, the main transition peak is at 976 nm, which corresponds to the transitions from the sub-level e to sub-level a. The emission peaks at wavelengths longer than 1 μm correspond to transitions from sub-level e to sub-levels b, c and d.

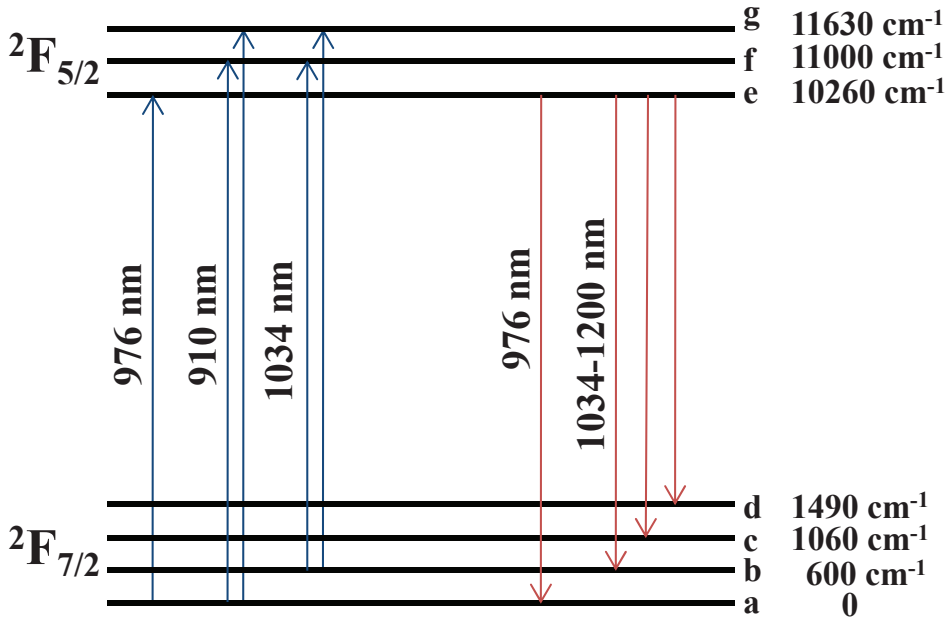

FIGURE 6.1: Energy level structure of Yb^{3+} in silica glass.

The detailed structure of the Stark sub-levels can vary depending on the chemical composition of the glass [2]. The optical properties of Yb^{3+} ions in alumino-silicate

or phospho-silicate glasses have been extensively studied and values of absorption and emission cross-sections determined in [3] are indicated in Fig. 6.2. One can see that Yb^{3+} ions in the alumino-silicate glass have larger emission cross-section, especially at wavelengths longer than 1070 nm, which makes alumino-silicate host fibre preferable for the long wavelength generation of Yb-doped fibre. In addition, the spectroscopic properties are temperature dependent [4].

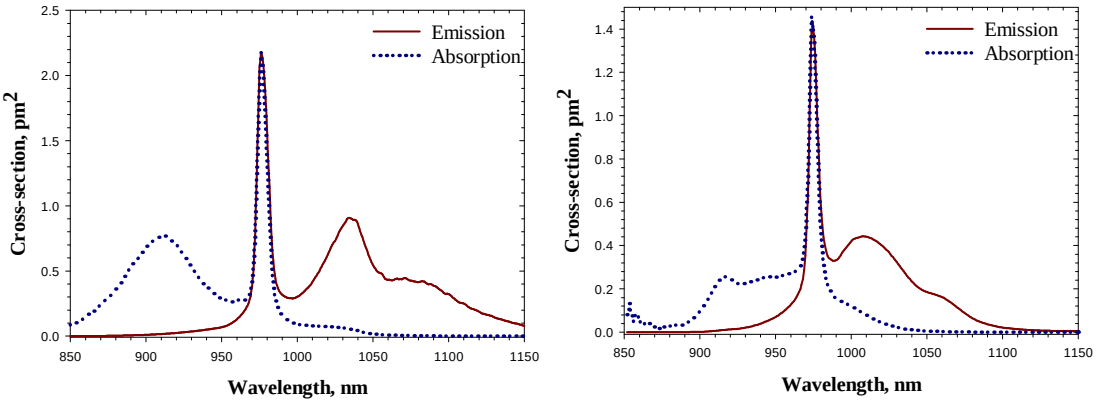

(a) Alumino-silicate (b) Phospho-silicate

FIGURE 6.2: Absorption and emission cross-sections of Yb^{3+} in (a) alumino-silicate and (b) phospho-silicate host [3].

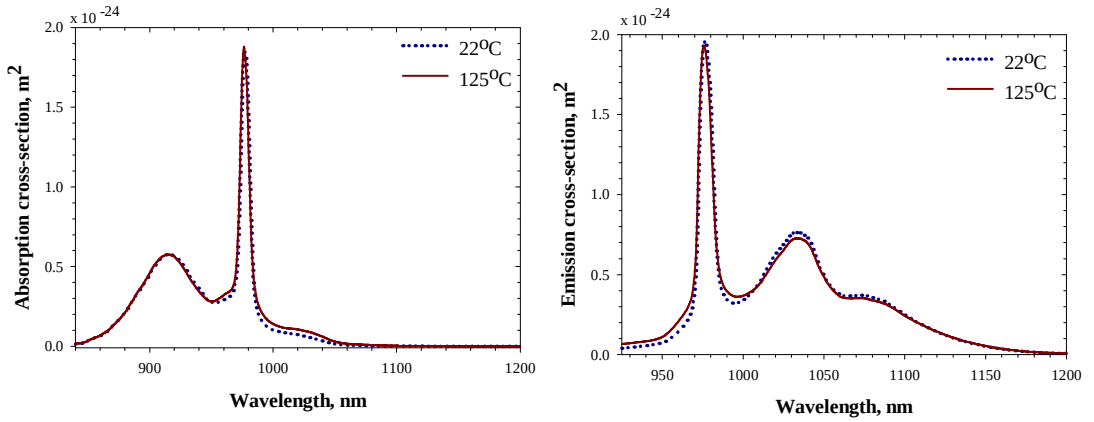

(a) Absorption Cross-section (b) Emission Cross-section

FIGURE 6.3: Experimental measurements of the temperature dependance of (a)absorption and (b)emission cross sections of the Yb-doped fibre.

The absorption and emission cross-sections of the Yb-doped alumino-silicate fibre were measured at various temperatures ranging from 22^{o}C (room temperature)

to 125^{o}C (Fig. 6.3). The absorption and emission cross-sections of the Yb-doped alumino-silicate fibre at different temperature conditions were measured by Luis Vazquez-Zuniga at ORC. One can see a decrease in the absorption strength at 910 and 976 nm with increasing temperature which corresponds to decrease in ground state populations i.e. in sub-level a. With the reduction of the population of sub-level a, the population of the other sub-levels, i.e. b, c, and d increases resulting in the increment of the absorption strength in the wavelength range of 1034 nm. However, for wavelengths longer than 1150 nm, the temperature dependence of the absorption cross-section is almost negligible. On the other hand, the emission cross-section decreases at 976, 1030, and 1080 nm with increasing temperature. These wavelengths correspond to the transitions from sub-level e to sub-levels a, b, and c respectively, which indicates a significant reduction in the population of sub-level e at higher temperatures. It was also noted that, for longer wavelengths, temperature has no influence on the emission cross-section.

6.3 Yb-doped fibre lasers at 1179 nm

6.3.1 Experimental procedures

The Yb-doped alumino-silicate fibre (T0166-L30109) used in this work was fabricated in-house by MCVD and the solution doping technique. The preform was drawn into a fibre with 125 μm outer diameter with higher index polymer coating materials. The fibre had a 10 μm Yb-doped core diameter with an NA of 0.11. The Yb concentration in the core was estimated to be 14000 ppm-wt. The background loss in the fibre was less than 10 dB/km, measured at 1285 nm with a high resolution OTDR.

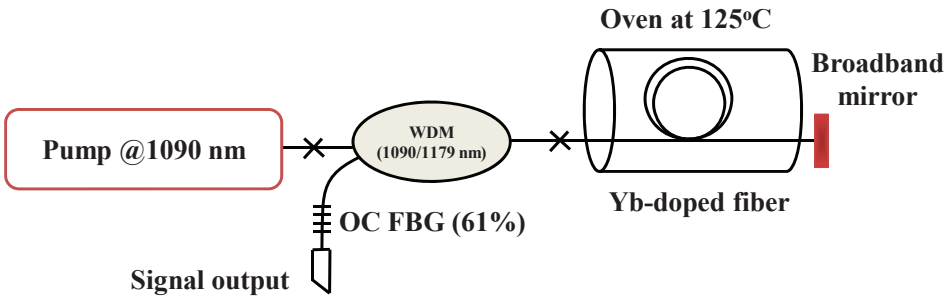

FIGURE 6.4: Experimental setup of the 1179 nm fibre laser; OC: Output Coupler, FBG: Fibre Bragg Grating.

The configuration used for 1179 nm fibre laser was a simple Fabry-Perot cavity. Figure 6.4 shows the schematic of the Yb-doped fibre laser experimental set-up. The fibre laser consisted of a 20 m long Yb-doped fibre that is fusion spliced to a 1090-1179 nm WDM coupler. The pump power is coupled into the core of the Yb-doped fibre through the WDM coupler. The pump consists of a GTWave based Yb-doped fibre laser at 1090 nm, pumped by two 915 nm PUMA laser diodes (SPI Laser). The available output power at 1090 nm was 30 W. The WDM coupler was mounted on a heat sink to remove excess heat and avoid damage during the high power operation. The other end of the doped fibre was flat cleaved and butted to a broadband mirror with high reflectivity, both at the pump and signal wavelengths. Index-matching liquid was applied to the fibre end to reduce the coupling loss with the broadband mirror. An FBG, acting as an output coupler, was spliced to the 1179 nm arm of the WDM coupler to select the lasing wavelength. The reflectivity of the FBG was 61% at 1179 nm with 3 dB bandwidth of 0.25 nm. The Yb-doped fibre was placed inside an oven (Carbolite, TZF 12/38/400), which was maintained at 125^{o}C to increase the pump absorption at 1090 nm.

6.3.2 Experimental results

Figure 6.5(a) shows the output power of the 1179 nm fibre laser as a function of the launched pump power. A total signal output power of 12.3 W at 1179 nm was obtained for 30 W of launched pump power at 1090 nm. The slope efficiency was estimated to be 43% with respect to the launched pump power. No roll-off or saturation of the output power was observed even at the maximum available pump power, indicating that the extracted output power was limited by the available pump power. It is to be noted that the reflectivity of the output coupler FBG was not optimised; instead the fibre length was optimised for the maximum output power. No change in output power was observed with further increase in temperature above 125^{o}C.

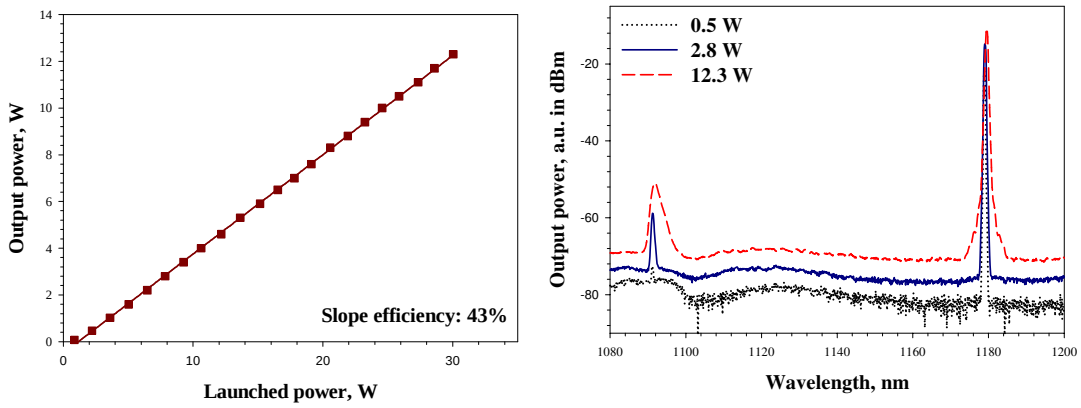

(a) Slope efficiency (b) Output spectrum

FIGURE 6.5: (a) Output power and (b) output spectrum (taken with an optical spectrum analyzer with 0.5 nm resolution) of Yb-doped fibre laser operating at 1179 nm.

A Yokogawa AQ-6370 OSA was used to measure the output spectrum. The measured spectrum of 1179 nm laser at different output power levels is shown in Fig. 6.5(b). The suppression of the ASE was better than 50 dB even at the maximum output power. The 3 dB linewidth of the laser spectrum at the maximum output power was less than 0.38 nm, measured with 0.02 nm OSA resolution (Fig. 6.6). The laser linewidth broadens slightly with increasing pump power as

expected in typical fibre laser. The results seem to indicate that pumping at 1090 nm helps to suppress the parasitic lasing at shorter wavelengths.

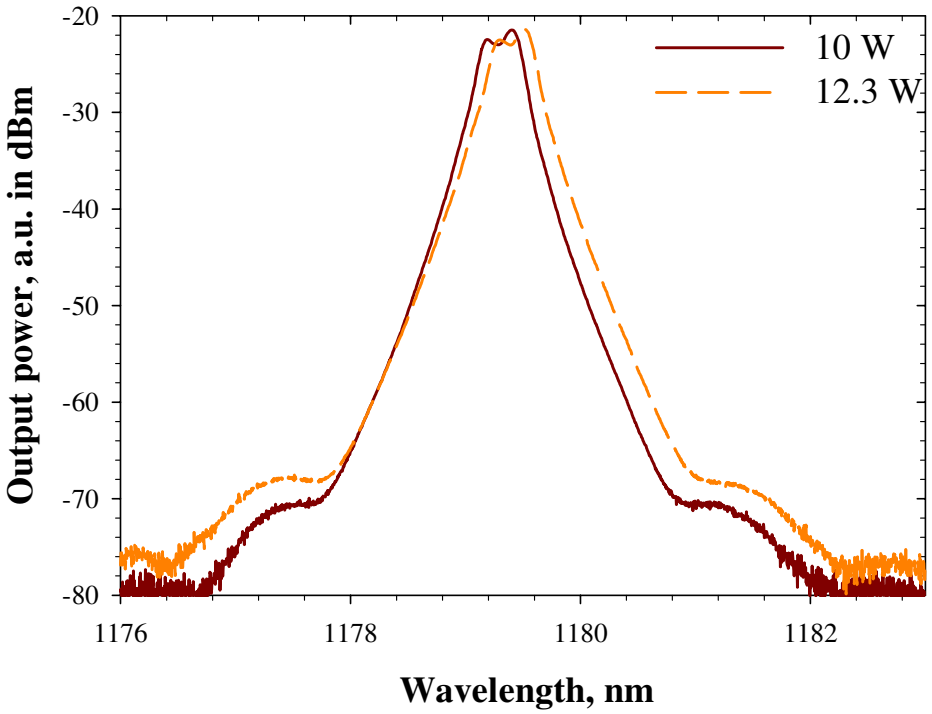

FIGURE 6.6: Output spectrum of the fibre laser at different signal power (optical spectrum analyzer resolution 0.02 nm)

No change in the output power was observed over the course of the experiments. However, the fibre strength seems to decrease after several days of operation, due to the degradation of the coating material at 125^{o}C. Nonetheless, the temperature handling capability of the fibre can be further improved at least up to 400^{o}C by using hybrid glass protective coating materials [5] or by using polyimide coated fibre [6]. Metal coated fibre using pure metals of copper, aluminium and gold are also available, which give better strength to the fibre at higher temperatures. Recently, low cost CuBALL [7] coating has allowed use at temperature up to 500^{o}C for long periods. These coating materials of high thermal stability can offer reliable and long term operation without any deterioration of the active fibre.

6.4 Modeling and interpretation

To optimise the fibre laser cavity for maximum output power a numerical simulation, using a commercial software (OptiSystem 8.0), was carried out. The model is based on the solution of the rate and propagation equations 6.1 and 6.3 of a two level system [8, 9],

$$-\frac{dn_1}{dt} = \frac{dn_2}{dt} = \sum_k \frac{\sigma_{ak}\Big|_{T=398K} P_k i_k}{h\nu_k} n_1(r,\phi,z) - \sum_k \frac{\sigma_{ek}\Big|_{T=398K} P_k i_k}{h\nu_k} n_2(r,\phi,z) - \frac{n_2(r,\phi,z)}{\tau} \quad (6.1)$$

$$n_t(r,\phi,z) = n_1(r,\phi,z) + n_2(r,\phi,z) \quad (6.2)$$

where n_t is the local Yb^{3+} ion density with n_1 and n_2 the populations of the lower and upper levels respectively; P_k is the total power at position z of the kth beam with wavelength centred at λ_k; τ is the spontaneous life time of the upper level; ν_k is the frequency and h is Planck's constant; σ_{ak} and σ_{ek} are the absorption and emission cross-sections respectively at temperature 398K. The normalised intensity is given by $i_k(r,\phi) = I_k(r,\phi,z)/P_k(z)$; where $I_k(r,\phi,z)$ is light intensity distribution of the kth beam.

The propagation equation describes the propagation of the beams through the doped fibre,

$$\frac{dP_k}{dz} = u_k\sigma_{ek}\Big|_{T=398K} \int_0^{2\pi}\int_0^{\alpha} i_k(r,\phi) n_2(r,\phi,z) r dr d\phi (P_k(z) + mh\nu_k\Delta\nu_k) - u_k\sigma_{ak}\Big|_{T=398K} \int_0^{2\pi}\int_0^{\alpha} i_k(r,\phi) n_1(r,\phi,z) r dr d\phi (P_k(z)) \quad (6.3)$$

where $mh\nu_k\Delta\nu_k$ is the spontaneous emission contribution from the local metastable

population n_2 and $\Delta\nu_k$ is the frequency interval between two successive wavelengths considered in the simulation. Also, beams traveling in the forward direction are indicated by $u_k = 1$, and beams traveling in the backward direction are indicated by $u_k = -1$.

With this simulation tool, the fibre laser configuration was optimised to enhance the output power of the fibre laser. It is to be noted that the tool could be used to study the influence of the fibre parameters on the laser efficiency as well, which was not attempted due to time constraints.

The model was applied to the experimental results reported in Section 6.3. The fibre laser was core pumped by a CW laser at 1090 nm and the cavity was built with a 20 m long fibre. The fibre parameters were selected to be the same as the fabricated Yb-doped fibre characterised in Section 6.3. With 61% output coupler at 1179 nm, a slope efficiency of 43% was reported. In Fig. 6.7 we have compared the simulation to the experimental data. The agreement is excellent.

The reflectivity of the output coupler was then optimised to maximise the output power. In the first instance, the fibre length was kept constant at 20 m. Output coupler reflectivity in the range of 30 to 75% was tested and the results are summarized in Fig. 6.8. For output coupler reflectivity of 35% a slope efficiency of 38% can be obtained while increment in slope efficiency was observed with higher output coupler value. A maximum slope efficiency of 53% with respect to launched pump power was achieved for 40% output coupler reflectivity [Fig. 6.8(b)]. The corresponding output power was projected to be more than 15 W as shown in Fig. 6.8(a). However, with further growth in output coupler reflectivity, the efficiency dropped down to 31% at 75% output coupling.

Figure 6.9 illustrates the slope efficiency as a function of fibre length for three different output coupler reflectivities. One can see that the optimum fibre length

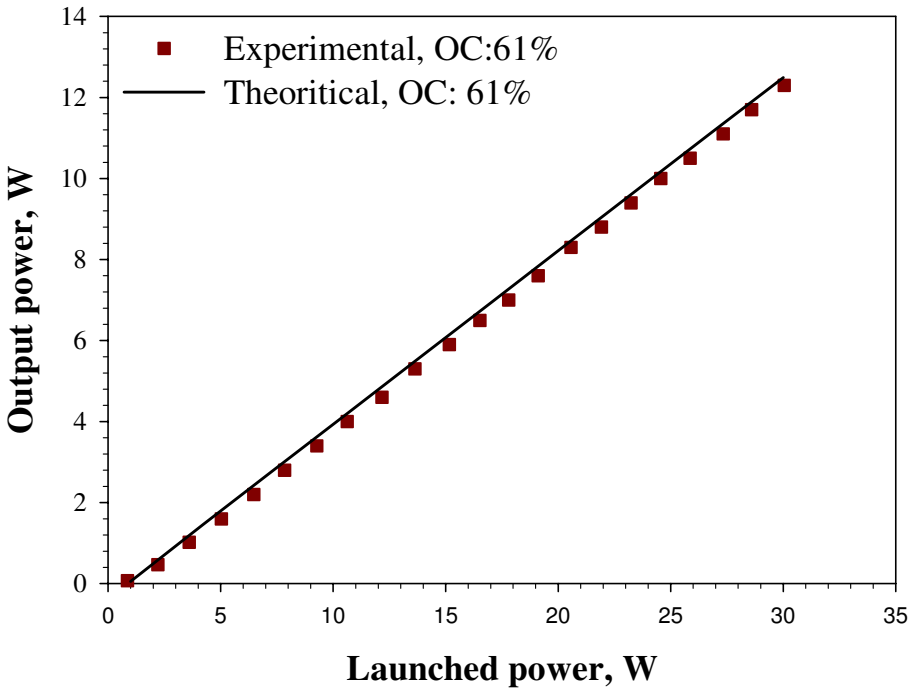

FIGURE 6.7: Comparison of experimental and simulated results of the slope efficiency

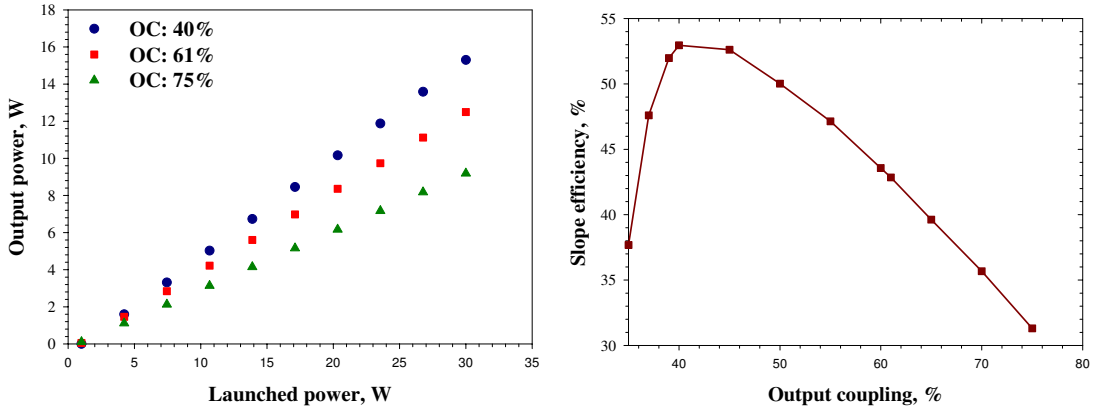

(a) Simulated slope efficiency

(b) Output coupler optimisation

FIGURE 6.8: (a). Output power vs. launched pump power with different output coupler transmittance, experimental and theoretical value, and (b) dependance of slope efficiency on the output coupler transmittance.

strongly depends on the coupler reflectivity. It is worth mentioned that, we did not observe any short wavelength ASE build up with the numerical model as well.

The calculation of population inversion of the Yb-doped fibre in the optimised

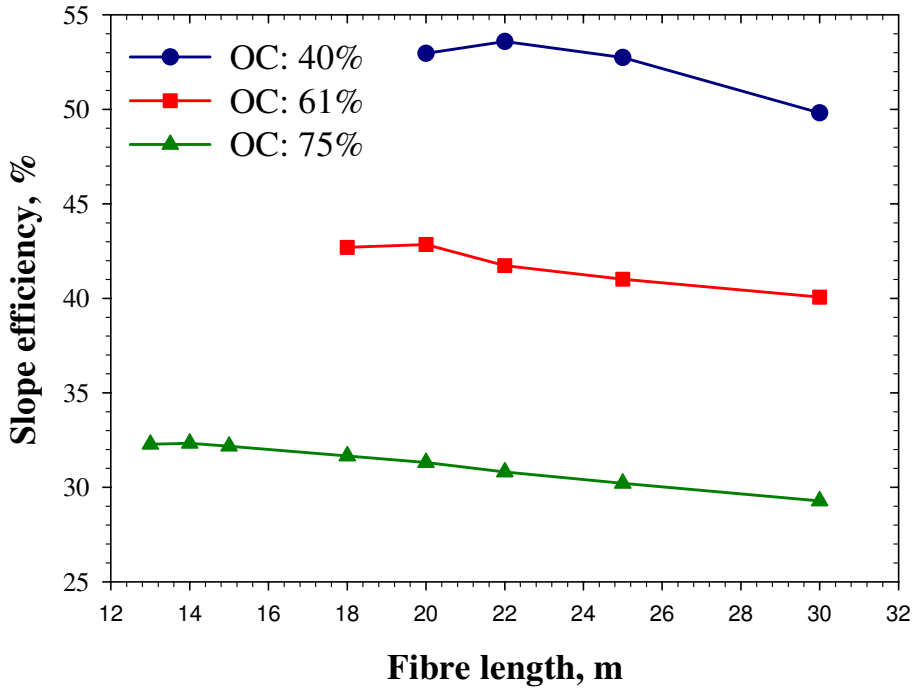

FIGURE 6.9: Slope efficiency vs. active fibre length for different output coupler reflectivity.

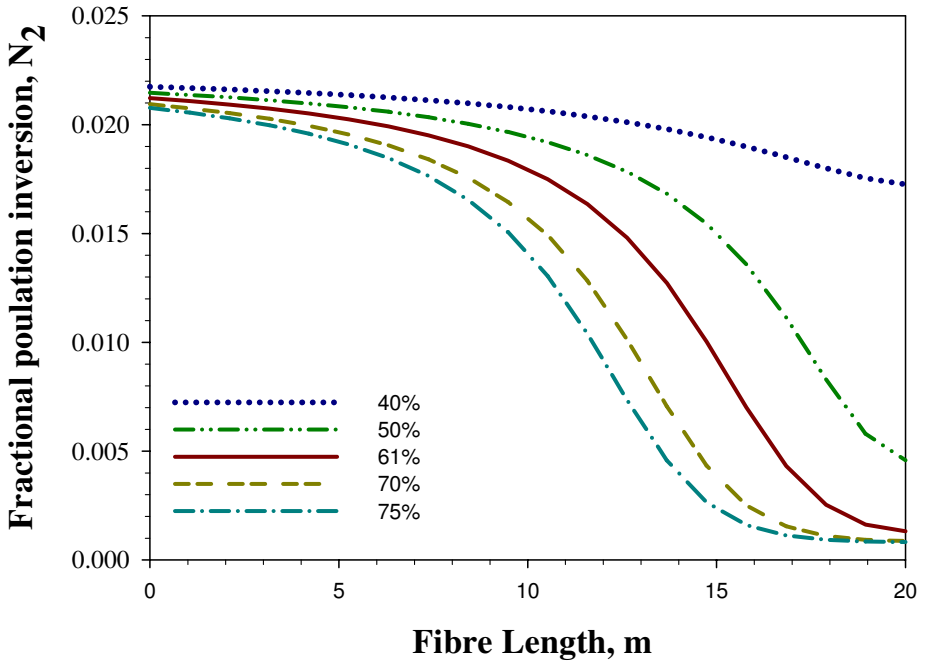

FIGURE 6.10: Evolution of population inversion along the fibre length in different output coupling.

cavity shows that the population inversion along the fibre was less than 2.5% for the 1179 nm laser (Fig. 6.10). Photodarkening can be greatly reduced when the population inversion is low [10]. Hence, the results suggest that potentially photodarkening effect will be negligible in the long wavelength operation of Yb-doped fibre laser when pumped at 1090 nm and an output power of more than 250 W is achievable before being limited by the Raman process [11]. The minimum linewidth that can be achieved with the fibre laser cavity would be around 1 GHz; which can be reduced to 1 MHz using a single frequency, single polarization fibre ring laser with ultra narrow-band FBG. Another approach could be using a single frequency seeded master oscillator power amplifier (MOPA) configuration [12]. Furthermore, for efficient frequency doubling, polarisation maintaining Yb-doped fibre is required. Power scaling of single frequency MOPA is usually limited by the on set of stimulated Brillouin scattering (SBS), which can be mitigated by using innovative fibre design and advanced experimental techniques [13].

6.5 Conclusion

In this chapter, a 1090 nm pumped, high power, narrow linewidth Yb-doped fibre laser operating at 1179 nm have experimentally been demonstrated. The simple and robust configuration is capable of generating more than 12 W output power with a slope efficiency of 43%. Numerical modeling was also carried out to optimise the laser cavity as well as to understand the maximum power extractable from this architecture. Numerical results suggest that the slope efficiency and hence the output power can be improved by optimising the output coupler reflectivity. Slope efficiency as much as 53% is possible by decreasing the output coupler reflectivity from 61% to 40%. Further enhancement in output power is possible by using high power single mode pump sources at 1090 nm. With accessibility to 1090 nm fibre

laser sources with hundreds of watts of output power and with the availability of high power passive optical components (e.g. WDM couplers, FBG), the proposed cavity architecture demonstrates the potential to achieve output power in excess of 250 W. This would open the door to high power yellow light sources for laser guide star applications and many more.

References

[1] H. Pask, R. Carman, D. Hanna, A. Tropper, C. Mackechnie, P. Barber, and J. Dawes, "Ytterbium-doped silica fiber lasers: versatile sources for the 1-1.2 μm region," IEEE *Journal of Selected Topics in Quantum Electronics* **1**(1), pp. 2 –13, 1995.

[2] M. Weber, J. Lynch, D. Blackburn, and D. Cronin, "Dependence of the stimulated emission cross section of Yb^{3+} on host glass composition," *IEEE Journal of Quantum Electronics* **19**(10), pp. 1600 – 1608, 1983.

[3] M. A. Melkumov, I. A. Bufetov, K. S. Kravtsov, A. V. Shubin, and E. M. Dianov, "Lasing parameters of ytterbium-doped fibres doped with P_2O_5 and Al_2O_3," *Quantum Electronics* **34**(9), p. 843, 2004.

[4] D. A. Grukh, A. S. Kurkov, V. M. Paramonov, and E. M. Dianov, "Effect of heating on the optical properties of Yb^{3+}-doped fibres and fibre lasers," *Quantum Electronics* **34**(6), p. 579, 2004.

[5] A. B. Wojcik, K. Schuster, J. Kobelke, C. Chojetzki, C. Michels, K. Rose, and M. J. Matthewson, "Novel hybrid glass protective coatings for high temperature applications," in *Proc. 54th Int. Wire & Cable Symp*, **368**, 2005.

[6] "Fibercore." `http://www.fibercore.com`.

[7] "Oxford electronics." `http://www.oxford-electronics.com`.

[8] C. R. Giles and E. Desurvire, "Modeling erbium-doped fiber amplifiers," *Journal of Lightwave Technology* **9**(2), pp. 271–283, 1991.

[9] R. Paschotta, J. Nilsson, A. Tropper, and D. Hanna, "Ytterbium-doped fiber amplifiers," IEEE *Journal of Quantum Electronics,* **33**(7), pp. 1049 –1056, 1997.

[10] J. Koponen, M. Soderlund, H. J. Hoffman, D. A. V. Kliner, J. P. Koplow, and M. Hotoleanu, "Photodarkening rate in Yb-doped silica fibers," *Applied Optics* **47**(9), pp. 1247–1256, 2008.

[11] G. P. Agrawal, *Nonlinear fiber optics*, Academic Press, San Diego, 3rd ed., 2001.

[12] Y. Jeong, J. Nilsson, J. Sahu, D. Payne, R. Horley, L. Hickey, and P. Turner, "Power scaling of single-frequency ytterbium-doped fiber master-oscillator power-amplifier sources up to 500 W," *IEEE Journal of Selected Topics in Quantum Electronics* **13**(3), pp. 546 –551, 2007.

[13] M.-J. Li, X. Chen, J. Wang, S. Gray, A. Liu, J. A. Demeritt, A. B. Ruffin, A. M. Crowley, D. T. Walton, and L. A. Zenteno, "Al/Ge co-doped large mode area fiber with high SBS threshold," *Opt. Express* **15**(13), pp. 8290–8299, 2007.

Chapter 7

Conclusion

Bi-doped fibre presents an attractive medium for fibre laser and amplifier in the 1.1 μm wavelength band. The work on this thesis explored some of the fundamental spectroscopic properties of Bi-doped fibre and identified the suitability of this fibre for practical device applications.It also presents the achievement on Yb-doped fibre laser at longer wavelengths and possible future directions of investigations.

A series of Bi-doped preforms and fibres were fabricated using three different fabrication routes: a) MCVD and the solution doping technique, b) MCVD based chemical-in-crucible deposition technique, and c) the PIT technique in which a silica tube is filled up with a mixture of SiO_2, Bi_2O_3 and Al_2O_3 powder, before drawing into fibre. A fabrication set up has been designed and developed for the MCVD based chemical-in-crucible deposition technique for rare earth doped fibre development and successfully applied to Bi-doped fibre fabrication. The powder-in-tube technology can subsequently provide a method for fabricating high concentration Bi-doped fibres. Bi-doped fibre fabricated by the PIT technology, shows similar luminescence properties to those of Bi-doped glasses made using conventional glass melting technique.

Bi-doped fibre with different host glass compositions were investigated. It was observed that the behaviour of Bi-doped fibre strongly depends on their host material. The use of silica doped with P shifts the Bi luminescence spectra to a longer wavelength. The peak position of the emission band shifts to longer wavelengths in presence of P in the core. In case of alumina-silicate and alumina-germano-silicate fibres, under 1090 nm excitation, the luminescence peak position is at 1130 nm while in phospho-alumino-germano-silicate and phospho-germano-silicate fibres the peak shifts to longer wavelengths of 1220 nm. The emission characteristics including fluorescence spectra and lifetimes are also dependant on the wavelength of excitation. The fluorescent spectra was measured at different pumping wavelengths from 915 to 1090 nm. The fluorescence peak shifts towards longer wavelengths and become narrower with longer pump wavelengths. The fluorescence decay time seems to depend on the pumping wavelengths and was measured at 915, 977, 1047 and 1090 nm. The recorded time was 750 μsec under 1090 nm pumping, but it reduced to 670 μsec under 915, 977 and 1047 nm pump. It was observed that the measured lifetime data deviates from single exponential behaviour. Analysis of fluorescence lifetime showed that Bi ions, which are responsible for 1160-1300 nm emission, possibly sit in different sites. The measured values of the Bi-lasers efficiency are essentially lower compared to the efficiencies of widely used rare earth doped fibre lasers. To find the mechanism of energy loss, the unsaturable loss of the Bi-doped fibre was determined by measuring transmission at different pump wavelengths. The unsaturable loss in Bi-doped fibre increased at shorter pump wavelengths and decreased at lower temperature. The ESA in Bi-doped fibres were measured in the 900 - 1300 nm range under 1047 nm pumping. A strong ESA appeared at 915 and 975 nm, whereas no significant ESA was found in the 1080 nm pumping band nor in the primary emission band of Bi-doped silicate fibre lasers. The measurement under 800 nm pumping revealed strong ESA from 900 - 1200 nm. The presence of ESA at 800 nm was inferred. The

pump ESA together with the observed signal ESA would limit the efficiency of the Bi-doped fibre laser under 800 nm pumping. The dependence of spectral characteristics in Bi alumino-silicate preform and fibre on different external treatment was investigated. The absorption in H_2-loaded fibre seems to increase but the excess molecular hydrogen can result in fluorescence quenching and a shortening of the radiative lifetime, which adversely affects the laser performance.

Experiments were carried out on Bi-doped fibre lasers emitting at 1160 and 1179 nm. A 25 m Bi-doped fibre laser at 1160 nm was demonstrated. The laser efficiency was impaired when unsaturable loss was high. The slope efficiency at room temperature was 10% and increased to 15% when cooled down to 10^{o}C. The temperature dependence of unsaturable loss and its influence on the efficiency of Bi-doped fibre laser operation was investigated. It was observed that effective heat removal can boost the laser performance in Bi system by reducing the temperature dependant unsaturable loss in the fibre. Optical amplification in a Bi-doped fibre at 1179 nm was demonstrated, with various seed power levels. A signal wave at 1179 nm and pump wave at 1090 nm counter-propagated in the fibre. It is observed that an efficient heat sink is helpful in enhancing the gain as well as the saturation output power in the Bi-doped fibre amplifier. The maximum gain achieved with water cooling was 19 dB at a signal seed power of 2.5 mW. In the power amplifier configuration, a slope efficiency of 16% was achieved at room temperature. The higher saturation power and higher efficiency at low temperature could be explained on the basis of low unsaturable loss at lower temperature in Bi-doped fibre at 1090 nm pump wavelength.

A 1090 nm pumped, high power, narrow linewidth Yb-doped fibre laser operating at 1179 nm have been experimentally demonstrated. The simple and robust configuration is capable of generating more than 12 W output power, limited by available pump power, with a slope efficiency of 43%. Numerical modeling was

also carried out to optimise the laser cavity as well as to understand the maximum power extractable from this architecture. Numerical results suggest that the slope efficiency and hence the output power can be improved by optimising the output coupler reflectivity. Slope efficiency as much as 53% is possible by decreasing the output coupler reflectivity from 61% to 40%.

Bi-doped optical fibre is a new promising material, which shows luminescence in the 1160-1300 nm spectral bands. Further fundamental investigation is necessary to fully understand the near infrared luminescence mechanism in the Bi-doped fibre. From the characterisation of Bi-doped fibre it is concluded that it is important to increase the Bi concentration in the fibre core for the construction of efficient fibre lasers based on core and cladding pumping scheme. It is also important to understand the luminescence processes in Bi-doped glasses, which will eventually lead to the engineering of efficient Bi-doped fibres for efficient devices. It was observed that the Bi gain characteristics depends on host composition, pump wavelength, and as a result can be adjusted to obtain desired properties, including gain spectrum. For this purpose, Bi-doped phospho-germano-silicate fibres can be developed, with pumping at different wavelengths, including 1200-1250 nm [1]. In an approach to understand the active centres responsible for Bi luminescence, co-doped system of Bi and a rare earth ion could be investigated. Valuable insight into the nature and properties of the Bi emission centre can be gained by studying energy transfer between the Bi and rare earth ions. Secondly, there are practical applications for co-doping, since the combined Bi/rare earth emission spectrum may be used in devices to create an ultra-broadband light source, or the rare earth ion can be used to sensitize the Bi emission.

References

[1] I. A. Bufetov and E. M. Dianov, "Bi-doped fiber lasers," *Laser Physics Letters* **6**(7), pp. 487–504, 2009.

Appendix A

Publications

Journal Publications

1. M. P. Kalita, S. Alam, C. Codemard, S. Yoo, A. J. Boyland, M. Ibsen, and J. K. Sahu, "Multi-watts narrow-linewidth all fiber Yb-doped laser operating at 1179 nm," Optics Express 18, 5920-5925, 2010.

2. M. P. Kalita, S. Yoo, and J. K. Sahu, "Influence of cooling on a bismuth-doped fiber laser and amplifier performance," Applied Optics 48, G83-G87, 2009.

3. S. Yoo, M. P. Kalita, J. Nilsson, and J. Sahu, "Excited state absorption measurement in the 900-1250 nm wavelength range for bismuth-doped silicate fibers," Optics Letters 34, 530-532, 2009.

4. M. P. Kalita, S. Yoo, and J. K. Sahu, "Bismuth doped fiber laser and study of unsaturable loss and pump induced absorption in laser performance," Optics Express 16, 21032-21038, 2008.

5. A. J. Boyland, A. S. Webb, S. Yoo, F. H. Mountfort, M. P. Kalita, R. J. Standish, J. K. Sahu, D. J. Richardson, D. N. Payne, "Optical fiber fabrication using novel gas phase deposition technique," Journal of Lightwave Technology, 2011.

Conference Publications

1. M. P. Kalita, S. Yoo, A. S. Webb, R. J. Standish, M. Ibsen, and J. K. Sahu, "Modification of spectroscopic properties of bismuth doped silica fiber by post-fabrication process and different fabrication methods," OFC/NFOEC, San Diego, 21-25 March, 2010.

2. M. P. Kalita, S. Yoo, and J. K. Sahu, "Bismuth doped fiber laser performance on effective fiber cooling," CLEO/Europe-EQEC Conference 2009, Munich, 14-19 June, 2009.

3. J. K. Sahu, M. P. Kalita, S. Alam, M. Ibsen, and A. Boyland, "12 W ytterbium doped all-fiber laser at 1179 nm" CLEO/Europe-EQEC Conference 2009, Munich, 14-19 June, 2009.

4. M. P. Kalita, S. Yoo, and J. K. Sahu, "All fiber narrow linewidth high power bismuth doped fiber amplifier at 1179 nm," CLEO/QELS 2009, Baltimore, 31 May-5 June, 2009.

5. M. P. Kalita, S. Yoo, R. S. Quimby, and J. K. Sahu, "Pump wavelength dependance of bismuth doped fibre laser," International Conference on Fiber Optics and Photonics, Photonics 2008, Delhi, India, 13-17 December, 2008.

6. S. Yoo, M. P. Kalita, J. K. Sahu, J. Nilsson, and C. Oton, "Excited state absorption measurement in bismuth-doped silicate fibers for use in 1160 nm fiber laser," 3rd EPS-QEOD Europhoton Conference, Paris, 31 August-5 September, 2008.

7. S. Yoo, M. P. Kalita, J. K. Sahu, J. Nilsson, and D. N. Payne, "Bismuth-doped fiber laser at 1.16 microns," CLEO/QELS 2008, San Jose, 4-9 May, 2008.

8. A. J. Boyland, A. S. Webb, M. P. Kalita, S. Yoo, C. A. Codemard, R. J. Standish, J. Nilsson and J. K. Sahu, "Rare earth doped optical fiber fabrication using novel gas phase deposition technique," CLEO/QELS 2010, San Jose, 18-20 May, 2010.

9. J. K. Sahu, M. P. Kalita, and S. Yoo, "Bismuth-doped fibres for near-infrared light sources: progress and prospects," International Conference on Fiber Optics and Photonics, Photonics 2010, Guwahati, India, 11-15 December, 2010 (Invited).

Selected Other Publications

1. M. P. Kalita, A. S. Webb, A. J. Boyland, S. Yoo, and J. K. Sahu "Novel fiber fabrication methods benefit fiber lasers," Laser Focus World 46, 63-65, 2010.

2. S. Yoo, M. P. Kalita, A. J. Boyland, A. Webb, R. J. Standish, J. K. Sahu, M. C. Paul, S. Das, S. K. Bhadra, and M. Pal, "Ytterbium doped Y_2O_3 nanoparticle silica optical fibers for high power fiber lasers with suppressed photodarkening," Optics Communications 283, 3423-3427, 2010.

3. M. C. Paul, S. W. Harun, N. A. D. Huri, A. Hamzah, S. Das, M. Pal, S. K. Bhadra, H. Ahmad, S. Yoo, M. P. Kalita, A. J. Boyland, and J. K. Sahu, "Wideband EDFA based on erbium doped crystalline zirconia yttria alumino silicate fiber," Journal of Lightwave Technology 28, 2919-2924, 2010.

4. A. Hamzah, S. W. Harun, N. A. D. Huri, A. Lokman, H. Arof, M. C. Paul, M. Pal, S. Das, S. K. Bhadra, H. Ahmad, S. Yoo, M. P. Kalita, A. J. Boyland, J. K. Sahu, "Multi-wavelength fiber laser with erbium doped zirconia fiber and semiconductor optical amplifier," Optoelectronics and Advanced Materials - Rapid Communications 4, 1431-1434, 2010.

5. M. C. Paul, S. Bysakh, S. Das, S. K. Bhadra, M. Pal, S. Yoo, M. P. Kalita, A. J. Boyland, and J. K. Sahu, "Y_2O_3 doped YAG nano-crystallites in silica based core glass matrix of optical fiber preform," Materials Science and Engineering B 175, 108-109, 2010.

6. M. C. Paul, S. W. Harun, N. A. D. Huri, A. Hamzah, S. Das, M. Pal, S. K. Bhadra, H. Ahmad, S. Yoo, M. P. Kalita, A. J. Boyland, and J. K. Sahu, "Performance comparison of Zr-based and Bi-based erbium-doped fiber amplifiers," Optics Letters 35, 2882-2884, 2010.

7. A. Hamzah, M. C. Paul, S. W. Harun, N. A. D. Huri, A. Lokman, M. Pal, S. Das, S. K. Bhadra, H. Ahmad, S. Yoo, M. P. Kalita, A. J. Boyland, and J. K. Sahu, "Compact fiber laser at L-band region using Erbium-doped Zirconia fiber," Laser Physics 21, 176-179, 2011.

8. S. W. Harun, N. A. D. Huri, A. Hamzah, H. Ahmad, M. C. Paul, S. Das, S. K. Bhadra, S. Yoo, M. P. Kalita, A. J. Boyland, J. K. Sahu, "Zirconia-Based Erbium-Doped Fiber Amplifier," Book Chapter in Optical Amplifiers, Chapter IV, Nova Publishers, 2011.

9. J.K. Sahu, S. Yoo, A.J. Boyland, A. Webb, M. Kalita, J. N. Maran, Y. Jeong, J. Nilsson, W. A. Clarkson and D. N. Payne, "Fiber design for high power fiber lasers," Proc. SPIE 7195, p. 719501, 2009.

10. S. Yoo, M. P. Kalita, A. J. Boyland, A. Webb, R. J. Standish, J. K. Sahu, M. C. Paul, S . Das, S. K. Bhadra and M. Pal, "Ytterbium doped nano-crystalline

optical fiber for reduced photodarkening," CLEO/QELS 2010, San Jose, 18-20 May, 2010.

11. J. K. Sahu, M. C. Paul, M. P. Kalita, A. Boyland, C. Codemard, S. Yoo, A. Webb, R. J. Standish, J. Nilsson, S. Das, S. Bhadra, M. Pal, A. Dhar, and R. Sen, "Ytterbium doped nanostructured optical fibers for high power fiber lasers," CLEO/Europe-EQEC Conference 2009, Munich, 14-19 June, 2009.

12. J. K. Sahu, S. Yoo, A. J. Boyland, A. Webb, M. Kalita, Y. Jeong, J. Nilsson, and D. N. Payne, "Advances in active fibres for high-power and high-brightness fibre sources," International Conference on Fiber Optics and Photonics, Photonics 08, Delhi, India, 13-17 December, 2008 (Invited).

13. J. K. Sahu, S. Yoo, A. J. Boyland, C. Basu, M. P. Kalita, A. S. Webb, C. L. Sones, J. Nilsson, and D. N. Payne, "488 nm irradiation induced photodarkening study of Yb-doped aluminosilicate and phosphosilicate fibers," CLEO/QELS 2008, San Jose, 4-9 May, 2008.

14. J. K. Sahu, S. Yoo, A. J. Boyland, A. Webb, M. Kalita, J. N. Maran, Y. Jeong, J. Nilsson, W. A. Clarkson, and D. N. Payne, "Fiber design for high power fiber lasers," Photonics West, San Jose, 24-29 January, 2008 (Invited).